

October 2022

ANALYSIS OF FOOD COLORANTS USING RAMAN SPECTROSCOPY

Haochen Dai
University of Massachusetts Amherst

Follow this and additional works at: https://scholarworks.umass.edu/dissertations_2



Part of the [Food Chemistry Commons](#)

Recommended Citation

Dai, Haochen, "ANALYSIS OF FOOD COLORANTS USING RAMAN SPECTROSCOPY" (2022). *Doctoral Dissertations*. 2610.

<https://doi.org/10.7275/30047001> https://scholarworks.umass.edu/dissertations_2/2610

This Open Access Dissertation is brought to you for free and open access by the Dissertations and Theses at ScholarWorks@UMass Amherst. It has been accepted for inclusion in Doctoral Dissertations by an authorized administrator of ScholarWorks@UMass Amherst. For more information, please contact scholarworks@library.umass.edu.

ANALYSIS OF FOOD COLORANTS USING RAMAN SPECTROSCOPY

A Dissertation Presented

By

HAOCHEN DAI

Submitted to the Graduate School of the
University of Massachusetts Amherst in partial fulfillment
of the requirements for the degree of

DOCTOR OF PHILOSOPHY

September 2022

Department of Food Science

© Copyright by Haochen Dai 2022
All Rights Reserved

ANALYSIS OF FOOD COLORANTS USING RAMAN SPECTROSCOPY

A Dissertation Presented

By

HAOCHEN DAI

Approved as to style and content by:

Lili He, Chair

Eric A. Decker, Member

Jiakai Lu, Member

Nianqiang Wu, Outside Member

Lynne A. McLandsborough, Department Head

Food Science Department

DEDICATION

To my grandparents, parents, loving fiancé overseas,
And any of my friends (especially Gen Li, Ziheng Wang, Zhiwei Tang, and Qian Feng)
who supported me throughout the course of my Ph.D. study.

ACKNOWLEDGMENTS

I would like first to thank my Ph.D. advisor, Prof. Lili He, for her tremendous support, guidance, and patience throughout my entire doctoral studies. Her expertise and scientific attitudes have shaped me imperceptibly. And her excellence as a researcher and mentor will guide me forever.

Next, I would like to sincerely acknowledge my committee members, Prof. Eric A. Decker, Prof. Jiakai Lu, and Prof. Nianqiang Wu, for their constructive feedback and suggestions for my research.

I would like to thank all my research colleagues, especially my undergraduate students, Qixiang Gao, Benjamin Goldberg, and Adam Forbes, for their hard work and advice. I also thank Dr. Zhiyun Zhang and his family for their generous advice and friendships.

At last, I would like to express my sincere and deepest gratitude to my family for their unconditional love and accompany. Next, I want to thank my fiancé Chang Guo for supporting me as a soul mate and life partner. I would not have come this far without your encouragement!

ABSTRACT

ANALYSIS OF FOOD COLORANTS USING RAMAN SPECTROSCOPY

SEPTEMBER 2022

HAOCHEN DAI, B.E., BEIJING TECHNOLOGY AND BUSINESS UNIVERSITY

M.S., UNIVERSITY OF MASSACHUSETTS AMHERST

Ph.D., UNIVERSITY OF MASSACHUSETTS AMHERST

Directed by: Professor Lili He

Color is one of the most important quality attributes that affect consumers' selection of food. The increasing demand of consumers for natural colorants over artificial ones has placed challenges in both product development and regulatory practices. However, current analytical solutions for food colorants are mostly limited to a sophisticated laboratory setting with tedious sample preparation procedures. Herein, this research focuses on the analytical developments toward cost-effective determination of colorant adulteration and stability analysis. The main technique explored is Raman spectroscopy, which measures the inelastic light scattering and allows one to obtain unique molecular fingerprints for specific molecules. Compared with chromatographic methods, e.g., high-performance liquid chromatography (HPLC) or gas chromatography (GC), Raman spectroscopic

methods show great potential in the analysis of food colorants due to their fingerprinting capability non-destructive nature, good portability, and easy preparation protocols. In addition, the integration of gold or silver metallic nano substrate to Raman spectroscopy, known as surface-enhanced Raman spectroscopy (SERS), improves detection sensitivity tremendously.

The first study was aimed to develop a fast screening and quantification method combining thin-layer chromatography (TLC) and Raman spectroscopy for saffron powder analysis, which is one of the most expensive agricultural products in the world. Sample solutions of pure saffron and spiked saffron were prepared and dropped on TLC chips for the identification of pure saffron quality as well as discrimination of spiked saffron. The result indicated that Raman spectroscopy was capable of quantifying the major coloring compound, crocin, on dried TLC sample patterns. The method achieved excellent prediction capability for crocin concentration (expressed via absorbance value at 440nm, according to ISO3632) in the range of 0 to 400 with an RMECV of 13 and an R^2 of 0.99 using partial least squares (PLS) regression model. The TLC patterns between adulterants (safflower, turmeric, red 40, and yellow 5) were distinct under bright and UV lights. Their variation was demonstrated using principal components analysis (PCA). The lowest adulteration degrees that can be detected were 2.59% for red 40, 4.15% for yellow 5, 31.01% for safflower, and 41.98% for turmeric respectively, using the PLS analysis. The next study was aimed to utilize data fusion strategies to improve the classification and quantification accuracies of saffron adulteration. In the data processing protocol, the

imaging data and featured Raman data were concatenated into one data matrix. The model performance of the fused data was compared against each data block. The result indicated that the classification accuracy for saffron adulterants were greatly improved with a classification accuracy of 99% among 4 different adulterants ranging from 2% to 100% (w/w) using the fused data block as compared to the imaging data (84% accuracy) or Raman data (86% accuracy) alone. The quantification performances of the developed PLS model were improved slightly using the fused data block, achieving higher R^2 values with lower errors.

To improve the detection capability of TLC-Raman for adulterant analysis, a mirror “stamping” TLC-SERS approach was developed. The aim of this study was to build a simple approach for sample separation (TLC) and signal enhancement (SERS) using easily available materials. Homemade silver nanoparticles were fabricated, formed to a mirror, and stamped on developed TLC patterns for Raman signal amplification. Pure saffron (1000 ppm) and spiked saffron (200 ppm red 40) solutions were used as a model system. The result indicated that both saffron colorant(crocin) and adulterated colorant (red 40) exhibited a strong characteristic peak using the mirror stamp approach, whereas there was no or little signal without the mirror application.

An arising challenge was reported when food manufacturers were trying to develop products that contain natural colorants with iron fortification. In detail, the natural colorant, anthocyanins, developed unwanted blue color shifts due to iron-anthocyanin co-pigmentation. Thus, the last study was aimed to establish a quantitative model for the

prediction of anthocyanin color stability in the presence of dissolved iron. Nine anthocyanin extracts obtained from various sources were purified and measured using SERS. The PCA model successfully discriminated anthocyanins from different plant sources. The stabilization index of each anthocyanin extract was measured using UV-vis spectroscopy under pH 3 and 6 with and without iron fortification (ferric sulfate) and used as input for PLS model. The PLS model demonstrated high accuracy of predicting the stability index with an RMSECV of 2.16 nm (bathochromic shift) and an R^2 of 0.98 for external validations.

The results from these studies demonstrated the capability of Raman or SERS conjoined with TLC techniques and multivariate analyses for natural colorant adulteration and stability analysis. The Raman/SERS spectral data obtained in the present studies provide useful references for the food colorant research. The established methods could provide useful methodologies for industry applications in regard to fast raw ingredients screening for food companies as well as quality control for natural colorant manufacturers.

TABLE OF CONTENT

	Page
ABSTRACT	vi
LIST OF TABLES	xiv
LIST OF FIGURES	xv
1. ANALYSIS OF FOOD COLORANTS USING RAMAN SPECTROSCOPY	1
1.1 Abstract	1
1.2 Introduction	1
1.2.1 Synthetic colors.....	2
1.2.2 Natural colors.....	6
1.3 Current analytical methods and limitations	10
1.4 Raman and surfaced-enhanced Raman spectroscopy	12
1.5 Applications of Raman or SERS on food colorant analysis.....	14
1.6 Current limitations and future perspective	20
1.7 Conclusion	22
2. RAPID DETERMINATION OF SAFFRON GRADE AND ADULTERATION BY THIN-LAYER CHROMATOGRAPHY COUPLED WITH RAMAN SPECTROSCOPY	23
2.1 Abstract	23
2.2 Introduction	24
2.3 Material and method.....	29
2.3.1 Chemicals, reagents, and plant materials.....	29
2.3.2 Preparation of pure saffron and adulterated saffron powder samples....	29
2.3.3 Sample preparation for imaging analysis and TLC-Raman.....	30
2.3.4 Determination of the crocin color strength using the standard ISO method.....	31
2.3.5 Raman reference spectrum analysis of saffron and saffron adulterants.	31
2.3.6 Analysis of pure and spiked saffron samples using the TLC-Raman and TLC imaging method.....	32
2.3.7 Statistical analysis.....	33

2.4 Results and discussion	34
2.4.1 Reference saffron sample analysis using the ISO and Raman spectroscopic methods.....	34
2.4.2 Establishment of two PLS calibrations for quantifying the saffron color strength based on L*a*b* values and Raman spectra, respectively.....	35
2.4.3 Identification of saffron adulterants based on TLC patten.....	37
2.4.4 Confirmation of saffron adulterants based on Raman spectroscopy.....	40
2.4.5 Validation the established methods and models using adulterated samples with optically identical property.....	42
2.5 Conclusion	45
3. IMPROVING CLASSIFICATION AND QUANTIFICATION ACCURACY OF SAFFRON ADULTERATION USING DATA FUSION STRATEGIES.....	46
3.1 Abstract	46
3.2 Introduction	47
3.3 Material and method... ..	50
3.3.1 Chemicals and reagents.....	50
3.3.2 Sample preparation.....	50
3.3.3 Data acquisition.....	51
3.3.4 Data fusion.....	54
3.3.5 Partial least squares discriminant analysis.....	55
3.3.6 Partial least square (PLS) regression of quantification.....	55
3.4 Result and discussion	56
3.4.1 The effect of mid-level fusion on classification performance.....	56
3.4.2 Mid-level fusion model validation for adulteration classification.....	59
3.4.3 The effect of data fusion on PLS model quantification performances.....	60
3.5 Conclusion	63
4. A MIRROR STAMPING APPROACH FOR IMPROVED SEPARATION AND DETECTION OF COLOR ADULTERANTS USING THIN-LAYER	

CHROMATOGRAPHY AND SURFACE-ENHANCED RAMAN SPECTROSCOPY.....	65
4.1 Abstract.....	65
4.2 Introduction.....	66
4.3 Material and method.....	68
4.3.1 Silver mirror fabrication.....	68
4.3.2 Pure and spiked sample preparation.....	70
4.3.3 Silver mirror application.....	71
4.4 Results and discussion.....	72
4.4.1 Detection of pure saffron sample on TLC.....	72
4.4.2 Separation performance of different mirror application methods on TLC.....	74
4.4.3 Detection of Allura red signal in adulterated saffron samples on TLC...	76
4.4.4 Detection of saffron signal in adulterated saffron samples on TLC.....	77
4.5 Conclusion.....	79
5. PREDICTION OF ANTHOCYANIN COLOR STABILITY AGAINST IRON CO-PIGMENTATION BY SURFACED-ENHANCED RAMAN SPECTROSCOPY.....	80
5.1 Abstract.....	80
5.2 Introduction.....	81
5.3 Material and method.....	84
5.3.1 Raw material and chemical reagents.....	84
5.3.2 Sample preparation.....	84
5.3.3 Anthocyanin quantitation (pH differential method).....	85
5.3.4 Iron stabilization index acquisition.....	86
5.3.5 Anthocyanin SERS reference spectra acquisition.....	87
5.3.6 Data analysis.....	88
5.4 Results and discussion.....	89

5.4.1 Stabilization index analysis of anthocyanin extracts against iron incorporation.....	89
5.4.2 SERS analyses of anthocyanin extracts from natural colorants.....	91
5.4.3 PCA analysis of tested anthocyanin SERS spectra.....	95
5.4.4 PLSR analysis between SERS spectra and stabilization index of each anthocyanin extract.....	98
5.4.5 Study of anthocyanin’s iron stability on SERS signal.....	101
5.5 Conclusion.....	104
6. SUMMARY AND FUTURE RESEARCH.....	106
BIBLIOGRAPHY.....	110

LIST OF TABLES

Table		Page
1	Summary of certified synthetic colorants in the U.S.....	4
2	Summary of major natural colorants in the USA and EU.....	9
3	Summary of Raman or SERS analytical approaches of food colorants in recent publications.....	18
4	Comparison of UV-vis and TLC-Raman analytical methods for identifying saffron color strength.....	42
5	TLC-PLS calibration validation with adulterated samples.....	44
6	Misclassification table of spiked saffron samples based on A. Imaging data, B. Featured Raman data, and C. Fused data as training group.....	58
7	Misclassification table of validation group based on the fused data block.....	59
8	Statistics for each data block in external and cross-validations.....	62
9	Major anthocyanin structures and plant sources.....	82
10	Stabilization indexes of collected anthocyanin extracts.....	89
11	Band wavenumbers and their tentative assignments of anthocyanin extracts.....	94
12	Statistics for each stabilization index in cross- and external validations..	99

LIST OF FIGURES

Figure		Page
1	Physical observation of pure saffron extract (a) and its TLC pattern (b) under different lighting conditions (ambient light on the top half, 365nm UV light on the bottom half); c. Predict vs. actual color strength PLS plots for saffron specimens using L*a*b* data.....	36
2	a. Raman Spectrum of pure saffron extract measured on TLC plate; b. Predict vs. actual color strength PLS plots for saffron specimens using Raman spectrum data.....	37
3	TLC pattern of pure saffron and spiked saffron with different adulteration level (ambient light on the top half, 365nm UV light on the bottom half) ..	38
4	a. Principal component analysis of pure saffron and max adulterated samples based on TLC pattern L*a*b* values. Predict vs. actual color strength plots for adulterated saffron specimens based on L*a*b* data of b. safflower; c. turmeric; d. Allura red; e. tartrazine.....	40
5	a. Pure saffron and pure adulterants Raman spectrum (80% ethyl extracts). b. Principal components analysis (PCA) of pure saffron and adulterants Raman spectrum (all sample solutions were prepared with a concentration of 1 mg dry matter/ml water)	41
6	Comparison of TLC pattern, crocin Raman spectrum (a, b, and d) and adulterant Raman spectrum (c, e, and f) among three validation samples. (Note: Unless specifically mentioned, all Raman spectra were acquired at the center of each TLC drop)	43
7	Raman spectra of adulterated saffron samples collected on TLC substrates.....	52
8	TLC pattern and imaging data collection scheme.....	53
9	Schematic view of mid-level data fusion processing.....	54
10	PLS-DA 3D-plots of (A). Imaging data; (B). Featured Raman data; (C). Fused data.....	56
11	Predict vs. actual PLS plots of spiked saffron samples using imaging, featured Raman, and fused data blocks.....	61
12	Physical observation of different AgNP mirror formation phases. a. AgNPs reacting with meditating solution; b. AgNP mirror formation and condensation; c. fully stabilized AgNP mirror; d. drying process of AgNP on a gold slide.....	69
13	Sample pretreatments: a. standard Raman approach on TLC chip; b. mirror first TLC-SERS approach; c. mirror last TLC-SERS approach; d. mirror stamp TLC-SERS approach.....	70

14	a-f. Raman and SERS signals of pure saffron solution collected under different sample pretreatments; g. Characteristic Raman peak intensity of saffron collected on TLC substrates under various sample pretreatments....	72
15	Physical observation of adulterated saffron solutions under different pretreatments on TLC substrates. a. standard Raman-TLC (no mirror); b. SERS-TLC treatment 1 (mirror first); c. SERS-TLC treatment 2 (mirror last); d. SERS-TLC treatment 3 (mirror stamp).....	75
16	Raman and SERS signal of Allura red from adulterated saffron specimens collected on TLC substrates under various sample pretreatments: a. standard Raman-TLC (no mirror); b. SERS-TLC treatment 1 (mirror first); c. SERS-TLC treatment 2 (mirror last); d. SERS-TLC treatment 3 (mirror stamp).....	76
17	Raman and SERS signal of crocin from adulterated saffron specimens collected on TLC substrates under various sample pretreatments: a. standard Raman-TLC (no mirror); b. SERS-TLC treatment 1 (mirror first); c. SERS-TLC treatment 2 (mirror last); d. SERS-TLC treatment 3 (mirror stamp).....	78
18	Structure of major anthocyanin-3-O-glucoside (R3).....	81
19	Bathochromic (Index 1 and 2) and hyperchromic (Index 3 and 4) shifts of co-pigmented anthocyanin measured by UV-vis spectroscopy.....	86
20	Surface-enhanced Raman spectra of anthocyanin extracts from different plant sources (dried acidified solution).....	93
21	PCA scores of collected anthocyanin SERS signal.....	96
22	Principal component spectra of anthocyanin extracts.....	97
23	Actual vs. prediction PLS plot in external validation for each stabilization index.....	100
24	PLS loading spectra for stabilization index 1 using anthocyanin's SERS signal.....	102

CHAPTER 1

ANALYSIS OF FOOD COLORANTS USING RAMAN OR SURFACE- ENHANCED RAMAN SPECTROSCOPY

1.1 Abstract

The use of food colorants, either natural or synthetic, aims to improve the appearance of food products or dye transparent foods to give them certain flavor perceptions. However, the illegal use of carcinogenic synthetic dyes, misuse, or adulteration of natural colorants poses risks to public health. Thus, fast and sensitive detection methods are crucial for food safety and quality by identifying banned or adulterated colorants. This review provides a general background of currently certified colorants, common detection methods, and an introduction to surface-enhance Raman spectroscopy (SERS) as a novel method for colorant analysis. This article also focuses on established SERS methods for colorant detection, their limitations, and potential solutions for improvements.

1.2 Introduction

The perceptions of consumers play a crucial on the food industry. Over the years, products with more appealing and delightful characteristics have been produced to meet consumers' expectations.¹ Among the characteristics of a food product, the product's color is usually one of the most impressive attributes that affect consumers' first impression of whether the food is fresh, safe, or delicious.^{2,3} However, the final color expression of a food product is ultimately affected by many aspects, such as processing conditions or storage conditions. Thus, the addition of food colorant is an effective solution to mask unpleasant

colors or enhance existing colors in final food products. In addition, the incorporation of food colorant also helps dye products that are transparent or white, giving the consumer the impression of certain flavors related to the color.²

According to the Food & Drug Administration (FDA), a food colorant is defined as “*any dye, pigment or substance which when added or applied to a food, drug or cosmetic, or to the human body, is capable (alone or through reactions with other substances) of imparting color*”.⁴ In detail, they can be categorized into four major categories: synthetic colors, natural colors, nature-identical colors, and inorganic colors. However, in most cases, they are categorized into synthetic and natural colorants.^{5,6} The application of each type of the mentioned colorant and its potential risk to human health will be reviewed below.

1.2.1 Synthetic colors

Since the first synthetic color (mauvine) was developed by Sir William Henry Perkin in 1856, hundreds of colorants were produced and offered to the market.⁴ Synthetic colorants are easier to produce, less expensive, and more stable than their natural counterparts. Moreover, unlike most natural colorants, these chemically synthesized colorants can be easily homogenized in food matrices at a wide pH range with little or no unwanted flavors. Thus, synthetic colorants were well welcomed by manufacturers in the early 20th century.

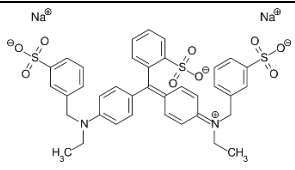
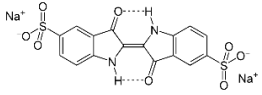
Today, commercially available synthetic colorants can be categorized into five groups, namely, (1) azo compounds, (2) triarylmethane-based compounds, (3) chinophthalon

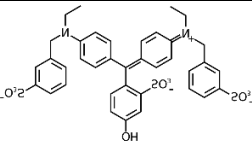
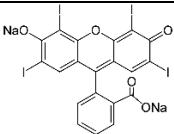
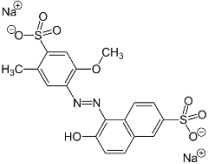
derivative-based compounds (Quinoline Yellow, E 104), (4) xanthene/erythrosine-based compounds, and (5) indigo-based compounds. However, the history of synthetic colorant application has always been related to abuse and safety concerns. Over the years, more food colorants have exhibited damage to human health. Carcinogenic effects or internal organ damage were found in many animal studies involving synthetic colorants (Green 1, Orange 2, Red 2, Red 4, Red 32, Yellow 1-4, Sudan Red, malachite green, rhodamine 6G, and others), which are nowadays banned but still used as color adulterants.^{7,8,9} The abuse of illegal synthetic colorants poses a great risk to public health. Such dyes are recognized or potentially recognized as carcinogens and are classified as category III by the International Agency for Research on Cancer.⁸ Direct consumption of these colorants at any level may potentially harm human health. However, there are substantial examples of deliberate adulterations and unlawful use of illegal dyes, in which carcinogenic artificial colorants were intentionally added to or indirectly contaminated food products.^{10,11}

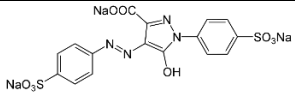
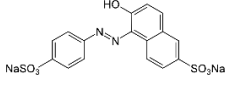
The use of synthetic colorants is now strictly monitored and legislated by numerous governments and agents across the globe, including the European Union (EU) and the Food and Drug Administration of the U.S.A. (USFDA). For instance, certified artificial colorants have been reduced to 7 from 700 being used in the U.S.A (Table 1).^{12,13} Nevertheless, no direct evidence were found in recent studies indicating severe adverse effects of existing certified colorants on human health.^{7,14,15} Studies still warn that synthetic colorant may pose risks to human health, including potential causes of hyperactivity in children.^{7,16} The result from recent cell studies or animal studies also observed different degrees of mutagenicity

or genotoxicity from certified food colorants at close to ADI levels or excessive concentrations.^{9,17,18} Consequently, manufacturers are actively developing products with natural alternatives due to increasing consumer pressure.

Table 1. Summary of certified synthetic colorants in the U.S.

Colorant	EU Code	Chemical Structure	Acceptable daily intake in the US (ADI mg/kg body weight)	Reported side effects	Ref.
FD&C Blue No. 1 (Brilliant Blue FCF)	E133	 <p>triarylmethane-based compounds</p>	6	May include allergic reaction, induced chromosome aberration in cell line (Chinese hamster fibroblast)	7,15,18,19,20
FD&C Blue No. 2 (Indigo carmine)	E132	 <p>indigo-based compounds</p>	2.5	Induced chromosome aberration in CHL cells, at 12 mg/mL,	19,20,21,22

				increased tumor incidence and/or mortality in at least one strain of hamster	
FD&C Green No. 3 (Fast green FCF)	E143	 <p>triarylmethane-based compounds</p>	2.5	Induced chromosome aberration in cell line (Chinese hamster fibroblast)	18,19,20
FD&C Red No. 3 (Erythrosine)	E127	 <p>xanthene/erythrosine-based compounds</p>	2.5	Induced DNA damage in mouse stomach and bladder at excessive intake level (>100 mg/kg).	17,19,20
FD&C Red No. 40 (Allura red AC)	E129	 <p>azo compounds</p>	7	May include allergic reaction, induced DNA damage in mouse colon at close to ADI level (10 mg/kg).	17,19,20

FD&C Yellow No. 5 (Tartrazine)	E102	 <p>azo compounds</p>	5	May include allergic reaction, induced DNA damage in mouse colon at close to ADI level (10 mg/kg). May induce hyperactivity in children.	13,17,19,20
FD&C Yellow No. 6 (Sunset yellow FCF)	E110	 <p>azo compounds</p>	3.75	May include allergic reaction.	19,20

1.2.2 Natural colors

Human has been using natural colorant in food for thousands of years. The evidence of incorporating natural colorants in food can trace back to 1500BC when ancient Egyptians used natural extracts in wine and candy to improve their appearance. Spices such as saffron and turmeric were also reported to be added to food as both spices and colorants.¹³

By definition, a natural colorant can be referred to as a substance obtained from plants, animals, or minerals that can be used to impart color. As is known, natural pigments are

widely assessable in fruits, vegetables, seeds, and roots in the form of thousands of compounds. In the kingdom of these bio-synthesized chemicals, carotenoids, chlorophyllin, anthocyanins, and betanin are four main categories of plant pigments utilized as natural colorants (Table 2).^{13,23,24} Other pigments from animals, such as heme proteins, are also used as natural food colorants in food, however, on a much smaller scale. In the meantime, humans also have a long history of consuming these pigments, which are vastly present in our diet. The “natural colorant” we consume daily in our food is significantly greater than those colorants we consume as colorants additives. Nowadays, 13 naturally derived colors are permitted in the EU (94/36/EC), whereas 26 colors are exempt from certification in the USA (21CFR Part 73), most of which are extracted from plants.¹³

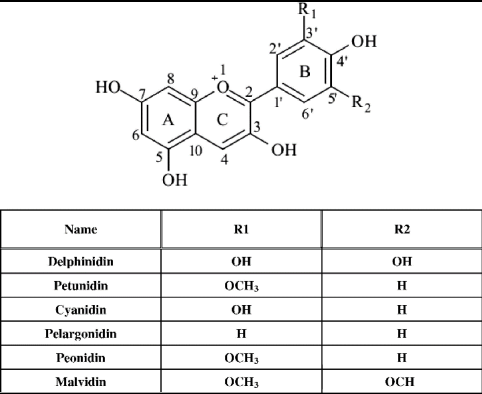
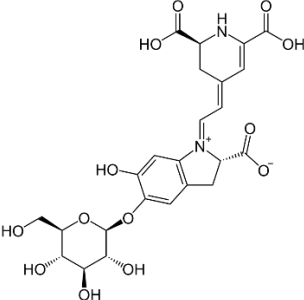
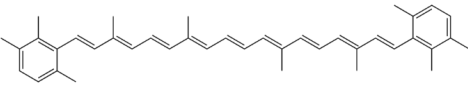
Many studies have proved the consumption of natural color pigments to have various health benefits compared to synthetic dyes. Compounds, like carotenoids and anthocyanins, exhibit great oxygen (O₂) quenching ability, antioxidant activity, free radical scavenging ability, anti-inflammatory effect, and others.²⁵⁻²⁸ Such chemo preventive activities can translate to better inhibition effects on cell mutation and cancer development. For instance, anthocyanins from different plant sources have proven to actively inhibit the growth of various cancer cells in vitro and the development of skin cancer, colon, and lung cancer in animals.²⁸⁻³⁰ Epidemiology studies in humans were also conducted with natural colorants due to these compounds' widely accepted safety and health benefits. Although most epidemiological studies did not directly link the

consumption of anthocyanin to reduced cancer risk in humans, studies suggest that anthocyanin intake may reduce certain parameters of oxidative damage.^{28,31,32,33} Similar epidemiological results were found in studies related to carotenoids, where inconsistent statements on the inhibitory effect of cancer in human bodies were observed.³⁴ Nevertheless, few studies reported that these compounds had a positive effect on inducing cancer development.

As compounds actively participate in biological activities, most natural pigments are sensitive to pH, temperature, and light.³⁵ In addition, the value of raw materials and the extraction process will inevitably increase the cost of natural colorants. Moreover, depending on the extraction process, intrinsic flavor compounds from the raw material may be carried together with target pigments, inevitably bringing unwanted flavor to the final food product. All these reasons hinder the application of natural pigments. As a result, natural colorants and spices suffer from various adulteration issues mainly due to economic considerations. Saffron, a natural colorant that produces water-soluble carotenoids, is a great example. Extraneous materials such as turmeric, calendula, and synthetic dyes have been used as adulterants to mimic saffron powders.⁸⁵

Thus, methods that can be used to either study or detect the behavior of both natural and synthetic colorants are needed for both scientific and regulatory purposes.

Table 2. Summary of major natural colorants in the USA and EU

Name	Base structure	Color	USA	EU																					
Anthocyanins	 <table border="1" data-bbox="493 680 971 865"> <thead> <tr> <th>Name</th> <th>R1</th> <th>R2</th> </tr> </thead> <tbody> <tr> <td>Delphinidin</td> <td>OH</td> <td>OH</td> </tr> <tr> <td>Petunidin</td> <td>OCH₃</td> <td>H</td> </tr> <tr> <td>Cyanidin</td> <td>OH</td> <td>H</td> </tr> <tr> <td>Pelargonidin</td> <td>H</td> <td>H</td> </tr> <tr> <td>Peonidin</td> <td>OCH₃</td> <td>H</td> </tr> <tr> <td>Malvidin</td> <td>OCH₃</td> <td>OCH</td> </tr> </tbody> </table>	Name	R1	R2	Delphinidin	OH	OH	Petunidin	OCH ₃	H	Cyanidin	OH	H	Pelargonidin	H	H	Peonidin	OCH ₃	H	Malvidin	OCH ₃	OCH	Red-blue-purple	Grape color extract, Grape skin extract, fruit juice, vegetable juice	E163
Name	R1	R2																							
Delphinidin	OH	OH																							
Petunidin	OCH ₃	H																							
Cyanidin	OH	H																							
Pelargonidin	H	H																							
Peonidin	OCH ₃	H																							
Malvidin	OCH ₃	OCH																							
Betanin		Red	Dehydrated beets	E162																					
Carotenoids		Yellow-orange-red	Annato extract, Canthaxanthin, β-Apo-8'-carotenal, β-Carotene, paprika,	E160 E161 E164																					

			<p>paprika</p> <p>oleoresin,</p> <p>saffron,</p> <p>tomato</p> <p>lycopene</p> <p>extract</p>	
Chlorophyllin		Green	<p>Sodium copper</p> <p>chlorophyllin</p>	<p>E140</p> <p>E141</p>

1.3 Current analytical methods and limitations

Target food colorants, either synthetic or natural, are subjected to extraction processes to acquire target analytes. Such practices usually include membrane filtration, solid-phase extraction (SPE), liquid-liquid extraction (LLE), and other extraction methods with the assistance of microwave or ultrasound.³⁶⁻⁴¹ The most adopted methods to determine food colorants are based on liquid chromatographic (LC) systems. Mass spectrometer (MS), ultraviolet-visible spectrometer (UV/VIS), diode-array detectors (DAD), and photodiode-array detectors (PDA) are often coupled with the LC system as signal detectors.^{10, 36, 37, 39,}

⁴² Depending on the LC system and the detector used, great resolution, as well as trace detection capabilities, can be achieved for a wide range of food colorant. However, most of these instruments require high operation and maintenance costs. In addition, such equipment needs laborious procedures for sample preparation, instrument setup, as well as dedicated laboratory conditions to operate, which limits its ability to perform any on-site detection.

Other methods exist with easier sampling and improved portability. For example, spectrophotometry is also used to quantify colorant concentrations in food due to the light absorption nature of colorant modules. Unlike HPLC or LCMS, it is one of the most cost-effective methods that do not require qualified personnel to operate. However, the simplicity of this method brings several major drawbacks, one of which is the poor specificity of visible absorption. Colorants with similar hues or shades can generate very similar spectra, making this method unsuitable for detecting mixtures.

Thin-layer chromatography (TLC) and capillary electrophoresis (CE) are economical methods with separation capabilities in food colorant studies.^{43,44} Moreover, both TLC and CE have shown great potential for rapid and onsite analysis. However, these methods struggle to provide useful data for quantitative analysis unless coupled with other techniques. For example, CE is usually coupled with UV/Vis or PDA detectors to achieve quantification capabilities.⁴⁵ Attempts have been made to use imaging data to quantify TLC patterns. However, such practice cannot provide good quantification accuracy, and the result may be compromised by color saturation problems.⁶⁷

Thus, a novel analytical technique that easily detects food colorants with great specificity and versatility would be useful. Such a method is desirable if it can detect, distinguish, and quantify colorant molecules with less tedious sample preparation protocols and faster measurement time.

1.4 Raman and surface-enhanced Raman spectroscopy

Raman scattering (inelastic) is ultimately a light-to-molecule interaction (laser excitation process), after which is observed as energy shifts of laser photons (Raman scattering emission process).⁴⁶ This technology is very useful and versatile for chemical analysis since it can generate unique molecular fingerprints for a specific molecule.

However, the Raman signal is often very weak to be effectively detected or generate useful data. Thus, an advanced Raman technique called surface-enhanced Raman spectroscopy (SERS) was applied to generate satisfactory results. SERS phenomenon occurs when the molecule is in the close vicinity or attached to nano-scale rough metal surfaces, which could greatly enhance Raman scattering up to 6 - 16 orders of magnitude.⁴⁷ Such an approach allows one to detect trace amounts of molecules or even one single molecule, making it one of the few techniques capable of reaching this analytical limit.⁴⁸⁻⁵⁰ Although many debates and studies have been conducted, there is still no concrete conclusion on the SERS mechanism.

Nevertheless, two main theories are dominant in explaining how it works, namely electromagnetic and chemical mechanisms.⁵¹⁻⁵³ It is known that surface plasmons played a

crucial role in electromagnetic theory. When incident light strikes metal nanostructures, localized surface plasmons are excited at the interface of nanostructures due to the plasmon oscillations of metal nanoparticles.⁵⁴ This process ultimately increases the density of conduction electrons in the vicinity, generating many pathways for both incident laser excitation and Raman scattering emission.⁵⁵ That is, such plasmonic metal surfaces offer many “hotspots” for nearby molecules to gain increased pathways for both excitation and emission.

Although the electromagnetic theory is widely accepted, it alone could not explain all the SERS phenomena. For example, molecules that chemically adsorbed on metal surfaces exhibited the largest signal enhancement with regard to molecules with similar Raman cross-sections. The charge transfer mechanism is believed to explain these phenomena.⁵⁶ According to this theory, depending on the energy level of involved metal and molecules, photo-induced electrons can transfer in either direction between the Fermi level of the metal locates and the highest occupied molecular orbital (HOMO) or the lowest unoccupied molecular orbital (LUMO) of the adsorbed molecule.⁵⁷ Thus, this charge transfer between metal conduction bands and the target molecules is responsible for the enhanced signal. The above two mechanisms do not usually exist alone but co-exist together to form the overall SERS signals.

Owning the advantage of high sensitivity, high specificity, and rapid detection of target molecules, SERS has advanced many applications in the field of chemistry, biology, food science, forensics, archeology, and others.⁵⁸⁻⁶² With the development of Raman

instruments, SERS can be coupled with a portable or handheld Raman spectrometer, which opens doors for rapid onsite analysis out of a lab setting.⁶³ Such performance cannot be achieved with traditional benchtop instruments, such as high-performance liquid chromatography (HPLC), gas chromatography (GC), or mass spectroscopy (MS). Moreover, SERS-imaging studies are capable of investigating a wide range of chemical systems or even directly on biological samples.⁶⁴

With all the mentioned strengths, one can execute both qualitative and quantitative analysis in SERS tests with the help of post-data processing techniques. Data processing (spike removal, baseline correction) and band assignment are usually performed prior to data analysis. For qualitative analysis, SERS is generally used to detect, identify, and classify target molecules. Multivariant analysis such as principal component analysis (PCA), partial least squares-discriminant analysis (PLS-DA), hierarchical cluster analysis (HCA), and others have been used to analyze spectroscopic data to achieve qualitative purposes.^{65,66} Multivariant analysis such as partial least square (PLS) is often adopted for quantitative work in SERS studies. Depending on the quality and characteristics of the collected SERS spectra, one peak or a group of peaks in different ranges can be loaded in the algorithm to quantify molecule concentrations.⁶⁷

1.5 Applications of Raman or SERS on food colorant analysis

Many studies have been conducted to determine, classify, and quantify food colorants or banned food colorants in food matrices. For example, Gukowsky et al. (2018)

established a SERS spectra database with 16 synthetic and natural food colorants, each of which was demonstrated with its characteristic SERS peaks. In addition, chemometric studies were also performed to successfully differentiate similar hue colorants using PCA analysis based on the characteristic SERS spectrum of each colorant. Besides qualitative analysis, his group successfully executed a quantitative test achieving a LOD of 5.9 ppm in Patent Blue V solution (a banned colorant in the U.S.). This work demonstrated that the SERS technique is suitable for detecting a wide range of food colorants with easy sample preparation and testing versatilities.¹⁹ In addition, table X summarizes the relevant research on the detection of food or prohibited colorants using SERS techniques.

Based on the substrate used, SERS methods for colorant analysis can be divided into two categories: solution-based and solid-substrate-based methods (Table 3). The solution-based method usually requires less sample preparation and SERS substrate preparation. Silver or gold nano structures are directly used as SERS substrates to amplify the target molecule's Raman signal. These nanostructures are usually chemically reduced from hydrogen tetrachloroaurate (HAuCl_4) or silver nitrite (AgNO_3) solution with various modifications.^{19,68,69} In addition, other fabrication steps and chemicals might be used to manipulate specific nanostructures, such as gold nano-dumbbells and silver nano flower flakes based on silver or gold seeds.^{5,68} Synthesized gold or silver nanoparticle solution is directly incubated with the sample solution, where interactions between nanoparticles and colorants take place either chemically or physically based on their chemical characteristics and surface charges.⁶⁸ The mixture is then pipetted and dried on a flat substrate, such as a

gold-coated slide or silicon wafer, prior to SERS analysis.^{5,19} Such practice will generate a distinct “coffee ring” of concentrated nanoparticles and target analytes, which results in an increased SERS signal due to higher concentrations of both substances.¹⁹

For different detection purposes, such as specific binding specific molecules or separating samples, solid substrate-based methods are developed with a broad range of substrate fabrication and modification. Such approaches are believed to be more sophisticated and more versatile in comparison to solution-based methods. SERS substrates can be developed into wide different varieties on different substrates owning specific characteristics and functions. For example, gold nanoparticles were grown on a synthesized metal-organic framework with an octahedral crystal structure in a recent study to detect food colorants.⁷⁰ The fabricated SERS platform formed porous network structures with the advantages of significant increases in surface area, which offers great conditions for nanoparticle-molecule interaction. As a result, the SERS substrate achieved higher R^2 and lower limit of detection (LOD) in two food colorants solutions (new cocine and orange II) in comparison to using gold nanoparticles alone. A similar approach was carried out using graphene/silver nanoparticle composite as SERS substrate for prohibited colorant detection.⁷¹ The SERS substrate was prepared by forming silver nanoparticles within the graphene structure during several chemical reduction steps. The substrate utilizes its plate-like structure to capture and form strong interactions with benzene rings, which are present in most food colorants. The result of this study confirmed the great detection power of the

newly fabricated SERS substrate with LODs as low as 10 μ M for all tested colorants (Amaranth, Erythrosine, Lemon yellow, and Sunset yellow).⁷¹

In addition to chemically synthesized SERS substrates, the oblique angle deposition (OAD) technique has been adopted in the fabrication of SERS substrates with recognized stability and efficacy. Metallic nanostructures can be fabricated and deposited on various surfaces. Glass slides or thin-layer chromatography (TLC) chips are ideal stationary substrates for nanostructure disposition using an e-beam deposition system.^{72,73} Thus, the detection performance can be further expanded depending on the characteristics of the base substrate. For example, OAD fabricated SERS-TLC chips are able to achieve good molecule LODs down to 10^{-6} M while having the ability to separate different analytes in a complex matrix.⁷³ However, one should be noted that the previously described approaches for SERS substrate fabrication usually require dedicated conditions and several specific instruments to complete.

Thus, other approaches with easier fabrication methods are emerging with good colorant detecting capabilities.^{69,74,75} Commercially available materials like filter paper and TLC chips are easy-accessible substrates for colorant detection. In brief, filter papers were incubated with nanoparticle colloid solution. The porous structure of cellulose fibers creates many tunnels and spots to absorb metallic nanoparticles. The nanoparticle-saturated filter paper can be later used as a SERS substrate on which sample solution is directly dropped or as a SERS wiper that wipes different sample surfaces after wetting.^{69,74} A simpler SERS-TLC approach was executed in which gold nanoparticle colloid solution was

directly dropped on developed TLC chips. SERS signal was later collected afterward. Despite the simplicity of these methods, they still achieved great colorant detection capabilities ranging from 1-6 ppm or 10-100 μM for selected colorants.

Table 3. Summary of Raman or SERS analytical approaches of food colorants in recent publications.

Target Colorant	Matrix	Sample pretreatment	Raman/SERS method	LOD/LOQ	Ref.
Sunset yellow, Lemon yellow, Orange II, Chrysoidin	Orange juice, Coke	Sample solution incubated with SERS substrate	Gold nanodumbbells as SERS substrate 785 nm Laser source from a portable Raman spectrometer.	LOD in orange Juice: Sunset yellow (50 ppm), lemon yellow (50 ppm), orange II (10 ppm), chrysoidin (10 ppm). LOD in coke: Sunset yellow (100 ppm), lemon yellow (100 ppm), orange II (10 ppm), chrysoidin (10 ppm).	68
Allura Red	Candy	Sample dissolved in solution, supernatant collected for analysis	OAD-fabricated silver nanorod on a glass slide using a custom E-Beam deposition system. The prepared chips were used as SERS substrates.	LOD: 0.05 ppm.	72
Food blue, Tartrazine, Sunset yellow, Acid red	Colorant solutions	Sample solution dropped and dried on SERS substrate	Flower-shaped silver nanostructures absorbed on Si wafer as SERS substrate 785 nm laser source.	LOD in water: Food blue (79.3 ppb), Tartrazine (5.3 ppb), Sunset yellow (45.2 ppb), Acid red (50.2 ppb).	5

New Coccine, Orange II	Colorant solutions	Sample solution incubated with SERS substrate	UiO-66(NH ₂)@Au as SERS substrate 633 nm laser source.	LOD in water: New Coccine (401.5 ppb), Orange II (54.6 ppb).	70
Amaranth, Erythrosine, Lemon yellow, Sunset yellow	Colorant solutions	Sample solution incubated with SERS substrate	Graphene and silver composite as SERS substrate 514.5 nm laser source.	LOD in water: Amaranth (10 μM), Erythrosine (0.1 μM), Lemon yellow (10 μM), Sunset yellow (10 μM).	71
Sunset yellow, Lemon yellow	Colorant solutions, Grape juice, Orange juice	Sample dissolved in DI water, then incubated with filter paper	Silver nanoparticle-based filter paper with polyelectrolytes as SERS substrate	LOD in water: Sunset yellow (10 μM), Lemon yellow (10 μM). LOD in both juice: Sunset yellow (100 μM), Lemon yellow (100 μM).	74
Rhodamine 6G, methylene blue, malachite green, crystal violet, Rhodamine B, bromophenol blue, erythrosine B sodium salt, crocein scarlet 3B, Auramine O	Traditional Chinese medicine herbs	Emerging herbs in dyes solution followed by drying. Wetting the dyed herb followed by wiping with SERS substrate.	Homemade silver nanoparticle-based wipers	LOD: 6 ppm or lower for all nine dyes.	69
Sudan I	Paprika powder	Sample solution dropped on TLC chips followed by AuNPs solution	Homemade thin-layer chromatography (TLC) chips, and homemade gold nanoparticles, 785 nm laser source	LOD: 1 ppm in spiked solution.	75

Methyl Orange (MO), Cresol Red (CR), Rhodamine 6G (R6G), Methylene violet 2B (MV)	Colorant Solutions	Sample solution developed on SERS-TLC chips	OAD-fabricated silver nanorod on TLC chips as SERS substrate	LOD in water: R6G (10^{-6} M) CR (10^{-5} M) MO (10^{-5} M) MV (10^{-5} M)	73
---	--------------------	---	--	--	----

1.6 Limitations and perspectives

In comparison to conventional techniques such as HPLC and GC, Raman spectroscopy of SERS offers a versatile and portable option for fast and sensitive detection of food colorants or prohibited colorants. Although the development of SERS substrates with targeted specificity and function has improved the reliability of this technique, there is still room for improvement. For instance, most current research focuses on improving the detecting capabilities of banned food colorants. In these studies, pure colorant solution or spiked solution with few components were used as analytes. However, little research has been done to study the interaction between food colorant and food components using Raman or SERS as a molecular fingerprinting tool. Such phenomenon is due to the limited capability for multi-analyte ($N > 5$) detection of Raman or SERS technique.⁷⁶ Although functional substrates can be used, as they can provide different degrees of separation capability, Raman or SERS methods are still considered as complimentary alternatives to chromatography methods, such as LC or GC-based techniques.

Attempts to combine SERS (or Raman) with other existing techniques, such as infrared spectroscopy (IR), and X-ray fluorescence spectroscopy (XRF), are promising toward overcoming their individual limitations.⁷⁷ In addition, an expanded research area of

SERS (or Raman) has been made possible by the integration of different techniques, enabling it to gain deeper research capabilities, such as chemical mechanism or real-time degradation studies at a molecular level. The previously described utilization of SERS-TLC substrate is a good example to demonstrate the benefit of SERS integration practice. In another example, UV-vis, Raman, and ¹H NMR were jointly used to determine characteristic compounds from the stigmata of *Crocus sativus* L, which is a natural spice and colorant. By integrating multiple techniques together, the 13-cis-digentiobiosyl crocetin and its all-trans isomer were detected and identified via UV-vis and Raman, respectively.⁷⁸ It was concluded that the integration offered a much more complete diagnostic molecular fingerprinting of samples. Such a statement was verified in another study where adulterated turmeric was tested via IR and Raman.⁷⁹ Instead of using Raman spectroscopy alone, the combination of the two techniques successfully discriminated and quantified adulterated turmeric samples with improved correlation coefficients of 0.97 and 0.95 for Sudan red and white turmeric adulterants, respectively.

Integrating multivariate chemometrics, machine learning, or data fusion with SERS is another promising way to achieve excellent predictive accuracies in complex matrices.⁸⁰ For example, the use of PCA, artificial neural networks (ANN), support vector regression (SVR), and PLS algorithms were reported in recent food colorant studies trying to improve quantification accuracies of prohibited Sudan red or other common food colorants.^{5,19,81} Cheung et al. (2010) had implemented ANN in an in-house program using collected SERS data to quantify Sudan-1 colorant. The result indicated that the ANN algorithm achieved a

smaller root-mean-square error of cross-validation value (RMSEV=0.123) and a better predictive squared correlation coefficient ($Q^2=0.977$) in comparison to common linear regression models (PLSR, RMSECV=0.084, $Q^2=0.916$). Despite the fact that few exposures have been found in food color analysis, Raman-involved data fusion applications are more widely accepted in forensic science and archaeology in determining writing inks and aging paintings. For example, a forensic study used the marriage between Raman and laser-induced breakdown spectroscopy (LIBS) to identify different writing inks. The collected Raman and LIBS spectra were fused into a single data matrix that provided information on two complementary aspects, namely, molecular and elemental composition. The result indicated the fused data block exhibited superior ink classification performances than those with individual data sets.⁸²

1.7 Conclusion

The previous sections have briefly reviewed current SERS applications in food colorant detection and quantification. Compared to golden analytical methods (HPLC, LC/GCMS), SERS holds significant potential for analyzing food colorant samples owing to the advantages of great versatility, specificity, and sensitivity. In addition, with the development of minimized Raman devices, SERS substrates, and post-data processing techniques, SERS (or Raman) shines in many aspects that conventional methods are not capable of doing, such as *in situ* detection, on-field analysis as well as great compatibility with other techniques.

CHAPTER 2

**RAPID DETERMINATION OF SAFFRON GRADE AND ADULTERATION BY
THIN-LAYER CHROMATOGRAPHY COUPLED WITH RAMAN
SPECTROSCOPY**

2.1 Abstract

Saffron, one of the most expensive spices around the world, is highly vulnerable to economic adulteration in its powder form. Plant materials and artificial colorants are commonly used as adulterants to reduce saffron concentration as well as maintain color strength in powdered saffron products. However, current analytical methods lack the ability to test samples accurately onsite. Therefore, the objective of this study is to develop a fast screening and quantification method combining thin-layer chromatography (TLC) and Raman spectroscopy for saffron powder analysis, including quantifying the main colorant crocin content and identifying possible adulterants out of a lab setting. A droplet of aqueous extract of saffron powder was deposited on a TLC plate, exhibiting a uniform yellow round pattern on the TLC plate. The content of crocin was analyzed using the ISO 3632 method and Raman spectroscopy separately. A quantitative model based on Raman spectra was established and validated using partial least square (PLS) with R^2 of 0.9955 and 0.9929 for calibration and validation of the PLS plot. Possible adulterants such as powders of safflower, turmeric powder, red 40 (Allura red), and yellow 5 (tartrazine) were mixed with saffron powder at various degrees. Their water extracts exhibited unique patterns under bright ambient light and UV light that can be discriminated from that of pure saffron

samples through visual observation and principal component analysis (PCA) based on the $L^*a^*b^*$ values. We also estimated the lowest adulteration degrees that can be detected were 2.59% for Allura red, 4.15% for tartrazine, 31.01% for safflower, and 41.98% for turmeric, respectively, using the PLS analysis. Further identification was evaluated using Raman spectroscopy, which provided fingerprint spectra for all adulterants except safflower. Combining TCL pattern and Raman spectroscopy, samples with identical optical properties to pure saffron but adulterated with multiple adulterants were analyzed and successfully detected. This study demonstrates the potential practical application of this method is the rapid analysis of saffron quality and adulteration.

2.2 Introduction

Saffron, the dried stigmas from the flower of *Crocus sativus* L., is known as a high-valued spice as well as a natural colorant. Due to the limited production amount and the tremendous labor to collect the flower stigmas by hand, saffron is listed as one of the most expensive agricultural products in the world. Each flower will produce approximately 6mg of saffron stigma; thus, approximately 150,000 - 160,000 flowers are used to produce 1 kg of saffron spice.^{83,84} The flower is mainly cultivated in Iran, India, Greece, and Spain. China, Turkey, and Azerbaijan also produce saffron with lower production.⁸⁵ The quality of saffron is affected by various factors, such as cultivation regions, climate, drying process, and storage conditions.^{85,86}

Saffron is mainly used as a flavoring and coloring agent in food, cosmetics, or perfume.⁸⁶ It is also used in many traditional medical practices due to its antioxidant activities,^{87,88} and anticarcinogenic properties.^{89,90} However, the high value of this product makes it very susceptible to economic adulterations. Particularly, the saffron powder is more vulnerable to adulteration since the characteristic appearance of the flower stigma is destroyed. Various adulteration methods are used to obtain the maximum profit with inexpensive saffron substitutes, such as mixing extraneous plant materials and adjusting the appearance of saffron with natural or artificial colorants.⁸⁵

Quality attributes of saffron products are mainly determined by the concentration of three constituents, namely crocin, picrocrocin, and safranal.^{84,85,91} These three compounds are responsible for the color expression, bitter taste, and unique aroma, respectively. The color strength of saffron is considered the major parameter in the trade market.⁹¹ The current ISO-3632/TS method is used to determine commercial saffron color strength, which is divided into three categories based on physical observation and chemical analysis by UV-vis spectroscopy (ISO 3632-1 2011; ISO 3632-2 2010).^{101,102} The absorbance of 1% saffron extract at 440 nm in a 1 cm quartz cell ($E_{1cm}^{1\%} 440\text{ nm}$) categorizes saffron specimens to category I ($E_{1cm}^{1\%} 440\text{ nm} > 200$), category II ($200 > E_{1cm}^{1\%} 440\text{ nm} > 170$), and category III ($170 > E_{1cm}^{1\%} 440\text{ nm} > 120$) (ISO 3632-1 2011).¹⁰¹ However, it was reported that the current ISO 3632-2 method is not able to detect saffron adulterants (safflower, marigold, and turmeric) up to 20% w/w.⁹² Moreover, this method is very

vulnerable to any natural or artificial colorant that produces yellow color, which increases the $E_{1cm}^{1\%} 440\text{ nm}$ value, resulting in a false reading.

To overcome this problem, thin layer chromatography (TLC) and high-performance liquid chromatography (HPLC) are applied to identify adulterants or specimen composition. Despite the great sensitivity and accuracy provided by the HPLC, it requires complicated sample preparation, well-trained operators, and high maintenance costs. Moreover, the bulk size of HPLC instruments makes it impossible to operate any onsite analysis. Hence, for food producers and companies, such an analytical method is not sustainable for routine measurement to monitor saffron quality during harvesting or production.

The objective of this study is to develop a rapid and facile approach that can be used to determine the crocin concentration for quality analysis and possible adulterants of saffron powders out of a lab setting. This approach combined thin layer chromatography and Raman spectroscopy. Thin-layer chromatography is widely implemented in the food industry as a convenient and low-cost approach for separating different chemical components, such as adulterants and contaminations.⁹³ However, traditional TLC techniques are usually time-consuming and challenging to perform quantitative analysis on the plate.⁹⁴ Herein, a modified TLC method was developed to reduce the sample preparation time and accommodate quantification measurement conducted by Raman spectroscopy. Optical images of pure and adulterated samples under both the bright and UV lights were captured via a digital camera and processed to L* a* b* data for further

evaluation using chemometrics. Then the TLC plate was analyzed by Raman spectroscopy for quantification measurement.

Raman spectroscopy measures molecular vibrations based on the inelastically scattered light from the target analyte. This technique allows for molecular fingerprinting as well as investigating the molecular structural changes in the target analyte in a rapid and non-destructive way.⁹⁵ The availability of a portable Raman instrument facilitates the potential onsite analysis. Compared to Infrared (IR) spectroscopy, Raman spectroscopy has been underexplored for food quality and authenticity analysis due to fluorescence interference. However, for the saffron analysis, Raman spectroscopy was reported to be more sensitive to crocin compounds than the IR methods,^{85,96} since the in-phase vibration of the conjugated double bonds in crocin is more Raman active.⁹⁷ Various chemometric models were built based on spectroscopic data (Infrared, Raman, laser-induced breakdown spectroscopy) to determine saffron quality as well as adulteration level;^{96,98,99,100} however, most of these researches did not focus on the exploration of the on-site capability for method development.

However, both methods struggle to work under an out-of-lab testing condition when used alone. TLC imaging is versatile in generating visual results with simple preparation procedures. But it fails to quantify saffron grade accurately with its color information. The variation of different lighting conditions from different testing cite may further contribute to inaccurate results. As mentioned before, Raman spectroscopy shows the potential to determine saffron quality as well as to detect potential adulterants in various

research.^{96,98,99,100} However, it cannot deliver a fast and intuitive result on-site as compared to the TLC method. Furthermore, it struggles to detect artificial adulterants with very low adulteration levels. The strong signal from crocin could easily cover any adulterant signals. Although it is possible to utilize tools like partial least square (PLS) and principal component analysis (PCA) to extract minor differences within spectra, it requires more time and calibrations to make the model work properly.

We could gain the advantage of both methods when they are combined and utilized in one method. As a separation method, TLC could be used to rapidly screen potential adulterants. In the meantime, it would also separate crocin and the potential adulterant within the same sample, making it easier for Raman spectroscopy to quantify crocin levels without the interference of potential adulterants. The separation process is also repeatable, meaning the adulterants could be concentrated if more sample drops are repeatedly dropped on the same spot. This approach could help gain a much more distinct TLC pattern as well as increase potential adulterants' Raman signals, which may be at a lower adulterant level.

As we mentioned before, similar research was conducted to determine saffron quality or adulteration.^{96,98,99,100} However, most studies adopted a sophisticated in-lab-setting to generate the result. Their accuracy and reliability may be affected when implementing the method out of a lab setting. In this study, we combined TLC for visual screening followed by Raman spectroscopy which directly measures the Raman signal of saffron water extracts on a TLC plate using a portable Raman instrument. Chemometrics models were established for quantifying crocin concentration as well as for identifying possible adulterants. The

combination of a low-cost TLC plate and a portable Raman instrument offers a potential solution to rapidly analyze the quality and authenticity of saffron powders out of a lab setting.

2.3 Materials and methods

2.3.1 Chemicals, reagents, and plant materials

HPLC grade ethanol was purchased from Decon laboratories, Inc. (King of Prussia, PA, USA). Saffron, turmeric powder, and safflower specimens were purchased from online sources. Each plant material was obtained from three different suppliers. Each artificial colorant (Allura red and tartrazine) was purchased from two suppliers, namely IFC solutions (Linden, NJ, USA) and Sigma Aldrich (Merk KGaA, Darmstadt, Germany). TLC aluminum plates (Silicagel 60W F254S) were purchased from EMD Millipore Corporation (Billerica, MA, USA).

2.3.2 Preparation of pure saffron and adulterated saffron powder samples

All specimens were subjected to size reduction. One gram of each plant material was pulverized by a Newtry high-speed food mill (Guangdong, China) at high speed for three minutes. A 500 μm mesh sieve was later used to uniform the particle size of all specimens. Prepared powder was transferred in a glass vial and stored in a desiccator. To help better evaluate the method, spiked samples are adopted in this study since they provide a wider range of adulteration than real samples. Furthermore, the differences in saffron crocin content due to different origins may disrupt the assessment of this method. Spiked samples

for calibration were prepared by mixing adulterants (safflower and turmeric) with pure saffron by weight percentages up to 100% (0, 20, 40, 60, 80, and 100%) on an analytical scale with a 0.0001g resolution. Artificial colorants are not used to replace saffron weight but instead adjust appearance and color expression. Therefore, synthetic dyes (tartrazine yellow and Allura red) were mixed with pure saffron powder with a lower weight percentage of 0, 2, 4, 6, 8, and 10% w/w compared to extraneous plant materials. After preparing all calibration standards, validation samples were prepared by mixing various amounts of plant adulterations as well as artificial colorants with saffron. Three validation samples were prepared, namely, sample 1 (no adulterants); sample 2 (49.4% safflower adulteration, 0.75% red 40 adulteration, w/w) and sample 3 (56.1% turmeric adulteration, 25.7% yellow 5 adulteration, w/w). The formula was created to generate similar color appearances when all samples were prepared as an aqueous solution with the same concentration (w/v).

2.3.3 Sample preparation for imaging analysis and TLC-Raman

Prior to analysis, TLC plates were cut to a dimension of 2.5×1 square inch, and the plate was then attached to a glass slide substrate to produce a flat surface. For each powdered specimen, a stock solution was prepared by extracting 50 mg of powdered samples with 50 mL of deionized water in the dark and agitated for 30 minutes, then filtered through a 0.45 μm PES filter (GE Lifesciences, Marlborough, MA, USA).

Three drops of 2 μL stock solution of each sample were dropped on the same spot on the TLC plate for further analysis. Each solution droplet would not be applied to the same

spot until the previous one had fully dried. After the final droplet, the dropping spot was dried under constant airflow for 5 minutes in order to remove any residual moisture within the silica gel.

2.3.4 Determination of the crocin color strength using the standard ISO method

The stock solution was then diluted according to the specification of ISO 3632-2. The color strength of water extracts at different concentrations was analyzed according to the specifications provided by ISO 3632-2:2010. Moisture and volatile content (W_{MV}) of the specimen powder were measured by an A&D MX-50 moisture analyzer (A&D Company, Tokyo, Japan), which was later used in the following equation. Sample water extracts were measured with a SpectraMax M2 spectrometer (Sunnyvale, CA, USA) at 440 nm. The color strength of each specimen was calculated by the following equation:

$$E_{1cm}^{1\%} 440 \text{ nm} = \frac{A \times 10000}{m(100 - W_{MV})}$$

where A is the sample absorbance at 440 nm, m is the weight of specimen expressed in grams, and W_{MV} is the moisture and volatile content measured previously. Each specimen was measured with three replicates.

2.3.5 Raman reference spectrum analysis of saffron and saffron adulterants

To collect the standard Raman spectrum of pure saffron and pure adulterant, 50mg of each powdered specimen was extracted via 50 mL 80% ethyl solution. All extracts were agitated for 30 minutes in dark and then filtered through 0.45 μm PES filters. Pure saffron and each adulterant ethyl extract were then dropped and dried on TLC plates before the standard spectra were collected at the coffee ring of the droplet by a DXR2xi Raman

imaging microscope (Thermo Fisher Scientific, Madison, WI, USA) equipped with a 780 nm laser source. For each coffee ring, 15 spectra were randomly measured with the spectral range of 200-2000 cm^{-1} . Each spectrum is an average of three independent measurements with an acquisition of 2 seconds under 2 mW laser power. Each sample was measured with triplicates.

2.3.6 Analysis of pure and spiked saffron samples using the TLC-Raman and TLC imaging method

Prepared pure and spiked saffron aqueous extracts with different concentrations were dried on TLC plates, and the center region of TLC patterns was analyzed by a portable Raman system (TSI Incorporated, Shoreview, MN, USA) equipped with a 532 nm laser source. Five sample points will be randomly measured on each droplet spot with an acquisition time of 10 s, max power. Each sample solution was measured with triplicates.

A digital camera (Fujifilm XH-1, Fujifilm) with a 35 mm lens was used to collect sample TLC pattern images. For ambient light images, the camera was mounted on a tripod with the focus distance fixed under consistent ambient light conditions. For UV light images, all ambient light was blocked, and a portable UV lamp (365 nm, Analytikjena, Upland, CA, USA) was installed at a fixed position to provide consistent illumination. All images were acquired with the following exposure settings: shutter speed 1/8 s, f stop 8.0, and ISO number 800.

All raw camera files (Fujifilm RAF files) were processed in Adobe Photoshop CC (version 20.0.4) to produce fused ambient and UV TLC pattern pictures (Fig. 3). A digital

color meter (Version 5.15, Apple Inc) was then used to translate color images to L*a*b* color space data. For each fused TLC pattern, four data regions (ambient inner circle, ambient ring, UV inner circle, and UV ring) were collected and translated into L*a*b* data. At each data region, five data points were randomly collected with three replicates.

2.3.7 Statistical analysis

Multivariate analysis was used for quantitative and qualitative analysis. The L*a*b* value of TLC patterns was translated to spectrum data using Microsoft Excel (Version 1911). All spectral data were first collected and preprocessed via OMNIC for Dispersive Raman 9.7.46 (Thermo Fisher Scientific) for baseline correction. Then, pathlength correction was processed with TQ Analyst 9.7.0.27 (Thermo Fisher Scientific) via a standard normal variate (SNV) filter with a spectral range between 889.9 cm⁻¹ and 952.7 cm⁻¹ for PLS or PCA calibration. The path length correction was computed in this manner because the spectral range between 889.9 cm⁻¹ and 952.7 cm⁻¹ is related to the distinct TLC Raman background. For determining the color strength, two partial least squares (PLS) regression models were established based on the L*a*b* and Raman data using the E₁cm^{^(1%)} 440 nm as the reference values, respectively. A total of 120 Raman spectra were collected to construct the regression model. Spectral regions 1581.42 - 1489.42 cm⁻¹ and 1313.37 - 1134.02 cm⁻¹ were selected for the calibration model to improve accuracy. Leave-One-Out cross-validation was performed to validate the calibration. The accuracy of the developed model was assessed by the correlation coefficient of the calibration, RMSEC, and RMSECV values. For identification of the adulterations, the different TLC

patterns and Raman spectra of pure and adulterated samples were analyzed using principal components analysis (PCA). PLS calibrations were also established to evaluate the sensitivity of the $L^*a^*b^*$ values to determine the degree of each adulteration. The Limit of detection (LOD) and the limit of quantification (LOQ) is calculated based on $3\sigma/S$ and $10\sigma/S$, where σ is the noise standard deviation and S is the slope of the calibration.

2.4 Results and discussion

2.4.1 Reference saffron sample analysis using the ISO and Raman spectroscopic methods

Reference saffron samples were obtained from three suppliers, and their crocin concentrations were analyzed using the ISO and Raman spectroscopic methods. According to ISO-3632-1, saffron1, 2, and 3 were recognized as category I with average ratings of 223, 217.9, and 214.3, respectively. As shown in Fig S1, all three saffron samples produced identical Raman patterns but different intensities. The intensity values obtained from samples 2 and 3 were lower than the intensity from sample 1. The result from Raman spectrum intensity also agreed with the result from the ISO-3632 method. This indicates a good correlation between the two methods since both results are affected by the crocin concentration presented in the pure specimen extract. The Raman characteristic peaks (Fig 2a and Fig S1) are produced from the crocin molecule, where the peak at 1543 cm^{-1} corresponds to conjugated C=C stretching.^{91,96,99,100} The peak at 1170 cm^{-1} is assigned to C-C stretching vibrations of the molecule skeleton.^{91,99} The medium peaks at 1285 cm^{-1}

and 1213 cm^{-1} are due to CH deformation and C-C stretching and C-H in-plane bending modes, respectively.^{91,103} The in-plane rocking of -CH₃ mode is reflected by the peak at 1025 cm^{-1} .^{91,99} In general, the Raman pattern of the present study is in good agreement with other groups' results.^{91,96,99,100} Based on these results, saffron sample 1 was used for further sample preparation for the establishment of chemometrics models for quality and adulteration analysis.

2.4.2 Establishment of two PLS calibrations for quantifying the saffron color strength based on L*a*b* values and Raman spectra, respectively

Saffron sample 1 was used to prepare the dilutions for establishing PLS calibrations. As shown in Fig. 1, with the increase of saffron extracts concentration, the color of extracts solutions turned from bright yellow to orange. When applied on a TLC plate, saffron extracts generated a uniform yellow circle with no significant coffee ring pattern under the bright light nor fluorescence pattern under the UV light (Fig. 1b). PLS calibrations were built based on the L*a*b* values against the absorbances of the ISO method. The correlation coefficient for calibration and cross-validation were 0.9805 and 0.9629, respectively. The RMSEC and RMSECV value of the calibration were 14.4 and 20.2, respectively. The R² value was 0.9272, which indicates a very good prediction of the regression (Fig. 1c). The LOQ of this method was calculated as 38.6, which is well under the limit of category III (120) based on ISO 3632-1 (2011).¹⁰¹

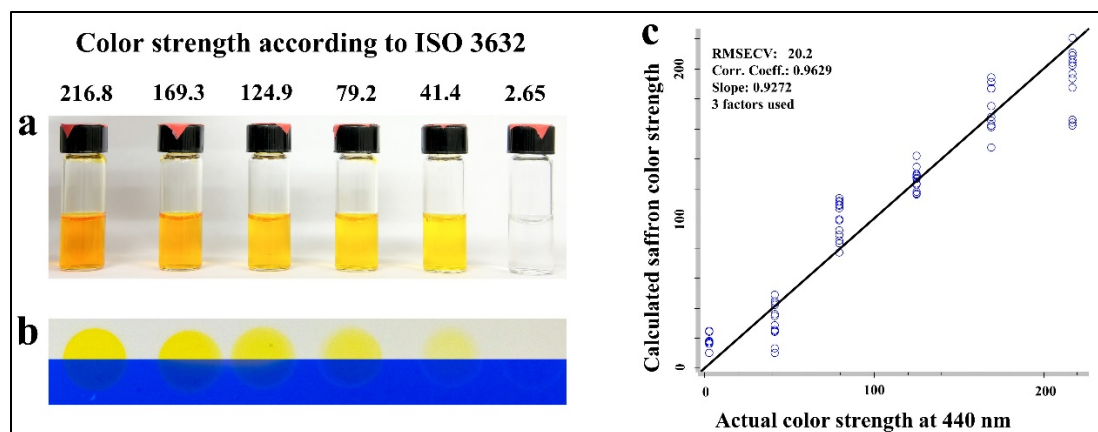


Figure 1. Physical observation of pure saffron extract (a) and its TLC pattern (b) under different lighting conditions (ambient light on the top half, 365nm UV light on the bottom half); c. Predict vs. actual color strength PLS plots for saffron specimens using L*a*b* data.

The Raman spectra of saffron specimens of various concentrations are shown in Fig.

2. The PLS calibrations were established based on the Raman spectrum intensity (spectral range from 1581.42 - 1489.42 cm^{-1} and 1313.37 - 1134.02 cm^{-1}) against the ISO values. The correlation coefficient for calibration and cross-validation are 0.9955 and 0.9929. The RMSEC and RMSECV value are 10.2 and 13.0, respectively. The R^2 value was 0.9858, which indicates a very good prediction of the regression (Fig. 2b). The LOQ is calculated as 64.14, which is also well under the limit of category III (120) based on ISO 3632-1 (2011).¹⁰¹

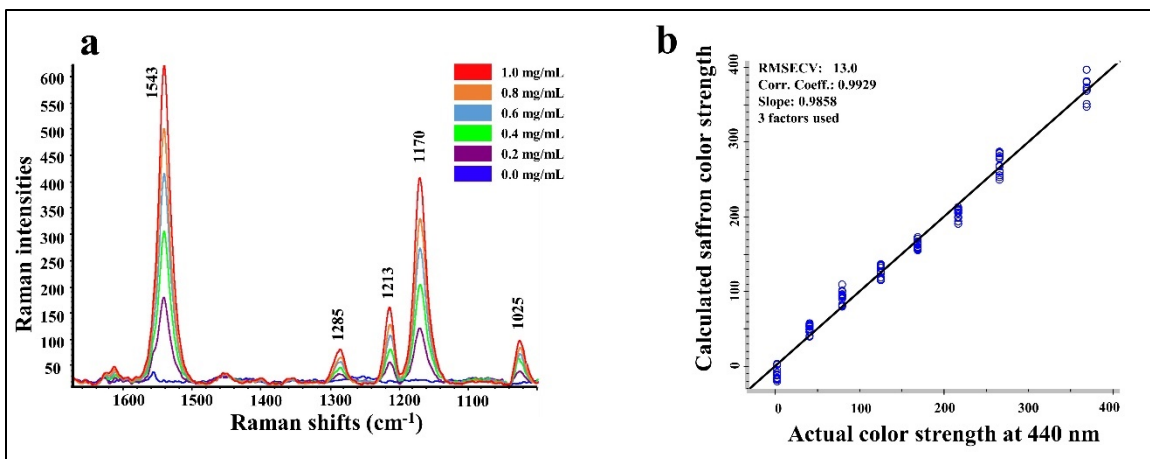


Figure 2. a. Raman Spectrum of pure saffron extract measured on TLC plate; b. Predict vs. actual color strength PLS plots for saffron specimens using Raman spectrum data. Both calibrations showed the potential to quantify saffron color strength.

The correlation between the Raman spectroscopic method and the ISO method was better than the L*a*b* method and the ISO method, although the LOQ L*a*b* method was lower than that of the Raman spectroscopic method. In addition, although the L*a*b* method was relatively easy and cost-friendly, this method was heavily dependent on lighting conditions, which is hard to control without a proper lighting setup. On the other hand, TLC-Raman could perform the measurement without ambient illumination, making it more consistent across different testing conditions.

2.4.3 Identification of saffron adulterants based on TLC pattern

Premium saffron and various adulterants were analyzed under two lighting conditions, namely ambient and UV light (Fig. 3). Visually, we could see premium saffron generated a uniform colored circle in both ambient and UV light, whereas safflower and turmeric formed a unique fluorescence ring and inner fluorescence circle, respectively. Tartrazine and Allura red were not mainly used to replace saffron weight; therefore, a lower

adulteration concentration was used. When incorporated in saffron, tartrazine generated a dark ring under UV light, and Allura red formed a distinct colored ring in both ambient and UV illumination. The characteristic of the described adulterant pattern became more prominent with the increase in adulteration level. The phenomenon of different TLC patterns could be explained due to the difference in photochemical and polarity of active components among the tested samples.

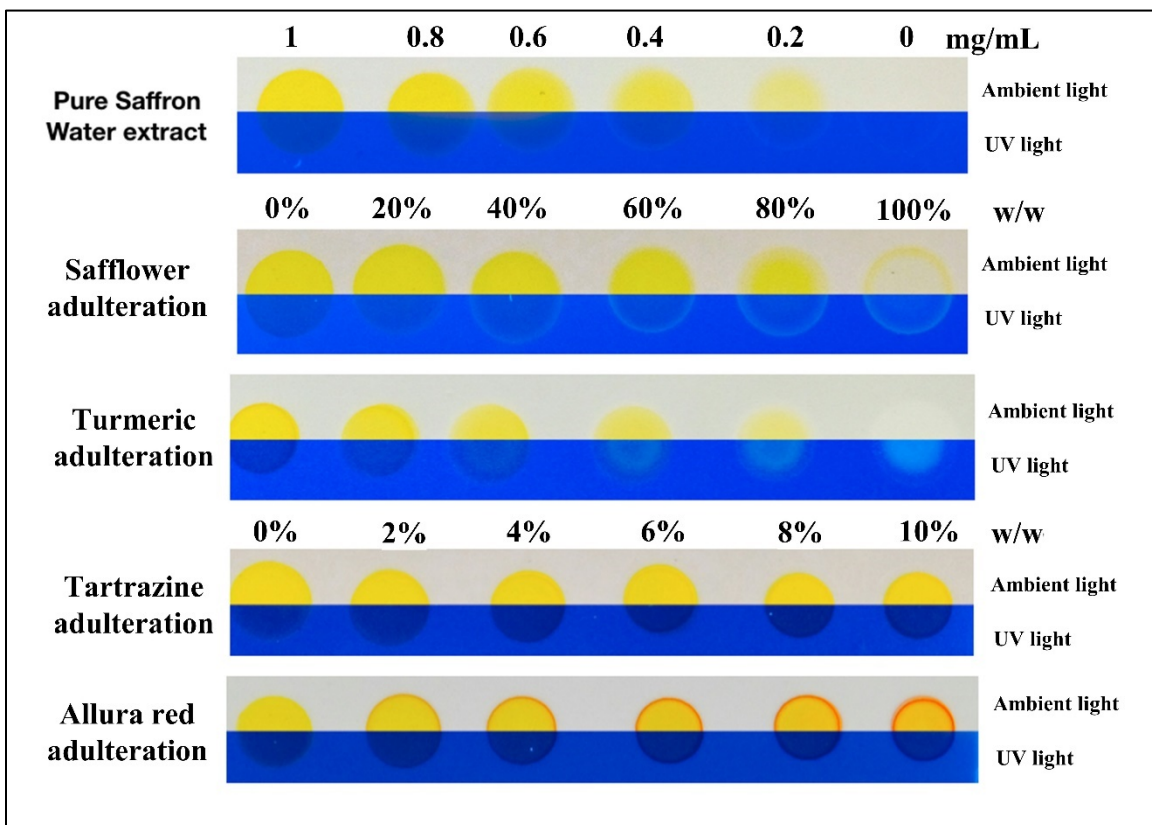


Figure 3. TLC pattern of pure saffron and spiked saffron with different adulteration levels (ambient light on the top half, 365nm UV light on the bottom half).

In addition to visual observation, we used PCA to analyze the variation between these samples. As seen in Fig. 4a, pure saffron and each adulterant were separated well in the PCA plot, demonstrating their inherent variation between these samples with a total

variation of 77.78% by three principal components. The sensitivity of the TLC method for individual adulterants was analyzed by calculating the LOD from each PLS plot (Fig. 4 b, c, d, and e). The result is shown as follows: Allura red (2.59%), tartrazine (4.15%), safflower (31.01%), and turmeric (41.98%). Based on RMSECV, R^2 value, and the correlation coefficient value for cross-validation, all three adulterants (Allura red, safflower, and turmeric) except for tartrazine show a good correlation ($R^2 > 0.8$) between the actual and calculated adulteration level. With a correlation coefficient (cross-validation) of 0.4636 and an R^2 value of 0.2149, it is challenging to identify tartrazine incorporation levels based on TLC images data (Fig. 4 b, c, d, and e). The yellow coffee ring of tartrazine was difficult to distinguish and specifically hard to quantify color intensity under white ambient light since the color became saturated on top of the yellow background of saffron (Fig. 3). The same phenomenon also occurred in safflower adulteration imaging under white ambient light, where the yellow background from saffron covers the yellow coffee ring from safflower. This is less of a problem for safflower since its coffee ring also generates fluorescence signals under UV light. The results demonstrated the feasibility of visually screening possible adulterants, particularly the artificial colorants, which were more sensitive than the natural colorants. The quantification remains a challenge for tartrazine, although accurate quantification is not a necessity as a screening method.

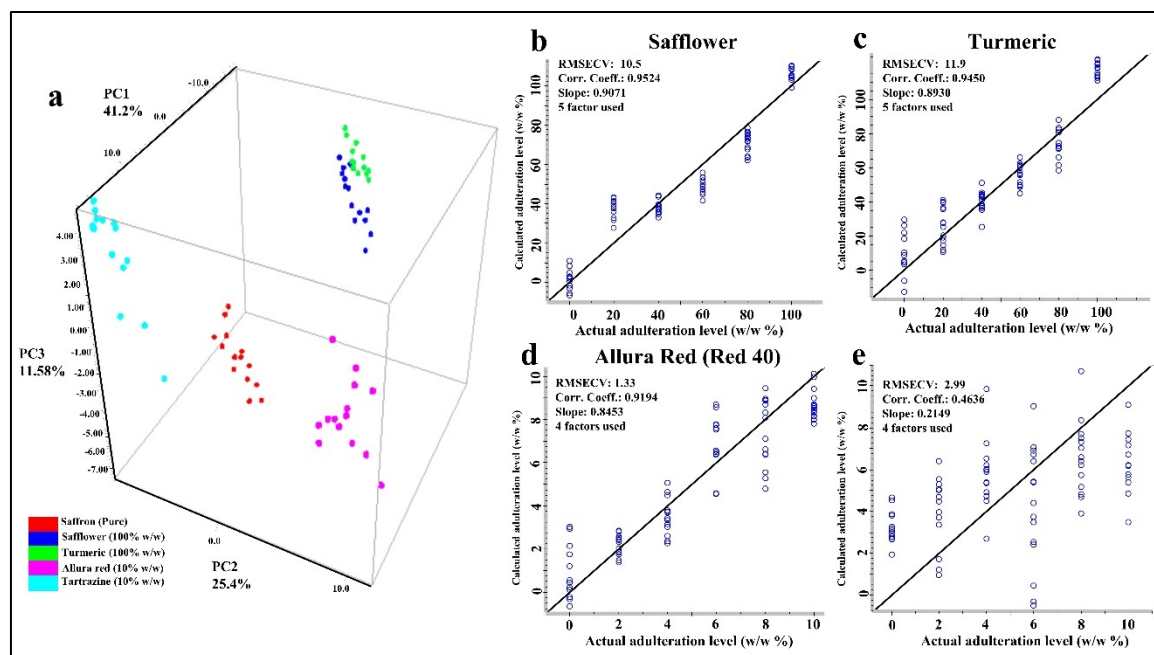


Figure 4. a. Principal component analysis of pure saffron and max adulterated samples based on TLC pattern $L^*a^*b^*$ values. Predict vs. actual color strength plots for adulterated saffron specimens based on $L^*a^*b^*$ data of b. safflower; c. turmeric; d. Allura red; e. tartrazine.

2.4.4 Confirmation of saffron adulterants based on Raman spectroscopy

Raman spectroscopy was used to evaluate its ability to confirm adulterants after the TLC presented adulterated sample patterns. Fig. 5a shows the standard spectrum of each adulterant of the concentrated ethyl extracts applied on TLC plates. Besides safflower concentrated extracts, all other adulterants exhibited their own unique characteristic peak for further identification. The reason we could not obtain the signal from safflower may be due to the relatively weaker Raman activity of carthamin under the tested condition. Due to different testing conditions and sample preparation, detection sensitivities and target Raman spectra might be different for different research groups. For example, Schmidt and Trentelman (2009) successfully detected the safflower spectrum in-situ within plant

materials with a 1064 nm laser source.¹⁰⁴ Bruni et al. (2011) detected the safflower spectrum in its extract using surface-enhanced Raman spectroscopy equipped with a 532 nm laser source. However, the Raman spectrum of safflower is different from these two groups.^{104,105} Nevertheless, the PCA plot of all tested Raman spectra shows well-separated clusters, indicating good discrimination between these compounds with a total variance of 38.1% by three principal components (Fig. 5b). Raman spectroscopy can be potentially used to identify or verify specific adulterants, followed by TLC visual screening.

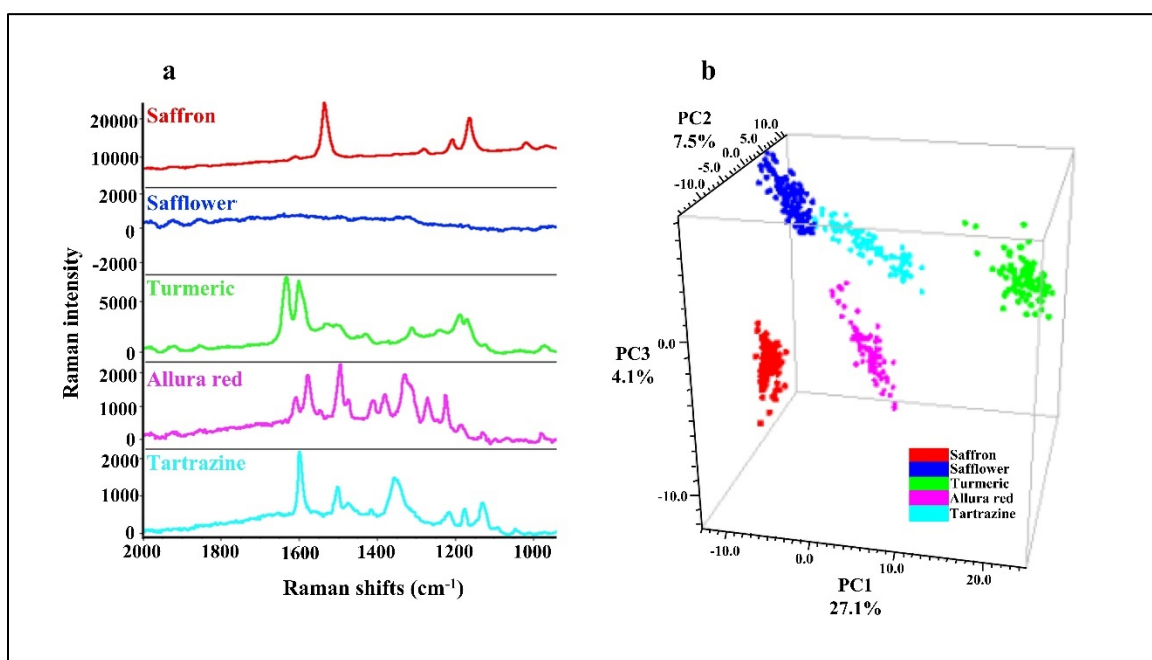


Figure 5. a. Pure saffron and pure adulterants Raman spectrum (80% ethyl extracts). b. Principal components analysis (PCA) of pure saffron and adulterants Raman spectrum (all sample solutions were prepared with a concentration of 1 mg dry matter/ml water).

2.4.5 Validation the established methods and models using adulterated samples with optically identical property

Three samples, namely pure saffron (Fig. 6 sample 1) and two adulterated saffron specimens (Fig. 6 sample 2 and Fig. 6 sample 3) were prepared to test the performance of the developed approach. As is shown in Figure 6, adulterated samples generated similar color strength as compared to premium saffron when adjusted by artificial colors in aqueous solutions., Sample 3 produced a similar $E_{1\text{cm}}^{1\%}$ 440 nm value as sample 1 (Table 4) using the ISO-3632 method, which demonstrated the weakness of the ISO method in analyzing samples with yellow 5 adulterations.

Table 4. Comparison of UV-vis and TLC-Raman analytical methods for identifying saffron color strength.

	UV-vis (ISO-3632)		TLC-Raman	
	Mean \pm SD	CV (%)	Mean \pm SD	CV (%)
Sample 1 (N=15)	179.0 \pm 0.8	0.4	198.0 \pm 11.3	5.7
Sample 2 (N=15)	104.1 \pm 1.8	1.8	122.5 \pm 9.05	7.4
Sample 3 (N=15)	171.8 \pm 1.6	0.9	31.9 \pm 6.4	19.9

Note: The data from TLC-Raman were calculated value according to the Raman peak intensity at 1543 cm^{-1} of each sample. Mean values from UV-vis and TLC-Raman were all representing Saffron color strength grading values according to ISO-3632.

For visual screening, we can clearly see the TLC characteristic patterns of pure sample 1 and adulterated sample 2 and 3 show visual differences under ambient light as well as UV light. Compared to the standard images (figure 3), we could conclude the adulteration of sample 2 and 3. The distinct coffee ring pattern of red 40 and yellow 5 could be easily observed in sample 2 and 3 under ambient light, indicating the contamination of corresponding adulterants (Fig. 6). Due to the fluorescence characteristics of saffron natural adulterants, it was more easily to observe their distinct patterns under UV light.

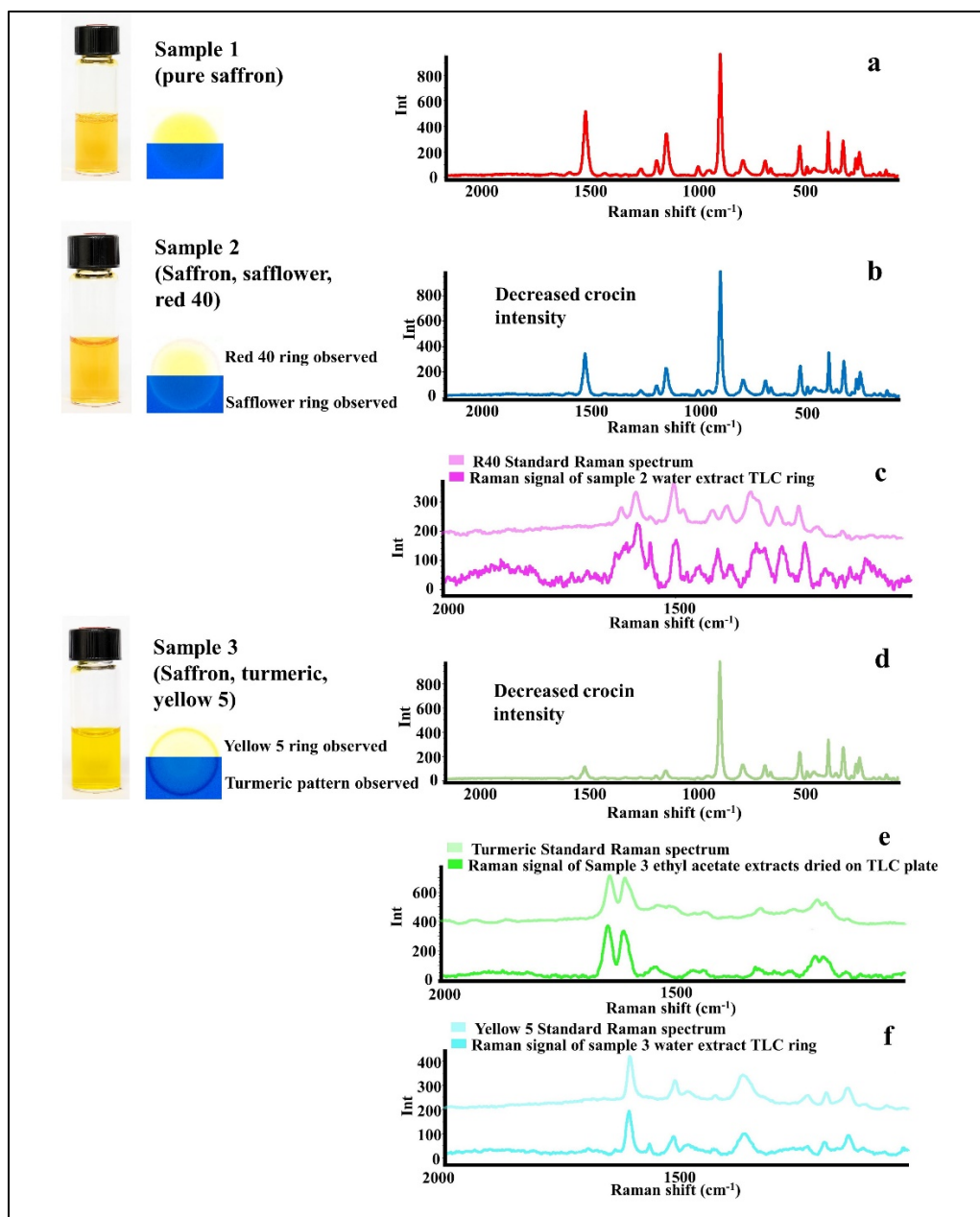


Figure 6. Comparison of TLC pattern, crocin Raman spectrum (a, b, and d), and adulterant Raman spectrum (c, e, and f) among three validation samples. (Note: Unless specifically mentioned, all Raman spectra were acquired at the center of each TLC drop).

Both safflower and turmeric fluorescence patterns could be observed as a coffee ring and inner circle in sample 2 and 3, respectively. Additional quantitative information can be

obtained from the L*a*b* data using the established PLS calibrations shown in Fig. 4 (b, c, d, and e). From the calculated results shown in table 5, red 40 and safflower recovery exhibited relatively better performance than turmeric and yellow 5. As previously discussed, the calibration of yellow 5 is inaccurate due to the color saturation phenomenon with the same yellow background.

Table 5. TLC-PLS calibration validation with adulterated samples.

Sample	Adulterants	Actual	Calculated adulteration (w/w %)		Recovery (%)
		adulteration (w/w%)	Mean ± SD	CV%	
2	Safflower	49.4	37.2 ± 5.4	14.6	74.3
	Red 40	0.75	0.81 ± 0.2	22.2	108.0
3	Turmeric	56.1	82.0 ± 6.3	7.7	146.4
	Yellow 5	25.7	6.5 ± 1.0	14.8	25.2

Spiked samples were then analyzed by Raman spectroscopy on TLC plates to confirm the decreased crocin intensity (Fig. 6 and Table 4) and the identification of adulterants. As can be seen in Fig 6, all samples with characteristic TLC adulterant patterns were confirmed with Raman spectroscopy except for safflower. It should be mentioned that artificial colorant was easy to detect even in low concentrations by repeatedly dropping sample solutions on the same spot. In this way, artificial colorants could easily concentrate on the coffee ring, making it easier to confirm the adulteration type using Raman spectroscopy. Both UV-vis (ISO-3632) and the TLC-Raman method had classified the pure validation sample (sample 1) as category I saffron (range from 170 to 200), confirming a good accuracy of this method for actual measurements.

2.5 Conclusion

In summary, the present study investigated a portable analytical approach to quantify saffron color strength as well as identifying saffron adulterants combining TLC and Raman spectroscopy. The developed approach exhibited great performance for quantifying pure saffron color strength as well as distinguishing adulterated saffron. Both the L^*a^*b method and the Raman spectroscopic methods had good correlations with the ISO method to quantify the crocin color strength for quality analysis.

For adulteration analysis, we could visually distinguish pure and adulterated saffron based on different TLC patterns. Further analysis based on the $L^*a^*b^*$ data extracted from TLC images could be potentially used to discriminate between pure and adulterated saffron specimens and estimate the level of adulteration with the help of chemometric models. Raman spectroscopy can be used to verify and identify possible adulterants when needed.

The result of this study demonstrated an alternative analytical method, which showed a potential advantage over the traditional UV spectroscopic method with less interference from adulterants. This approach could be applied to saffron quality control for local producers and small food companies with a limited budget. In the future study, we will further improve the data acquisition and analysis method to perform better quantification analysis.

CHAPTER 3

IMPROVING CLASSIFICATION AND QUANTIFICATION ACCURACY OF SAFFRON ADULTERATION USING DATA FUSION STRATEGIES

3.1 Abstract

High-valued agricultural crops have suffered from heavy economic adulteration around the globe. As one of the most expensive spices and colorants on the market, the saffron powder can be easily adulterated with the aid of extraneous plant materials or synthetic colorants. However, the current international standard method has several drawbacks, such as being vulnerable to yellow artificial colorant adulteration and requiring tedious laboratory measuring procedures. Previously, we developed a versatile and portable method to determine saffron quality using a thin-layer chromatography technique coupled with Raman spectroscopy (TLC-Raman). In this study, we aim to improve the adulteration classification and quantification accuracies with low and mid-level data fusion of TLC imaging data and Raman data. The best classification result was obtained from the mid-level fused partial least squares discriminant analysis (PLS-DA) model, which accurately determined saffron with artificial adulterants (red 40 or yellow 5 at 2 – 10 %, w/w) and natural plant adulterants (safflower and turmeric at 20 -100 %, w/w) with an overall accuracy of 99.52% and 99.20% in the training and validation group, respectively. The PLS quantification model built with the fused data block also showed improved quantification performance. The R^2 of each PLS model was improved using the fused data block. In the meantime, data fusion helped decrease quantification errors for most of the

PLS models, exhibiting lower RMSEP and RMSECV values. However, in comparison to sample classifications, data fusion strategies did not exhibit strong synergistic effects on improving quantitative accuracy. In conclusion, the present study demonstrated a great potential to fuse TLC imaging data and Raman data to improve the classification and quantification accuracy via the mid-level data fusion, which will facilitate rapid and accurate decision-making on site.

3.2 Introduction

Saffron, the stigma of *Crocus sativus* L, which is also called “the red gold”, is one of the most expensive agricultural products on the market. The finished saffron products have been used as medicines, spices, and colorants for centuries.^{86, 94} Historically, the economic adulteration includes mixing saffron with low-quality spices, adding plant materials, and forging saffron shades with natural or artificial colorants.¹⁰⁶

Color strength is one of the attributes to describe saffron quality. Currently, protocol ISO 3632-2, issued by the international organization of standardization, is used as the standard method for saffron color strength analysis.^{101, 102} In this method, UV-vis spectroscopy and high-performance liquid chromatography (HPLC) were used to determine saffron quality in color strength and its active ingredient responsible for color expression, crocin. However, despite the popularity of this method, it still suffers from some drawbacks. For instance, UV-vis spectroscopy is a well-developed technique with a wide range of applications. However, it can only detect saffron adulterants up to 20% w/w

and cannot identify artificial yellow adulterants that exhibit similar absorbance values as pure saffron.^{107,120} Other well-adopted methods, like HPLC and gas chromatography (GC), still have limitations such as long sample preparation, long test duration, high costs, and requiring laboratory settings and trained personnel.

Previously, we developed a rapid and field-deployable method based on thin-layer chromatography (TLC) and Raman spectroscopy to determine the saffron quality and saffron adulterations. Using TLC as a separation substrate, the optical TLC pattern of pure saffron and adulterated saffron specimens could be easily captured via a camera and converted to digital imaging data under ambient light and 365nm UV light.¹²⁰ Raman spectroscopy, in the meantime, provides molecular information on pure or adulterated saffron specimens from the TLC chip.⁹⁵ This established TLC-Raman method could determine saffron grades as well as identify common adulterations. However, we found some notable drawbacks when we further executed this method for adulterant quantification. In general, the Raman signal only provides information for pure saffron grade quantification, whereas the TLC patterns are used primarily for identifications of saffron adulterations. The lack of communication between these two data blocks prevents the method's full potential from being exploited. For instance, at high yellow 5 adulteration levels (6 - 10 % w/w), the optical method failed to accurately determine adulteration level due to color saturation problem on TLC chips. In the meantime, the decrease of crocin concentration due to the yellow 5 adulteration can be detected by the Raman spectrometer.

However, with no communications between these data blocks, the final decision-making relies on separate data analysis of the TLC pattern and Raman spectroscopy.

Data fusion, the analysis of concatenating several data sets into a single fused data block, has shown great potential to improve existing performance in spectroscopic analysis.¹⁰⁸⁻¹¹⁰ Compared to the analysis based on every single data set, concatenated data sets can interact and inform each other in the fused data, reducing the effects of spurious sources of variability and lowering prediction errors. The concatenation of data can be carried out and categorized at three different levels; namely, data level (low-level fusion), feature data level (mid-level fusion), and decision level (high-level fusion). With spectral data, data level and feature data level fusions are more suitable to be executed. In low-level data fusion, data from all measurement sources are simply combined into a single matrix after some data pretreatments for each individual data block. The mid-level data fusion would first extract relevant features of each data block separately. Then feature data are then concatenated to form a single array of data. In this case, features can be defined as relevant original or latent variables extracted via multivariate analysis models.¹⁰⁸⁻¹¹⁰

The aim of this paper is to evaluate the effectiveness of data fusion methodologies to improve the classification and quantification accuracies of adulterated saffron using Raman and TLC imaging data. This study evaluated a mid-level data fusion strategy for classification and quantification of saffron quality, respectively. In brief, saffron specimens were adulterated with artificial colorant or extraneous natural plant materials at different levels from 2% to 100%. Both adulterated and pure saffron specimens were prepared into

sample solution before each sample droplet was developed on TLC chips. Then, raw optical data and Raman raw were collected on the TLC chip. Subsequently, feature Raman data were generated by analyzing crocin characteristic Raman peaks. Variable influence on projection analysis (VIP) was also used to help extract feature Raman data. At last, the fused data matrix was completed by concatenating the imaging data and feature Raman data. The fused data were used for multivariate classification and regression via partial least squares discriminant analysis (PLS-DA) and partial least squares analysis (PLS), respectively. The classification and quantification results of saffron adulterants from the fused data were also compared against the analysis result based on each single data set.

3.3 Materials and methods

3.3.1 Chemicals and reagents

All of the natural specimens of this paper, saffron, turmeric powders, and safflower, were purchased from online sources. Each plant material was acquired from three different suppliers with a similar price range. Artificial colorants (Allura red and tartrazine) were purchased from two suppliers, which were IFC solutions (Linden, NJ, USA) and Sigma Aldrich (Merk KGaA, Darmstadt, Germany). TLC aluminum plates (Silicagel 60W F254S) were purchased from EMD Millipore Corporation (Billerica, MA, USA).

3.3.2 Sample preparation

All plant materials were pulverized by a Newtry high-speed food mill (Guangdong, China) at high speed for three minutes. Sample particle sizes were standardized by sieving through a 500 μm mesh sieve after pulverizing raw plant material. Collected powders were

contained in glass vials and stored in a light-sealed desiccator. Natural adulterants (safflower and turmeric) were mainly used to stuff weights. Spiked samples for calibration of natural adulterants were mixed with pure saffron by weight percentage (0%, 20%, 40%, 60%, 80%, 100%). We have considered using lower spike levels for natural adulterants. However, in normal practices, it is impractical to spike trace levels of natural plant materials in saffron for adulteration. For artificial adulterants (tartrazine yellow and Allura red), appearance and color intensity are the main aims of adulteration. Thus, the level of artificial adulterants mixing with pure saffron should not be added as much as natural adulterants, but with 0%, 2%, 4%, 6%, 8%, 10% w/w. For all samples, 50 mg of pure or spiked powdered samples were dissolved in 50 mL of deionized water to prepare raw sample solutions. The raw solutions were later filtrated through 0.45 μm PES filter paper. Then, three drops of 2 μL pure saffron or spiked saffron solutions were dropped on TLC plates at the same spot. Each droplet was dropped after the previous one had dried completely.

3.3.3 Data acquisition

Raw Raman spectral data were collected on TLC chips by a portable Raman system (TSI Incorporated, Shoreview, MN, USA) equipped with a 780 nm laser source. Each sample was measured in triplicates with five data collection spots for each replicate with an acquisition time of 10s. The measurements were carried out at max laser power with a spectral range from 100 to 2200 cm^{-1} . Thus, 75 spectra were collected for each type of adulteration, and 15 spectra were collected for pure saffron. A total of 315 spectra were

collected for data analysis in this study. Fig. 7 shows the adulterated saffron Raman spectra collected on TLC silica gel substrates. Featured Raman data (1000~1050 cm^{-1} , 1130~1240 cm^{-1} , 1270~1300 cm^{-1} , 1500~1580 cm^{-1}) was extracted by reviewing the main compounds responsible for saffron color expression. Feature selection was also referred to as the result of the Variable influence on projection (VIP, VIP value >1) from the SIMCA software, which summarizes the importance of each Raman peak in the PLS-DA model.

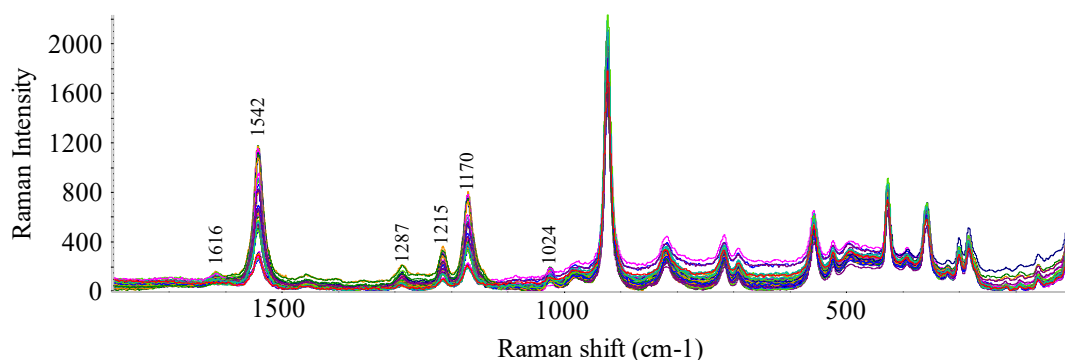


Figure 7. Raman spectra of adulterated saffron samples collected on TLC substrates.

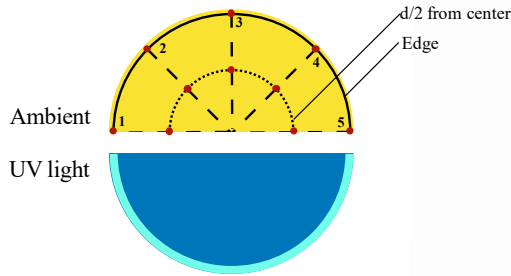
The collection and processing method of raw optical data from TLC chips could be found in our previous work with some modifications [10]. In brief, two separate images were collected under ambient and UV (365nm) light for each sample pattern, respectively. Furthermore, each adulteration level was measured in triplicates, and a total of 315 data were collected. Then, ambient and UV images were combined into one image, as shown in Fig. 8. An imaging data consists of millions of colored pixels with three layers of information in each pixel, namely, red (R), green (G), and blue (B). In addition, a typical 8-bit pixel has 0-256 shades of red, green, and blue, respectively. Thus, more details and

information can be observed and collected by separating the imaging data into three independent RGB channels. The optical data was collected using Adobe Photoshop CS6 (64-bit) under the green and blue channels. In brief, a color picker (32 * 32 pixels square) was used to collect 20 data points on each TLC pattern (5 points at ½ diameter distance from the center and 5 points on the TLC ring) under the full-color image, green and blue channels, respectively.

A. Sample TLC pattern



B. Imaging data collection point



C. Split Channels

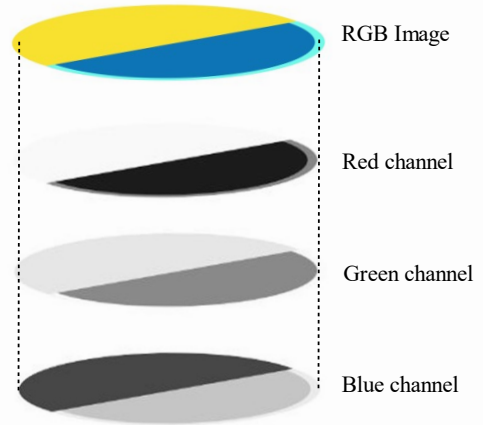


Figure 8. TLC pattern and imaging data collection scheme.

The imaging data can be expressed using the equation below:

$$X_{Ambient} = [X_{ambient\ RGB\ data} \ X_{ambient\ green\ channel\ data} \ X_{ambient\ blue\ channel\ data}]$$

$$X_{UV} = [X_{UV\ RGB\ data} \ X_{UV\ green\ channel\ data} \ X_{UV\ blue\ channel\ data}]$$

$$X_{Imaging} = [X_{Ambient} X_{UV}]$$

where RGB values in the color image (Fig. 8B) and the maximum, minimum, and average lightness values at blue and green channels (Fig. 8C) were collected at each sample collection point.

3.3.4 Data fusion

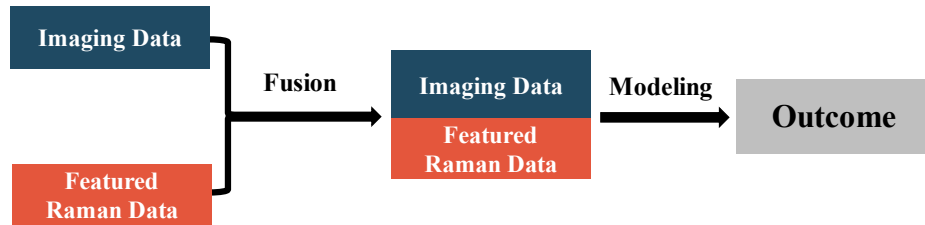


Figure 9. Schematic view of mid-level data fusion processing.

Fig.9 shows the fusion strategy, where featured Raman and raw optical data were measured and fused into one data block in the mid-level fusion model. Normalization was applied to both data blocks prior to the fusion according to the equation below.¹¹¹

$$X' = \frac{x - \min(x)}{\max(x) - \min(x)}$$

The fused data can be expressed via the equation below:

$$X_{Fused\ matrix} = [X_{Featured\ Raman} X_{Imaging}]$$

where $X_{Fused\ matrix}$ stands for the fused data block, $X_{Featured\ Raman}$ and $X_{Imaging}$ represent the single data block of featured Raman and imaging data, respectively. Next, $X_{Fused\ matrix}$, X

Featured Raman, and *X Imaging* data blocks were loaded in PLS-DA and PLS models for multivariate qualitative and quantitative analyses.

3.3.5 Partial least squares discriminant analysis

Partial least squares discriminant analysis (PLS-DA) was used for classification analysis in SIMCA (14.1) software. The entire classification model was classified by their adulterants type, and the scale type was used “Par” as the scaling model. The significant compounds were optimized via cross-validations. In the meantime, a total of 210 files from each data set were selected as the training group, including 50 spectra for each adulterant and 10 spectra for pure saffron. As a result, 3-D scattered point graphs (Fig. 10) and a misclassification table (Table 6) were generated.

In addition, the performance of the data fusion strategy was evaluated by the remaining 105 spectra working as an external validation group, which included 25 spectra for each type of spiked saffron and 5 spectra of pure saffron (Table 7).

3.3.6 Partial least square (PLS) regression of quantification

PLS-regression model was used to determine saffron adulteration levels. Raw data featured data, and fused data from the classification study were directly used in quantification analysis. Spectral data and imaging data were set up as variable X, whereas the adulteration level was set up as variable Y. The result was presented as predicted value versus observed value, as shown in Fig. 11. The performance of each PLS plot can be partially expressed by the maximum of R^2 values (goodness of fit) or the minimum of the

Root-Mean-Square Error of Prediction (RMSEP) values and the Root-Mean-Square of Cross-Validation (RMSECV) values.

3.4 Results and discussion

3.4.1 The effect of mid-level fusion on classification performance

As shown in Fig. 10A, the imaging data shows a mediocre cluster separation for natural adulterants, possibly due to similar TLC patterns at low adulteration concentration. In detail, safflower, turmeric, and yellow 5 adulterated samples are clearly distinguished from each other. However, heavy cluster overlapping is observed between turmeric and red 40; yellow 5, and pure saffron clusters. These results are also reflected in the misclassification table. In Table 6A, 20 out of 50 turmeric samples are misclassified as red 40. In addition, all pure saffron samples are misclassified as yellow 5 adulterated samples.

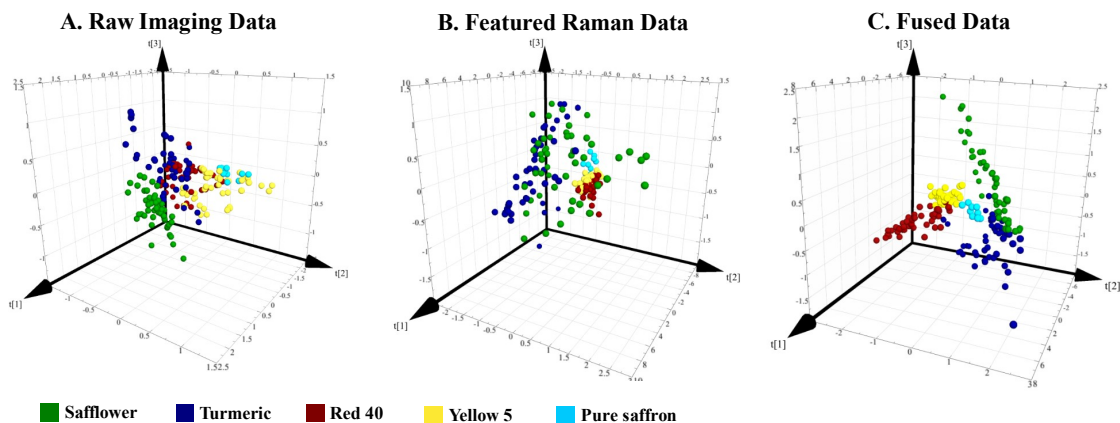


Figure 10. PLS-DA 3D-plots of (A). Imaging data; (B). Featured Raman data; (C). Fused data

As already discussed, one reasonable explanation for this phenomenon could be low pattern discrimination between these samples on TLC chips, which was also reported in our previous study [10]. One good example is the yellow 5 spiked sample, whose pattern characteristic is very similar to pure saffron at all tested concentrations (2-10% w/w). It also explains why all pure saffron samples are classified into the adulterated group.

In Fig. 10B, featured Raman data generates more scattered clusters for samples with natural adulterants. On the other hand, samples with artificial adulterants and pure saffron form tight and overlapping clusters. When looking at the result in Table 6B, it is evident that these tight clusters of artificial adulterants suffer from great misclassification issues. Nearly 20% (data not shown) of Red 40 and Yellow 5 adulterated samples are misclassified with each other. It is worth remembering that the collected Raman signal represents the sample mixtures on TLC chips. Its signal is jointly affected by the concentration of crocin and its adulterants. In the meantime, background signals from the silica gel are also part of the collected Raman data. In the featured Raman data block, variables are picked based on the most relevant peaks using VIP analysis. The feature extraction excludes background variables or instrument noises that contribute little to the model. As a result, those feature variables are mostly related to characteristic peaks of crocin, the main compounds responsible for saffron color expression. The presence of adulterants also causes nuances in the featured Raman data. However, these subtle differences can only be seen or analyzed with higher levels of adulteration, for instance, 20 – 100% w/w. However, at the given

spike level (2 – 10% w/w) for artificial adulterated specimens, there are few spectral differences, making it very difficult to differentiate these adulterated specimens.

Table 6 Misclassification table of spiked saffron samples based on A. Imaging data, B. Featured Raman data, and C. Fused data as training group.

	Members	Correct (%)	Safflower	Turmeric	Red 40	Yellow 5	Pure Saffron
A. Imaging data							
Safflower	50	100%	50	0	0	0	0
Turmeric	50	56%	2	28	20	0	0
Red 40	50	96%	0	0	48	2	0
Yellow 5	50	100%	0	0	0	50	0
Pure Saffron	10	0%	0	0	0	10	0
Total	210	83.81%	52	28	68	62	0
B. Featured Raman Data							
Safflower	50	94%	47	3	0	0	0
Turmeric	50	94%	3	47	0	0	0
Red 40	50	80%	0	0	40	10	0
Yellow 5	50	72%	0	0	14	36	0
Pure Saffron	10	100%	0	0	0	0	10
Total	210	85.71%	50	50	54	46	10
C. Fused data							
Safflower	50	100%	50	0	0	0	0
Turmeric	50	100%	1	49	0	0	0
Red 40	50	98%	0	0	50	0	0
Yellow 5	50	100%	0	0	0	50	0
Pure Saffron	10	100%	0	0	0	0	10
Total	210	99.52%	51	49	50	50	10

The result of mid-level data fusion on the classification accuracy can be seen in Fig. 10C and Table 6C. The PLS-DA plot and the misclassification table indicated significant improvements in cluster separation and correction rate compared to the result from each data block. In the meantime, the PLS-DA plot with mid-level fused data exhibited tighter clusters, yet each class was distributed with better separation, especially for red 40 and yellow 5 adulterated specimens (Fig. 10C). Each individual data block provides a complementary piece of information that helps classify spiked saffron samples. For instance, red 40 and turmeric spiked saffron samples that cannot be clearly differentiated

using the imaging data (Fig. 10A and Table 6A) can be separated in the PLS-DA plot when featured Raman data are used. Similarly, the introduction of the imaging data also helps enhance the classification capabilities of featured Raman data, which struggles to discriminate specimens with red 40 and yellow 5 adulterants (Fig. 10B and Table 6B). The synergistic effect between these two data blocks in the fused matrix achieves a satisfying accuracy of 99.52% (Table 6C).

3.4.2 Mid-level fusion model validation for adulteration classification

The performance of the PLS-DA model was validated using external validation samples (N=105), and the results are shown in Table 7. It is clear to see that the validation group has an excellent classification result among all adulterated specimens. Most samples with safflower, turmeric, and red 40 adulterants were correctly identified with adulteration levels ranging from 2% - 10% w/w for artificial adulterants and 20% - 100% for natural adulterants. The model achieved a correct rate of 99.2%, in which no adulterated specimens were classified as pure saffron in the validation group, giving it a 100% accuracy rate on adulterated sample determination.

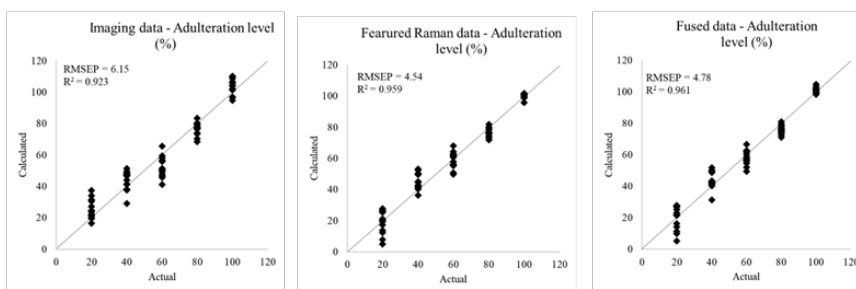
Table 7. Misclassification table of validation group based on the fused data block.

	Members	Correct (%)	Safflower	Turmeric	Red 40	Yellow 5	Pure Saffron
Fused data (external validation)							
Safflower	25	100%	25	0	0	0	0
Turmeric	25	100%	0	25	0	0	0
Red 40	25	96%	0	0	24	1	0
Yellow 5	25	100%	0	0	0	25	0
Pure Saffron	5	100%	0	0	0	0	5
Total	105	99.20%	25	25	24	26	5

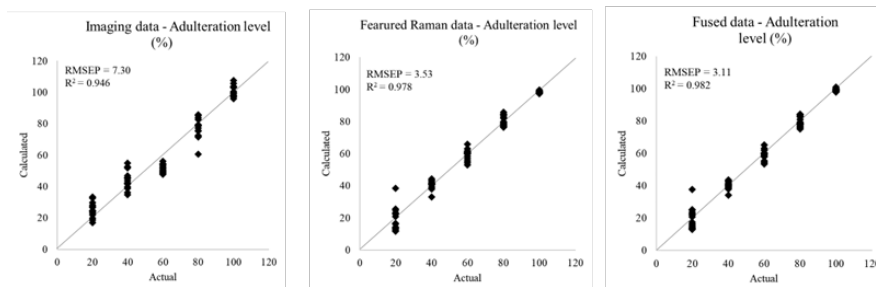
3.4.3 The effect of data fusion on PLS model quantification performances

Fig. 11 shows the PLS plots that predict spike levels in different adulterated saffron samples. Three data blocks, namely, $X_{Fused\ matrix}$, $X_{Featured\ Raman}$, and $X_{Imaging}$, were used to build each PLS plot. As can be seen, most of the plots, which project calculated and actual adulteration levels to the y and x-axis, establish good linear regressions. The R^2 and RMSECV values in Table 8 describe the model's goodness of fit and the model's ability to predict unknown samples. The RMSEP values indicate the goodness of the model's prediction using external validation samples (N=25). However, one should be noted that the RMSECV and RMSEP values are positively correlated to the scale of the data. In this case, samples with natural adulterants (20 - 100% w/w) were expected to have larger RMSECV and RMSEP values than artificial adulterants (2 - 10% w/w). Thus, artificial adulterants (red 40 and yellow 5) and natural adulterants (safflower and turmeric) should be compared separately due to the different adulteration levels. The PLS plots in Fig. 11 show poor prediction performances in red 40 and yellow 5 adulterated samples. As previously mentioned, low spiking level is the main reason behind this phenomenon. It also exposes one typical limitation of both imaging data and Raman data collected from TLC chips; low spike levels are insufficient to generate distinguishable patterns or spectral differences for quantification. One should be noted that sample droplets suffer from diffusion problems in every direction in TLC substrates. Thus the actual concentrations of the target adulterants on the chips are usually lower on the test spots. This issue can potentially be solved by concentrating the sample solution or dropping

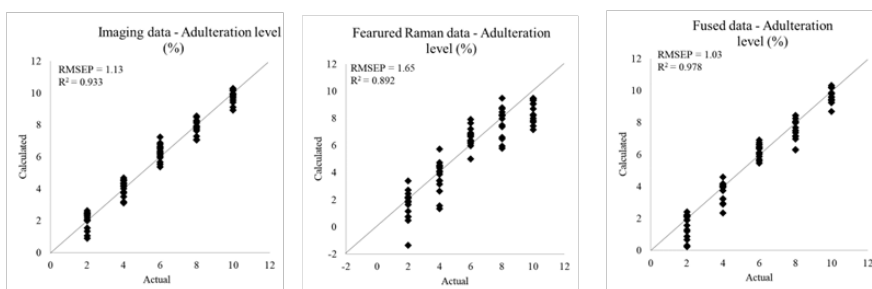
A. Safflower



B. Turmeric



C. Red 40



D. Yellow 5

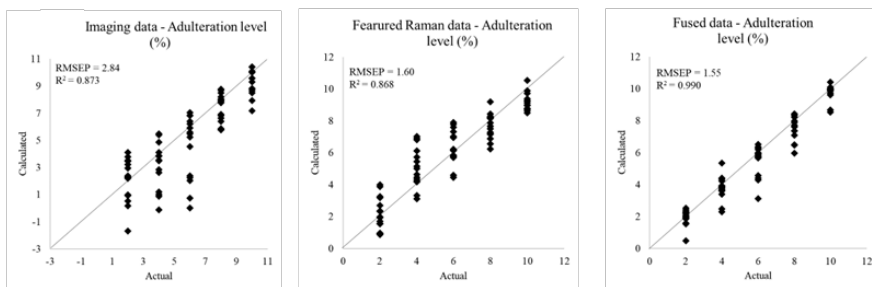


Figure 11. Predict vs. actual PLS plots of spiked saffron samples using imaging, featured Raman, and fused data blocks.

multiple sample droplets at the same spot. However, this approach may bring new detection challenges, such as stronger interference from crocin.

Table 8. Statistics for each data block in external and cross-validations

	Imaging data			Featured Raman data			Fused Data		
	R ²	RMSEP	RMSECV	R ²	RMSEP	RMSECV	R ²	RMSEP	RMSECV
Safflower	0.923	6.15	6.02	0.959	4.54	11.09	0.961	4.78	5.97
Turmeric	0.946	7.30	7.96	0.978	3.53	5.37	0.982	3.11	5.05
Red 40	0.923	1.28	0.82	0.892	1.65	1.37	0.978	1.03	0.97
Yellow 5	0.873	2.84	1.16	0.868	1.60	1.38	0.990	1.55	0.72

Thus, the data fusion strategy is still an ideal solution to improve quantification accuracy. When looking at the plots built based on the fused data (Fig.11), we can see some slight improvement in reduction in prediction errors. The most improvement is observed in Fig. 11D, where the fused data block significantly improves the plot's fittings. In Table 8, improvements can also be seen when we look into the statistics from the PLS model based on the fused data. For instance, most of the fused data blocks generate slightly higher R² values and lower RMSECV or RMSEP values compared to each individual data block. The imaging data and the featured Raman data achieve R² values ranging from 0.873 to 0.946 and 0.868 to 0.959, respectively. In the meantime, the fused data block has R² values from 0.961 to 0.990, which is considerably higher. The RMSECV values from the fused data PLS models are consistently lower, especially in yellow 5 specimens. This result indicates the synergistic effects when the imaging and featured Raman data are combined.

These effects, although not significant for most adulterated samples, still help improve the quantification capabilities of the model. A similar trend can be seen with the RMSEP values when using actual validation samples. That is, the model performs better using the fused data block for most adulterated samples, showing lower prediction errors.

Although most samples have better quantification performances using the fused data, some exceptions raise concerns about the model's effectiveness. For example, the reduction in RMSEP and RMSECV values is inconsistent when the fused data is used in PLS models. Samples spiked with safflower and red 40 show slightly higher RMSEP and RMSECV values in the fused data. It is reasonable to believe that sample variation may have caused this issue. But it still exposes one weakness of utilizing data fusion in quantification analysis. That is, the concatenation of different data blocks may cause deleterious effects when bad data blocks or outliers are introduced. This problem may not be very obvious in sample classifications since it is in favor of sample variation. However, it is very sensitive to quantification work. Taken together, our observation indicated that the fused data were best suited for quantitative analysis. But the improvements were not very consistent and significant.

3.5 Conclusion

The present study has examined the effectiveness of mid-level data fusion strategies in improving saffron adulteration classification and quantification accuracies using TLC-imaging data and Raman spectral data. Our results indicated that mid-level data fusion had

an excellent classification performance. Under this setting, all spiked samples were identified and distinguished from pure saffron samples. In the meantime, the validation result exhibited great capabilities to distinguish each adulterant with excellent accuracy (safflower, 100%; turmeric, 100%, red 40, 96%; yellow 5, 100%).

In the meantime, quantification accuracies of artificially and naturally adulterated samples showed better performances using the fused data block, achieving higher R^2 values with lower errors. However, from the result of external validation samples, the improvements were insignificant compared to the ones in the classification results.

Further work must be done to establish better protocols for utilizing imaging data in quantitative analysis. Other data blocks can also be investigated and introduced to finalize classification and quantification models. Furthermore, the established result can be further concatenated to produce a high-level fused result, which consists of both classification and quantification results. First, the PLS-DA model obtains classification results from mid-level data fusion. Then, corresponding quantification algorithms will be chosen based on the classification result. Depending on the classification results, the quantification results could be either expressed as saffron grade or adulterant level. Eventually, the final developed algorithm would be able to automatically determine saffron authenticity, adulterant identification, spike level, and pure saffron grade simultaneously to facilitate fast decision-making on site.

CHAPTER 4

**A MIRROR STAMPING APPROACH FOR IMPROVED SEPARATION AND
DETECTION OF COLOR ADULTERANTS USING THIN-LAYER
CHROMATOGRAPHY AND SURFACE-ENHANCED RAMAN
SPECTROSCOPY**

4.1 Abstract

Combining thin-layer chromatography (TLC) and surface-enhanced Raman scatterings (SERS) is a promising approach for analyte separation and detection. Herein, we developed a novel and simple TCL-SERS approach based on silver mirror stamping, which is achieved by pressing a layer of aggregated silver nanoparticles on top of the target analytes on the developed TLC chip. The performance of the stamping method was evaluated on the separation and signal enhancement of a mixture of saffron adulterated with Allura red as a model matrix, as compared to the other two methods. The result indicated that the mirror stamping method achieved the best separation performance with strong SERS signals, owing to the less sample disruption and less sample dilution from the internal solution in the application process. Thus, the mirror stamping approach has shown a great potential to be used in TLC-SERS analysis for the analyte separation and detection.

4.2 Introduction

Surface-enhanced Raman spectroscopy (SERS), a variant of Raman spectroscopy utilizing nanoscale metallic surfaces to enhance the Raman scattering, has been widely explored in many analytical applications.^{112, 113} Despite many advantages such as high sensitivity, fingerprinting characterization, and rapid detection, one major drawback of the SERS technique is the lack of separation capabilities when analyzing complex matrices such as food or biological samples.¹²³ Colloid-based nanosubstrates, the most commonly used SERS substrates, face another challenge. That is low signal reproducibility due to the difficulty of controlling their aggregation.

Thin-layer chromatography (TLC) is a simple and widely applied technique for constituents separation. This technique utilizes molecules' different affinities and solubilities in the stationary and mobile phases to achieve sample separation in complex matrices. Thus, the marriage of TLC and SERS has shown strong potential to be an effective and economical approach to improving the detection performances of complex samples. The fabrication of TLC-SERS substrates is now well established in many published works. For example, one usually needs to attach metallic nanoparticles on or into TLC substrates. Metal nanoparticles can be either synthesized within the stationary phase or, more commonly, applied or sprayed directly on the sample spot.^{114-118, 124} To start, Shen et al. utilized concentrated silver nanoparticles (AgNPs, 50-60 nm) droplets to enhance analytes' Raman signal on homemade diatomaceous earth TLC chips. The AgNPs colloid droplets were dropped onto every developed sample spot on the TLC chip.¹¹⁴ Similar

practices were also adopted by other groups to detect hydrophobic markers or water pollutants.^{115, 116} However, when the colloid solution was dropped or sprayed on the stationary phase, water was inevitably introduced to the sample spots, resulting in a secondary dilution to decrease the target molecule concentration. In addition, the applied nanoparticles may also spread unevenly on the TLC chip since they also follow the same principle of TLC separation. Thus, the disrupted sample may struggle to produce satisfactory signal consistency. Another strategy is incorporating metallic nanoparticles within or firmly attached to the stationary phase, such as cardboard, paper, or silica gel.^{117, 118, 124} These attempts successfully solved the previous problems. However, the substrate preparation is rather complicated and requires additional equipment to fabricate the stationary phase. For example, electro beam evaporation systems are usually required to perform metal (Ti or Ag) deposition on stationary substrates under pressurized or depressurized conditions.^{117, 124} Although the prepared substrate generates good SERS signals with little sample disruption by the nanoparticles, this method is relatively expensive and not readily accessible for a general analytical lab.

Thus, sample disruptions, secondary diffusion, and sophisticated fabrication protocols remain the key challenges many researchers or companies face in producing easy-to-prepare TLC-SERS substrates.

Herein, we aim to develop a novel and simple approach for TLC-SERS based on a commercially available TLC plate and a SERS active silver mirror we developed previously. The novelty of the techniques can be concluded into two points: 1. This method

utilized a simple silver mirror preparation protocol to integrate TLC and SERS seamlessly;

2. The present method has shown good TLC-SERS capabilities while keeping the sample pattern intact on TLC chips.

The homemade silver mirror was fabricated using a simple lab-modified protocol with all commercially available reagents. Our previous studies have validated that the silver mirror exhibits uniform and consistent Raman signal enhancement and great versatilities to conjunct with various substrates.¹¹⁹ To adopt the silver mirror to the TLC-SERS, we evaluated three methods: mirror first, mirror last, and mirror stamping. In brief, silver mirrors were directly dropped on TLC chips before and after sample application or stamped on dried sample patterns on TLC chips. The performance of these three methods was evaluated based on the separation and detection of a high-value-added agricultural product, saffron, spiked with an artificial colorant (Allura red). This matrix was previously studied using the combination of TLC and Raman spectroscopy which serves as a good model system for this study.¹²⁰

4.3 Material and method

4.3.1 Silver mirror fabrication

Silver mirrors were fabricated according to the method reported in our previous work with some modifications.¹¹⁹ In brief, an aqueous solution of capping agent (branched polyethylenimine, 0.1%, w/v) was added to silver nitrate solution (0.1%,w/v) to form the developing solution for silver colloid. The homemade silver colloid stock solution was then

synthesized by exposing the developing solution under 365 nm UV light for 80 minutes.¹²⁰

The stock solution was later used to prepare silver mirrors.

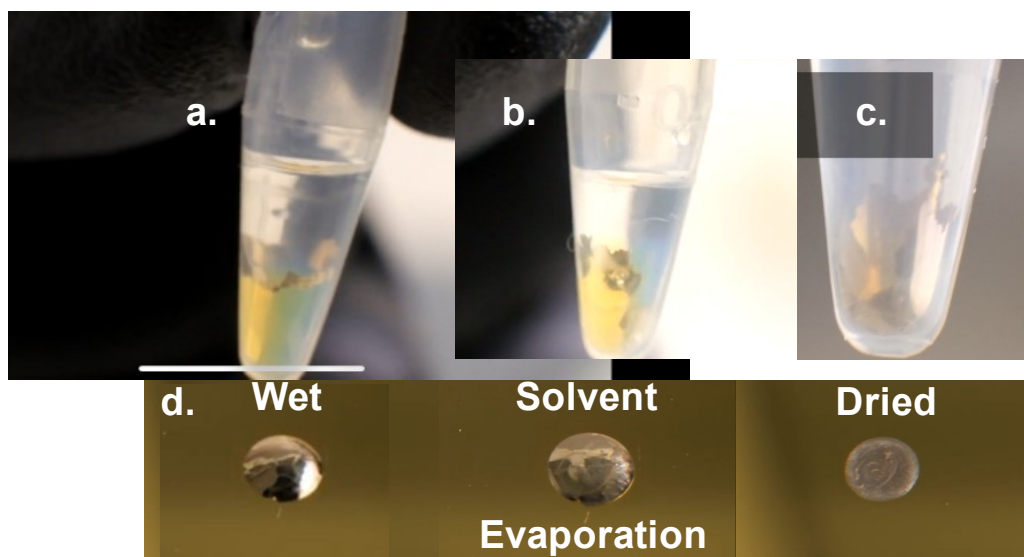


Figure 12. Physical observation of different AgNP mirror formation phases. a. AgNPs reacting with meditating solution; b. AgNP mirror formation and condensation; c. fully stabilized AgNP mirror; d. drying process of AgNP on a gold slide.

As shown in Fig. 12, a piece of the silver mirror was fabricated by gently adding 100 μl stock silver colloid solution to 100 μl of meditating solution (bottom layer of 1:1 volume mixed hexane and acetonitrile). Silver nanoparticles were immediately aggregated and aligned by the meditating solution to form a thin layer of silver mirror, which was later pipetted on a glass slide or a TLC chip for analysis.¹¹⁹ In addition, different mirror application sequences (Fig.13) were evaluated to compare their signal enhancement performances.

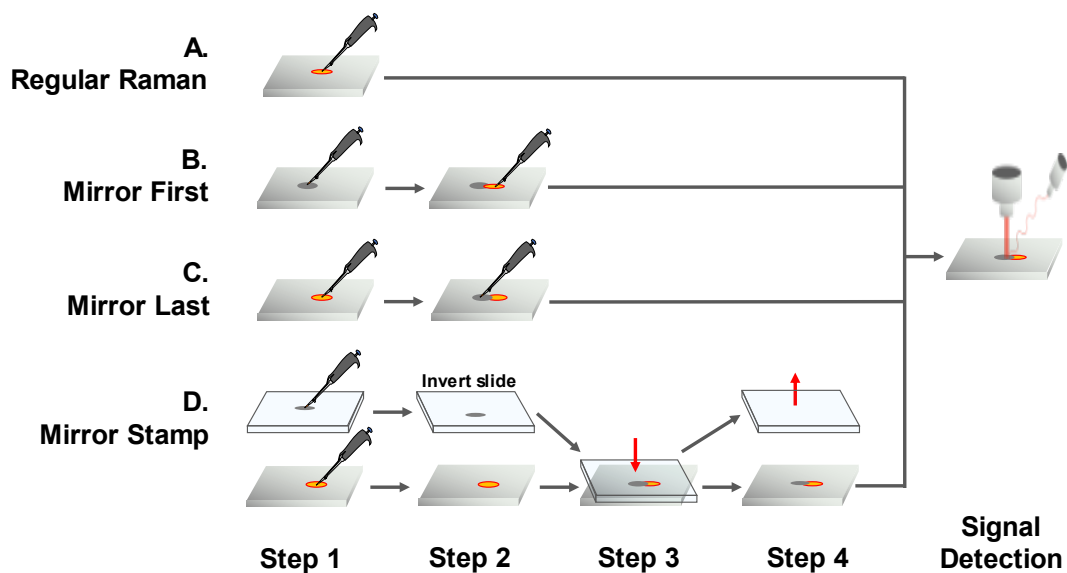


Figure 13. Sample pretreatments: a. standard Raman approach on TLC chip; b. mirror first TLC-SERS approach; c. mirror last TLC-SERS approach; d. mirror stamp TLC-SERS approach.

4.3.2 Pure and spiked sample preparation

A similar sample preparation protocol was adopted according to our previous study.¹²⁰ Briefly, pulverized saffron sigma was mixed with deionized water to prepare a bulk saffron extract (1,000 ppm). The extract was then filtered to obtain a clear saffron solution. Allura red solution (1000 ppm) was prepared in the same manner. In this study, a pure saffron sample (1,000 ppm) and a saffron adulteration sample (800 ppm and 200 ppm Allura red aqueous solution) were used to evaluate the performance of this method in terms of signal enhancement and sample separation performances. The spiked saffron solution was prepared by mixing pure saffron solution and Allura red solution at a 4:1 volume ratio. Prior to SERS measurements, three drops (1 μ L each) of saffron (or spiked saffron) solution

were added to the TLC chip at the exact same spot for an ideal testing concentration. This process would also simulate a standard TLC developing condition, where the feeding droplets imitate the flowing mobile phase.

4.3.3 Silver mirror application

As mentioned before, three different mirror application approaches were used: mirror first, mirror last, and mirror stamp (Fig. 13). The “mirror first” protocol was prepared by dropping the liquid AgNP mirror on the TLC substrate before the sample droplets. On the other hand, the sample solution was applied prior to the liquid AgNP mirror in the “mirror last” protocol. The mirror stamping protocol was finished by stamping a nearly dried AgNP mirror (Fig. 12d) over dried sample droplets on the TLC substrate (Fig. 13). In pure saffron samples, the silver mirrors were applied at the center of each TLC pattern, whereas, in the spiked saffron samples, the edge of the TLC pattern was aimed for different mirror applications.

All samples were measured with triplicates by a portable Raman system (TSI Incorporated, Shoreview, MN, USA) equipped with a near-infrared (780 nm) laser source. Five random spots were collected at each measuring area within each replicate. The collected data were processed via OMNIC for Dispersive Raman 9.7.46 (Thermo Fisher Scientific). Statistical analysis was performed on Microsoft Excel (Version 1911).

4.4 Results and discussion

4.4.1 Detection of pure saffron sample on TLC

Both TLC-Raman (Fig.14c) and TLC-SERS (Fig. 14def) techniques could detect characteristic crocin characteristic Raman peaks, which agrees with reports from other studies.^{121, 122} It is clear to show the signal intensities from the TLC-SERS group were much higher compared to the one without any silver mirror. Although the mirror stamp method did not give the highest signals, possibly due to several factors such as the effect of the solvent or the silver concentration on the silver mirror, the signal of the mirror stamp group was still comparable to the other two TLC-SERS groups and shared the same order of magnitude signal enhancement.

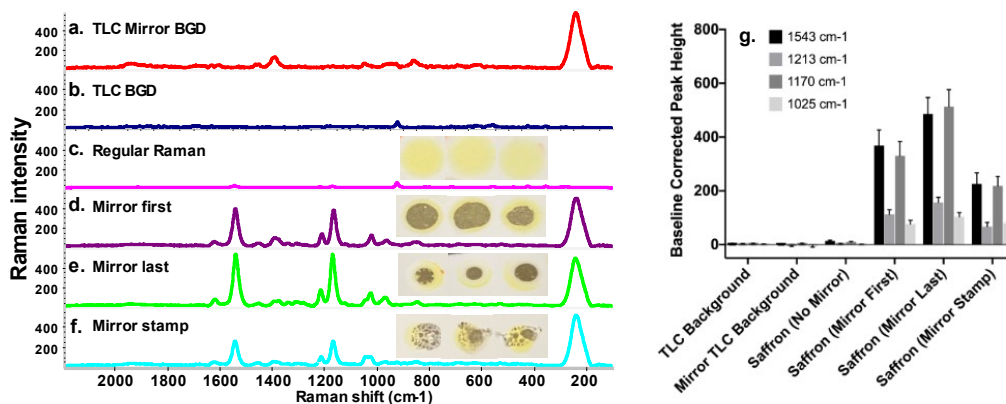


Figure 14. a-f. Raman and SERS signals of pure saffron solution collected under different sample pretreatments; g. Characteristic Raman peak intensity of saffron collected on TLC substrates under various sample pretreatments.

It is apparent that the shapes of the silver mirror and saffron droplets were associated with different mirror application procedures (Fig.14). Looking at Fig.14d, we can see that the TLC-silver mirror substrate did not affect the saffron droplet development when each

droplet was aimed at the center of the silver mirrors. When the silver mirror was applied after saffron droplets, the silver mirror droplet exhibited less secondary dilution than regular water droplets or silver colloid solution, owing to the fact that the thin layer of the silver film would contain and fix the sample inside of its edge. On the other hand, the sample outside of the silver mirror edge was flushed away from the mirror, forming a concentrated saffron ring (Fig. 14e). By pressing silver mirrors on TLC slides, the pressure from both surfaces caused the silver mirrors to break, forming a group of scattered smaller mirrors (Fig. 14f). This phenomenon is possibly due to the large surface tension of the mirror droplet. In addition, it is worth mentioning that the appearance of the stamped mirror is jointly affected by many factors, such as the pre-drying condition of silver mirrors, pressing forces, and pressing speed. This process may affect the density of silver nanoparticles per unit area on TLC chips, which was reflected on the SERS signal. However, as previously mentioned, the reduced signal recovery in the mirror stamp group is also possibly related to the presence of fewer solutions in the droplets.

When looking at Fig. 14g, it is interesting to see that the mirror stamp group retains a similar signal consistency compared to the other two methods, even though the appearance of the stamped mirror is broken and scattered. One reasonable explanation for this phenomenon is that upon breaking the large mirror droplet, tiny droplets of mirrors are instantly formed due to large surface tensions. These small silver mirrors, although scattered, have remained similar consistencies in terms of silver concentration and uniformity.

4.4.2 Separation performance of different mirror application methods on TLC

Sample separation and signal enhancement performances were evaluated on standard TLC and silver mirror-assisted TLC chips using adulterated saffron solutions. Fig.15 summarizes the physical appearances of different silver mirror application sequences on the TLC substrate. Clearly, mirror application sequences significantly affected the separation characteristic of TLC substrates. On a standard TLC chip, the adulterated saffron solution showed an excellent separation between red 40 and saffron extract with a distinct red ring (Fig. 15a). When dropped next to mirror-modified TLC, the TLC-SERS substrates selectively allowed saffron content to penetrate through the edge of the mirror-TLC, whereas the red 40 solutes were rejected at the edge (Fig. 15b). It could be seen from Fig. 12d that the mirror droplet contains the meditating solution from the preparation process as it is a necessary component to transport the silver mirror. Therefore, the solution within the silver mirror droplet would inevitably disrupt the original TLC pattern after the mirror droplet has been applied on top of the dried sample pattern, pushing both saffron and Allura red content away from the silver mirror coated TLC. However, as mentioned in section 4.3.1, the TLC pattern remained uninfluenced within the mirror area, where the initial impact happened. It could be seen from Fig. 15c that the mirror layer trapped the Allura red ring and saffron inner circle from mobilizing even though the meditating solution was pushing other parts of the analytes away from the mirror layer.

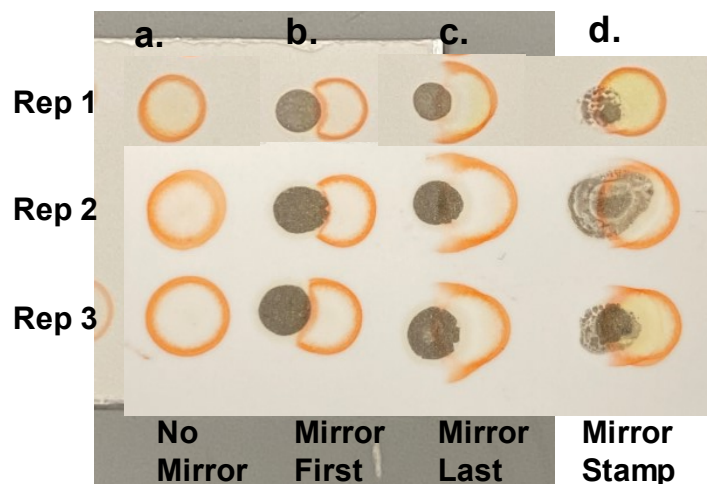


Figure 15. Physical observation of adulterated saffron solutions under different pretreatments on TLC substrates. a. standard Raman-TLC (no mirror); b. SERS-TLC treatment 1 (mirror first); c. SERS-TLC treatment 2 (mirror last); d. SERS-TLC treatment 3 (mirror stamp).

At last, the mirror stamping technique allowed the silver mirror to attach the sample without major disruption to its pattern or concentration on the TLC substrate. Although there were still some meditating solution residuals within the mirror, as it is necessary to perform the stamping process, most of the TLC patterns were unaffected and could be easily identified (Fig. 15d). The advantages of this technique were obvious. First, unlike the mirror first technique, the mirror was applied after the sample droplets had dried. Thus, the TLC substrate could use its full potential to separate all analytes within the sample solution. Secondly, since most of the mirror's meditating solution had evaporated before the mirror application, the remaining solvent would have little impact on disrupting sample distribution. At last, the mirror stamp technique simplified the data acquisition process since the pattern was less disturbed and easier to be aimed at by the laser.

4.4.3 Detection of Allura red signal in adulterated saffron samples on TLC

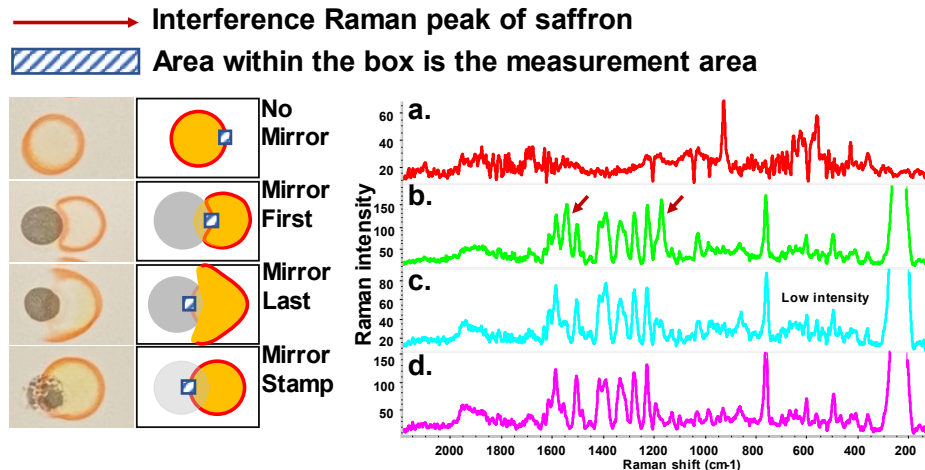


Figure 16. Raman and SERS signal of Allura red from adulterated saffron specimens collected on TLC substrates under various sample pretreatments: a. standard Raman-TLC (no mirror); b. SERS-TLC treatment 1 (mirror first); c. SERS-TLC treatment 2 (mirror last); d. SERS-TLC treatment 3 (mirror stamp).

Fig.16 summarizes the Raman and SERS signal of red 40 across all four types of sample pretreatments, namely, standard Raman (no mirror), mirror first, mirror last, and mirror stamp. No meaningful peaks were detected in the standard TLC-Raman measurement to reflect the presence of red 40 adulterants. On the other hand, red 40 characteristic peaks were detected in the TLC-SERS group (Fig. 16bcd). However, it should be noted that mirror first treatments failed to separate the red 40 signal and saffron signal. Two saffron characteristic peaks at 1543 cm^{-1} and 1170 cm^{-1} were detected in the mirror first samples when measuring the red 40 signals (Fig. 16b). As previously described, the dried silver mirror will selectively accept crocin content to pass through the edge of the complex while rejecting red 40 content. Thus, crocin was flushing through the Allura red segment while the mirror-TLC complex kept rejecting red 40 from entering the complex.

Eventually, this process defeated the purpose of using TLC as a separation tool since two components were mixed again at the mirror complex edge.

4.4.4 Detection of saffron signal in adulterated saffron samples on TLC

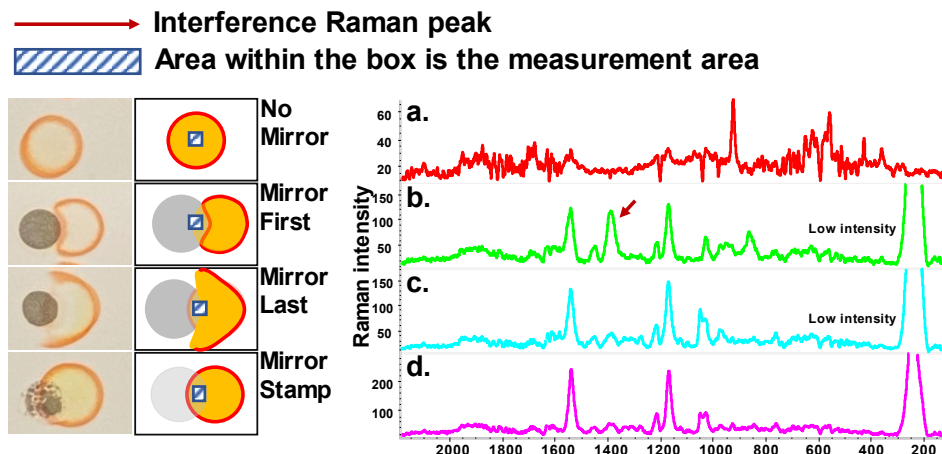


Figure 17. Raman and SERS signal of crocin from adulterated saffron specimens collected on TLC substrates under various sample pretreatments: a. standard Raman-TLC (no mirror); b. SERS-TLC treatment 1 (mirror first); c. SERS-TLC treatment 2 (mirror last); d. SERS-TLC treatment 3 (mirror stamp).

Two weak characteristic peaks of crocin were detected at 1543 cm⁻¹ and 1170 cm⁻¹ on a TLC substrate (Fig. 17a), whereas the silver mirror group generated much stronger crocin signals with more crocin characteristic peaks emerging at 1213 cm⁻¹ and 1025 cm⁻¹ (Fig. 17bcd). Two silver mirror background peaks were spotted in the mirror first spectrum (Fig. 17b) at 1390 cm⁻¹ and 1450 cm⁻¹, which were also detected in the other two spectra (Fig. 17cd). Generally, it is very common to see irrelevant background signals from SERS substrates, as they usually consist of enhanced Raman signals of various compounds such as colloid stabilizers or remaining reducing agents. But it was still unclear what caused the strong background signal in the mirror first treatment. One possible explanation was that

the mediating solution played a role in helping reduce the background signal by adjusting the surface charges of the silver nanoparticles when the silver mirror was attached to the crocin molecule. In the mirror first treatments, the silver mirror was thoroughly dried before any sample application. This condition was changed in mirror last and mirror stamp treatments, where the mediating solution was present during mirror attachment. Therefore, the presence of meditating solutions might have changed the binding behavior between the silver mirror and crocin molecule, resulting in less background signal. For now, we could only conclude that the presence of water or organic solution may greatly alter SERS behaviors on mirror-modified TLC-SERS substrate.

We observed different signal enhancement characteristics from the mirror first, last, and stamp methods. For example, the mirror stamp method behaved differently in the pure saffron analysis and spiked saffron analysis, where an apparent improvement in SERS signal recovery was observed in the latter study. This discrepancy could be attributed to the dropping spot of silver mirrors. Since the dropping point (or stamping point) was aimed at the edge of the TLC pattern, the developed sample is more likely to migrate to the blank TLC area, making it more prone to suffer from sample dilution problems. As we already discussed, other factors may also affect the signal recovery of target analytes, including the role of mediating solvents, mirror stamp pressure, and pre-evaporation time. Besides, the sample's secondary dilution factor by the mediating solvent and concentration of aggregated silver nanoparticles are considered to be the leading factors affecting the overall signal recovery in this study. In fact, the SERS binding mechanism between each specific

SERS substrate and target molecule should be studied extensively to present a convincing explanation.

It is worth remembering that the present study aims to enhance Raman signals on TLC chips with minimal disruption to developed samples. In this regard, the mirror stamp method outperforms the other two preparation methods regardless of detailed SERS signal recovery results. There is no denying that the main weakness of the mirror stamp approach is the paucity of effective protocols to produce consistent stamped mirrors, which may eventually lead to inconsistent signal recovery. However, these results warrant future investigation on improving signal consistency with the mirror stamping protocol.

4.5 Conclusion

This study has developed and evaluated a novel and simple TLC-SERS approach by combining our previously developed silver mirror with commercially available TLC chips. The mirror stamping method yields the best overall performance regarding sample separation and Raman signal enhancements. In addition, the mirror stamp technique significantly reduced substrate preparation time to 5 minutes compared to other TLC-SERS techniques.¹¹⁴⁻¹¹⁷ Furthermore, the silver mirror-assisted TLC-SERS substrates were made from readily available materials on the market without any dedicated instruments or strictly controlled synthesis conditions. Thus, the developed mirror stamping method could be used to help us design faster and more affordable approaches to analyze complex food matrices.

CHAPTER 5

PREDICTION OF ANTHOCYANIN COLOR STABILITY AGAINST IRON CO-PIGMENTATION BY SURFACED-ENHANCED RAMAN SPECTROSCOPY

5.1 Abstract

The color change resulting from anthocyanin and iron co-pigmentation has been a significant challenge in many iron-fortified food matrices. This present study aims to establish a quantitative model to predict the degree of color stability in the presence of dissolved iron using surface-enhance Raman spectroscopic (SERS) spectra. SERS spectra of anthocyanin extracts from 7 different plant sources were measured and analyzed by principal component analysis (PCA). Discrimination among different sources of anthocyanin was observed in the PCA plot. Stability indexes of each sample were established based on UV-vis analysis of anthocyanin at pH 3 and 6 with and without ferric sulfate. Partial least square (PLS) regression models were applied to establish the correlation between SERS spectra and stability index. The best PLS model was built based on the stability index calculated from the bathochromic shift (UV-vis spectral range: 380-750 nm) in pH3 buffer and the SERS spectra, achieving an RMSEP of 2.16 nm and an R^2 of 0.98. In conclusion, the present study developed a feasible approach to predict the quality of anthocyanin colorants, which is reflected as the degree of color shifts with the fortification of iron. The developed model can be used in real-life applications for quick screenings of raw ingredients for food manufacturers and food developers.

5.2 Introduction

The color of food products is one of the most important sensorial attributes for consumers' preferences. Currently, seven artificial dyes have been certified to be used as food colorants. However, recent reports post some emerging risks and concerns on these colorants, such as their ability to induce allergic reactions in a human child or potential carcinogenic effects when consumed in large quantities in some animal studies.^{7, 9, 16, 17, 18.} Hence, consumers are shunning away from artificial colorants and switching to more label-friendly ones, natural colorants.

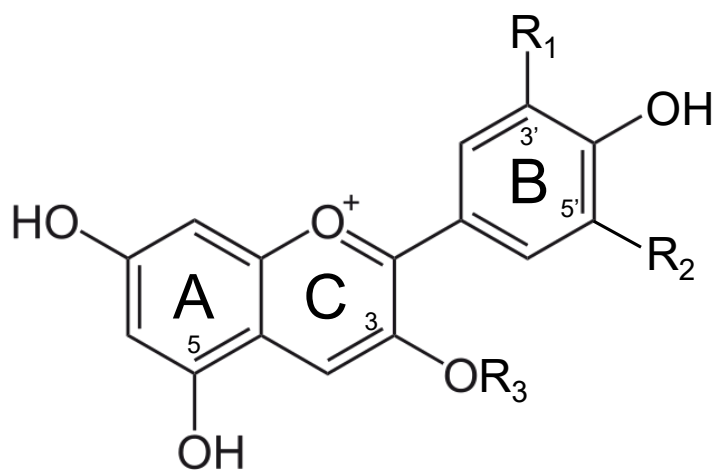


Figure 18. Structure of major anthocyanin-3-O-glucoside (R3).

Besides carotenoids, chlorophylls, and betalains, anthocyanins are the most abundant natural colorants in thousands of plants. The anthocyanin compounds are chemically defined as glycosylate polyhydroxy or poly methoxy derivatives of 2-phenylbenzopyrilium with two benzyl rings, as is shown in Fig. 18.^{134, 135, 146.} The major anthocyanins and their plant sources can be found in Table 9.^{136-138, 144, 146}

Table 9. Major anthocyanin structures and plant sources.

Anthocyanin	Abbrev.	R ₁	R ₂	Plant sources
Cyanidin	CYN / Cy	OH	H	Acai, black currant, elderberry, purple carrot, purple sweet potato
Delphinidin	DEL / Dp	OH	OH	Black currant, blood orange, purple carrot, red cabbage
Petunidin	PET / Pt	OH	OCH ₃	Bilberry, grape
Pelargonidin	PEL / Pg	H	H	Acai, red radish, strawberry
Peonidin	PEO / Pn	OCH ₃	H	Grape, purple sweet potato
Malvidin	MAL / Mv	OCH ₃	OCH ₃	Bilberry, grape

However, the color stability of extracted anthocyanin is affected by many factors such as pH, heat, light, and the presence of other chemical compounds. Given that many food manufacturers are fortifying iron in their formulation to fight global iron deficiency, especially for baby food, metallic ions are considered one of the leading compounds affecting the color stability of isolated anthocyanins within the food matrix.¹²⁶⁻¹³³ The major reaction involved between anthocyanin and metallic ions is called co-pigmentation. The anthocyanin-metal complex is formed due to the metal-binding capability of the ortho-dihydroxyl groups on the B ring (Fig.18).¹³⁹ Most anthocyanin-metal co-pigmentation product is always a color shift to blue or violet hues.¹⁴⁰ However, this reaction product is not favorable in most food matrices, where anthocyanins are selected and preferred as red colorants. Thus, the organoleptic changes caused by the fortification of iron should be seriously investigated.

In the past few decades, a great number of works have been done to study the interaction between anthocyanin and ferrous/ferric ions. In addition, a considerable amount of literature has been published on the mitigation of metal-induced color shifts of

anthocyanin. Data from several groups suggest that acylated anthocyanins are consistently more stable against pH change and iron fortification.^{141-143, 145} It is believed that the acylated group is to protect the chromophore from the nucleophilic attack or the attack from ferrous/ferric ions.¹⁴⁵ Although most of these studies were conducted using HPLC-MS analysis, few published studies have attempted to investigate these compounds using Raman spectroscopy, let alone study different anthocyanin responses to iron co-pigmentation using Raman spectrometer.¹⁴⁸⁻¹⁵⁰ Nevertheless, there is a notable lack of knowledge gap between anthocyanins' Raman spectra and their corresponding stability with the presence of iron.

This study hypothesizes that there are underlying correlations between the Raman spectral fingerprints and the metal-induced color shifts of various anthocyanins. Thus, the aim of this study is to predict the color stability of anthocyanins with the incorporation of iron by means of surface-enhanced Raman spectroscopy. In the present work, a mathematical model was built for the prediction of anthocyanin color stability. Moreover, diagnostics of peak assignments were carried out to explain the relationship between SERS spectra and the color stability of anthocyanin extracts.

This study presents a fast-screening model to predict color-stable anthocyanin extracts in iron-fortified environments by means of SERS coupled with multivariate analysis. To our best knowledge, this approach was not achieved elsewhere. The outcome of this study has great potential to be used in real applications in raw material screenings for product development or quality control.

5.3 Materials and Methods

5.3.1 Raw material and chemical reagents

Plants extracts (7 different plant sources, N=9) were provided by three suppliers: Exberry, Food Ingredient Solutions, and Charles Bowman. Received powdered or liquid samples were kept in the dark at 4 °C until analysis. All samples were tested within 1 month after the reception. The choice of plants was made to maximize the structural differences of the dominant anthocyanin, which are based on their degree of acylation, and their B ring structures.

All chemical reagents are analytical grade unless specifically mentioned. Silver nitrate (AgNO₃) (assay 99.9%), potassium chloride (assay 99.8%), methanol (assay 99.8%), hexanes (assay 99.9%), acetonitrile (assay 99.9%), hydrochloric acid (min. 37%) were purchased from ThermoFisher; polyethylenimine (branched, average mv ~ 25,000), ethyl acetate (assay 99.8%), iron (iii) sulfate hydrate (assay 97%), sodium acetate (assay ≥ 99%) from Sigma-Aldrich. C-18 solid-phase extraction (SPE) column (500 mg sorbent) was obtained by ThermoFisher Scientific (Rockland, TN, USA). All buffers and solutions were prepared using ultrapure water (Micropure, TheroFisher Scientific, Langenselbold, Hungary). All buffers used in this study were monitored with an accumet AE 150 pH meter (ThermoFisher Scientific).

5.3.2 Sample preparation

Each sample was dissolved or diluted in acidified water (1% w/w) before being filtered through a PES filter (0.2 μm, Whatman, Buckinghamshire, U.K.). The extract was then

packed in a C-18 SPE column, pre-conditioned with 3 mL acidified methanol (0.01% HCl) and 3mL of acidified water (0.01% HCl). First, the column was washed with acidified water (0.01% HCl) followed by ethyl acetate to remove organic acids, free sugars, and phenolic compounds, which can work as co-pigments with iron. Next, the anthocyanin fraction was eluded with 3 mL acidified methanol (0.01% HCl). The collected eluent was concentrated by a HeizbadHei-UAP rotary evaporator (Heidolph Instrument, Schwabach, Germany) at 40 °C. Finally, concentrated anthocyanin stock solutions (acidified MeOH) were flushed with gentle N₂ streams and then stored under -20 °C until further analysis.

5.3.3 Anthocyanin quantitation (pH differential method)

All anthocyanin stock solutions were quantified using the pH differential method.¹⁴⁷ In brief, each stock anthocyanin solution was first diluted in 0.025 M potassium chloride buffer (pH 1) and 0.4M sodium acetate buffer (pH 4.5). Then, each buffer solution was measured in a SpectraMax M2 spectrometer (Molecular Devices, Sunnyvale, CA, USA) under 520nm and 700nm, respectively. Based on the absorbance difference, the concentration (cyanidin-3-glucose equivalent, C3G) of each stock solution can be calculated using the equation below,

$$C_{(\text{mg/L})} = \frac{A \times MW \times DF \times 1000}{\epsilon \times 1}$$

where A equals (A_{520-A700})_{pH1.0} - (A_{520-A700})_{pH4.5}, MW is the molecular weight for C3G (449.2 g/mol), DF is the total dilution factor, 1 stands for the curvet pathlength (1 cm), ε is the molar extinction coefficient in for C3G (26,900 L × mol⁻¹ × cm⁻¹), 1000 is the factor conversion from g to mg.

5.3.4 Iron stabilization index acquisition

Stock anthocyanin solutions were then diluted to 30 μM in 0.1 M pH 3 and 6 sodium acetate buffers. Iron (iii) sulfate was diluted in ultra-pure water at 200 mM and then diluted to 0.6 mM in both buffers. The iron solutions were then added to the anthocyanin solution with a 1:10 (ACN: Fe) ratio under their corresponding pH condition. The control sample was analyzed with the addition of buffers instead of iron solutions. The pH level of all tested samples was carefully monitored. Samples were mixed well and kept in the dark prior to the analysis of visible transmittance (SpectraMax M2, 380-700 nm, step size 5nm). Duplicates were evaluated for each sample.

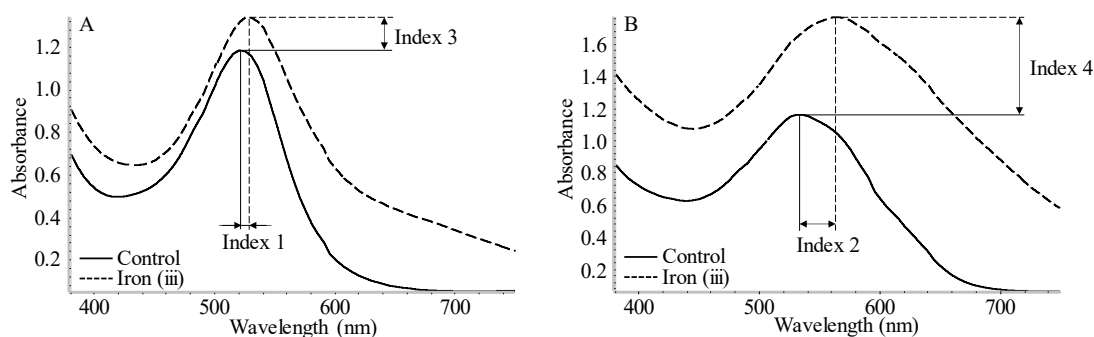


Figure 19. Bathochromic (Index 1 and 2) and hyperchromic (Index 3 and 4) shifts of co-pigmented anthocyanin measured by UV-vis spectroscopy.

The stabilization index was assigned to the bathochromic and hyperchromic shifts at both pH levels. As shown in Figure 19, index 1 and 2 corresponds to the bathochromic shift at pH 3 and 6. Similarly, index 3 and 4 translates to the hyperchromic shifts with the incorporation of iron at both pH conditions. Index 5 and 6 are calculated below as the root mean square of the conjunct bathochromic shifts and hyperchromic shifts.

$$Index\ 5 = \sqrt{\frac{(Index\ 1^2 + Index\ 2^2)}{2}}; \quad Index\ 6 = \sqrt{\frac{(Index\ 3^2 + Index\ 4^2)}{2}}$$

5.3.5 Anthocyanin SERS reference spectra acquisition

The silver colloid solution was prepared prior to SERS analysis of purified anthocyanin solutions. A modified light-assisted synthesis protocol was used to prepare the stock silver colloid solution.¹¹⁸ Briefly, the developing solutions, namely 0.2% silver nitrate and 0.2% branched polyethylenimine, were gently mixed with a 1:1 volume ratio. The mixture was then exposed under a UV lamp (365nm, Analytik Jena, Upland, CA, USA) in the dark for 8 hours under continuous stirring. Then the synthesized silver colloid solution was washed with ultra-pure water three times to remove the residual polymers. The washing process was achieved by centrifuging the colloid solution (17,000G, 5 minutes) and reconstituting using ultra-pure water (Sorvall Lynx 400 centrifuge, ThermoFisher Scientific, Amkalkberg, Germany).

Anthocyanin solutions were diluted with acidified water (0.01% HCl) and mixed with acidified silver colloid solution (0.01% HCl) at a final ACN concentration of 28 mg/L. The control sample was prepared by mixing acidified water with acidified silver colloid solutions. The mixture was dropped and evaporated on an aluminum foil-coated glass slide in the dark prior to analysis. The reference SERS spectrum of each anthocyanin under acidified conditions was collected using a DXRi Raman imaging microscope (ThermoFisher Scientific, Madison, WI, USA) equipped with a 780nm laser. Each sample was measured in triplicates with a laser power of 5 mW and a spectral range of 300 –

2000 cm^{-1} . Each anthocyanin SERS spectrum was an averaged result of 5 independent spectra with an exposure time of 1 second at a 50 μm slit aperture. A total of 15 averaged spectra were selected and used for each anthocyanin extract in the chemometric analysis.

5.3.6 Data analysis

Spectral data from the UV-vis spectrometer and the Raman imaging microscope were processed in the OMNIC software (version 9.7.46, ThermoFisher Scientific). Principal components analysis (PCA) and partial least square regression (PLSR) were executed in the TQ Analyst software (version 9.7.0.27, ThermoFisher Scientific). Standard normal variate (SNV) pathlength was used for correction after applying second derivatives for the anthocyanin SERS spectra for both PCA and PLS analysis. Spectral regions 370 – 918 cm^{-1} and 1099 – 1692 cm^{-1} were picked for PLSR analysis based on the distribution of characteristic peaks of anthocyanin. The performance of the PLSR model is evaluated by the root mean square error of cross-validation (RMSECV), root mean square error of prediction (RMSEP) values, and their corresponding correlation coefficient values (R^2), where the optimization of latent variables (factors) was also confirmed using the prediction residual error sum of square (PRESS) function for each stabilization indexes. For the calculation of RMSEP, samples were divided into training groups (75%, N=15) and validation groups (25%, N=5) for each index. The optimum model was chosen with the highest values of R^2 and the minimum of RMSECV/RMSEP.

5.4 Results and Discussion

5.4.1 Stabilization index analysis of anthocyanin extracts against iron incorporation

The stabilization indexes of each anthocyanin are summarized in Table 10. As can be seen from the table, anthocyanin extracts from different plant sources exhibit different stability indexes against iron incorporation. The larger the absolute value of each index indicates greater hue or intensity shifts with the addition of iron. In other words, lower color stabilities of anthocyanins are associated with increasing index values. Generally, greater index values occur at pH 6 rather than pH 3. This phenomenon was well observed in other studies.^{143, 146, 151} Index 5 and 6 (root mean square of indexes under pH 3 and 6) represent the overall stability under two different pH conditions.

Table 10. Stabilization indexes of collected anthocyanin extracts.

Anthocyanin Extracts	Stabilization indexes (mean \pm SD)					
	Index 1	Index 2	Index 3	Index 4	Index 5	Index 6
Purple sweet potato (S1)	2.64 \pm 1.54	11.64 \pm 0.06	-0.242 \pm 0.054	0.196 \pm 0.062	8.47 \pm 0.28	0.220 \pm 0.057
Purple carrot (S1)	24.59 \pm 1.22	41.26 \pm 0.49	0.048 \pm 0.004	0.349 \pm 0.031	33.97 \pm 0.14	0.249 \pm 0.022
Purple sweet potato (S2)	2.43 \pm 1.13	7.37 \pm 1.18	-0.149 \pm 0.041	0.144 \pm 0.003	5.50 \pm 1.04	0.147 \pm 0.022
Purple carrot (S2)	26.70 \pm 0.06	32.75 \pm 0.16	-0.0395 \pm 0.013	0.236 \pm 0.018	29.88 \pm 0.06	0.169 \pm 0.014
Grape juice color (S2)	-3.48 \pm 0.13	23.73 \pm 0.28	0.099 \pm 0.015	0.558 \pm 0.003	16.96 \pm 0.21	0.401 \pm 0.001
Red radish (S2)	-1.26 \pm 0.25	1.31 \pm 0.01	-0.111 \pm 0.083	0.113 \pm 0.016	1.29 \pm 0.13	0.112 \pm 0.031
Elderberry (S3)	22.57 \pm 0.35	44.72 \pm 1.23	0.089 \pm 0.004	0.413 \pm 0.015	35.42 \pm 0.67	0.298 \pm 0.010
Acai (S3)	5.35 \pm 0.24	51.38 \pm 2.12	0.085 \pm 0.025	0.261 \pm 0.181	36.53 \pm 1.47	0.199 \pm 0.113
Black currant (S3)	13.75 \pm 1.39	47.71 \pm 0.39	0.098 \pm 0.006	0.450 \pm 0.013	35.11 \pm 0.54	0.326 \pm 0.008

Note: S1 (Supplier 1); S2 (Supplier 2); S3 (Supplier 3)

The result from this study agrees with similar results from other groups where acylated anthocyanins tend to show better resistance than non-acylated anthocyanins against co-pigmentation from metal ions. Looking at index 5 and 6, acylated anthocyanins (purple sweet potato, purple carrot, red radish) score 1.29 – 33.97 for index 5 (bathochromic shift) and 0.112 – 0.249 for index 6 (hyperchromic shifts), respectively.^{152, 154, 155} For the

anthocyanins that are known to have less or little acylation (grape juice, elderberry, acai, black currant), a noticeable increase in both indexes was observed, ranging from 16.96 – 36.53 for index 5 and 0.199 – 0.401 for index 6.^{150, 153, 156-158, 160} According to index 5, which can translate to color hue difference, the overall color stability against iron from high to low are as follows: red radish > purple sweet potato > grape juice color > purple carrot > elderberry, acai, and black currant. Grape juice is generally considered to consist of non-acylated anthocyanins, such as Malvidin-3-O-glucoside or Peonidin-3-O-glucoside.^{157, 160} However, it should be noted that both of these anthocyanins only contains one hydroxy group on the B ring, which is not possible for metal chelation.¹⁶¹ Further evidence also indicates that the composition of some grape juices may vary significantly. For instance, acylated anthocyanin, Cyd 3-(p-coumaroyl) glucoside 5-glucoside, was found to be the dominant anthocyanin in Campbell Early (*Vitis labrusca*) grape juice.¹⁵⁷ Thus, considering its fair color stability in Table 10, it is reasonable to speculate that the grape juice color tested in the present study may contain acylated anthocyanin as the dominant anthocyanin. However, the detailed composition analysis of each extract is not the main objective of this study.

It is worth mentioning that each purified extract in the present study is a compound of a mixture of wide anthocyanin varieties whose chemical composition may be drastically different due to different glycosylation or acylation in different plant extracts. However, for anthocyanin extracts from the same plant sources, its primary anthocyanin contents were reported to be very similar unless great varieties of plant species were involved.¹⁵⁰⁻¹⁵⁸

Thus, it is not surprising to see that anthocyanin extracts from the same plant sources (purple sweet potato and purple carrot) showed very similar bathochromic shifts (index 1, 2, and 5). This indicates that the composition of the extracts from the same plant source is relatively similar using the applied purification protocol, and the index of the mixture could be used to represent the overall anthocyanin stability of certain plants.

5.4.2 SERS analyses of anthocyanin extracts from natural colorants

As previously mentioned, the anthocyanin extracts are mixtures of different anthocyanin variables. Thus, the collected SERS signals are not fingerprints for a specific type of anthocyanin but rather for a plant's total extractable anthocyanin composition, which is beneficial for food companies to evaluate the quality of the colorant extracts from the suppliers. Furthermore, based on the result from the previous section, it is clear that anthocyanin extracts used in this study can be used to represent plant sources with acceptable variations. Thus, collecting SERS spectra from anthocyanin extracts may help others gain more constructive knowledge on their co-pigmentation behavior for industry applications.

The SERS spectra of purified anthocyanin extracts are summarized in Fig. 20, with their corresponding Raman shift listed in Table 11. Although the tested anthocyanin extracts have different chemical compositions, they share some typical characteristic peaks. Such patterns can be used to identify the presence of anthocyanin. In detail, the peaks at ~ 1330 , 1370 , 1530 , 1570 , 1600 , and 1630 cm^{-1} are associated with ring stretching vibration modes of the A and B rings.^{148, 149, 159} The intense peaks at $\sim 1600\text{ cm}^{-1}$ are related

explicitly to the flavylium cationic form of the anthocyanins.¹⁵⁹ In addition, other strong peaks at $\sim 1330\text{ cm}^{-1}$ are attributed to the inter-ring bond stretching modes.^{148, 149, 159} The wavenumber of this band is closely related to the π -electron interaction between the B ring and the rest of the molecule. According to Zaffino et al. (2015), the wavenumber is positively correlated with the increase in the delocalization of the π -electron.¹⁴⁹

Two narrow bands at ~ 1080 and 1240 cm^{-1} are associated with the stretching of the C-O bond, whereas the bands at $\sim 1190\text{ cm}^{-1}$ are related to the bending modes of the hydroxyl groups. In addition, some skeleton in-plane and out-of-plane bending modes can be recognized at $\sim 420, 480, 630, 640\text{ cm}^{-1}$

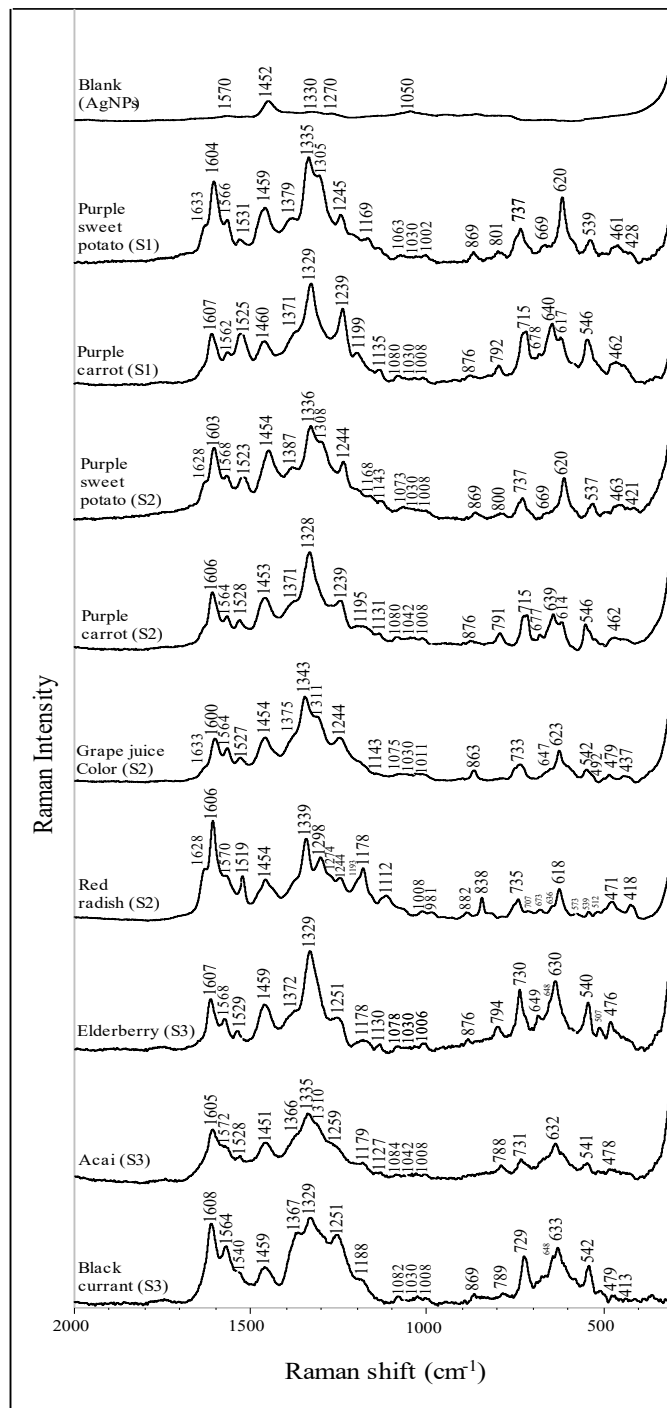


Figure 20. Surface-enhanced Raman spectra of anthocyanin extracts from different plant sources (dried acidified solution).

Table 11. Band wavenumbers and their tentative assignments of anthocyanin extracts.

	Purple sweet potato (S1)	Purple carrot (S2)	Purple sweet potato (S2)	Grape juice color (S2)	Red radish (S2)	Elderberry (S3)	Acet (S3)	Black currant (S3)	Blank (AgNPs)	Tentative Assignment
1633 (sh)	1628 (sh)	1633 (sh)	1628 (sh)	1633 (sh)	1628 (sh)	1607 (s)	1605 (s)	1608 (s)		v (ring A + B)
1604 (s)	1603 (s)	1606 (s)	1606 (s)	1600 (s)	1606 (s)	1568 (m)	1572 (sh)	1564 (m)	1570 (w)	v (ring A + B)
1566 (sh)	1562 (sh)	1564 (sh)	1564 (sh)	1564 (s)	1570 (sh)	1529 (m)	1528 (w)	1540 (sh)		v (ring B)
1531 (w)	1525 (s)	1523 (m)	1527 (m)	1519 (s)	1519 (s)	1459 (s)	1451 (s)	1459 (s)	1452 (s)	v (ring A + B)
1459 (s)	1460 (s)	1454 (s)	1454 (s)	1454 (s)	1454 (s)	1372 (sh)	1366 (sh)	1367 (sh)		v (cc)
1379 (sh)	1387 (w)	1371 (sh)	1375 (sh)	1375 (sh)	1339 (s)	1329 (s)	1335 (s)	1329 (s)	1330 (w)	v (ring B); δ (ch)
1335 (s)	1336 (s)	1328 (s)	1343 (s)	1343 (s)						v inter-ring coupled with a vibration of γ -pyrone
1305 (sh)	1308 (sh)		1311 (sh)		1298 (s)		1310 (sh)			
1245 (m)	1239 (s)	1244 (m)	1244 (m)	1244 (m)	1274 (sh)	1251 (sh)	1259 (sh)	1251 (m)	1270 (w)	v (co)
1169 (w)	1199 (w)	1168 (vw)	1195 (w)	1193 (sh)	1178 (s)	1178 (m)	1179 (w)	1188 (sh)		δ (oh)
									1050 (w)	δ (sh)
1063 (vw)	1135 (w)	1143 (w)	1131 (w)	1143 (vw)		1130 (m)	1127 (w)			
1030 (vw)	1082 (vw)	1073 (vw)	1080 (vw)	1075 (vw)	1112 (m)	1078 (vw)	1084 (vw)	1082 (vw)		Δ ccv (co)
1002 (vw)	1030 (vw)	1030 (vw)	1042 (vw)	1030 (vw)	1008 (w)	1030 (vw)	1042 (vw)	1030 (vw)		v (ring B), γ CH
			1008 (vw)	1011 (vw)	981 (w)	1006 (vw)	1008 (vw)	1008 (vw)		v (ring B), γ CH
869 (m)	876 (w)	869 (w)	876 (w)	863 (m)	882 (w)	876 (w)		869 (w)	948 (w)	γ (ch)
									861 (w)	
801 (m)	792 (m)	800 (w)	791 (m)	733 (m)	838 (m)	794 (m)	788 (m)	789 (w)		
737 (s)		737 (m)		733 (m)		730 (s)	731 (m)	729 (s)		aromatic system
669 (w)	715 (s)	715 (s)	715 (s)	707 (w)	707 (w)	679 (m)				
	678 (vw)	669 (sh)	677 (w)	673 (w)	673 (w)	648 (sh)				
	640 (s)	640 (s)	639 (s)	647 (sh)	636 (sh)	630 (s)			648 (w)	Δ (cc)
620 (s)	617 (sh)	620 (s)	614 (sh)	623 (s)	618 (s)		632 (s)	633 (s)		Γ (cc)
539 (m)	546 (s)	537 (m)	546 (s)	542 (m)	573 (w)	540 (s)	541 (m)	542 (s)		δ (cc)
				492 (sh)	539 (vw)	507 (m)				
461 (m)	462 (m)	463 (w)	462 (m)	479 (w)	471 (m)	476 (m)	478 (w)	479 (m)		Γ (cc)
428 (sh)		421 (w)		437 (w)	418 (m)			413 (w)		Γ (cc)

Note: v, stretching; δ , in-plane bending; γ , out-of-plane bending; Γ , skeleton out-of-plane bending; Γ , inter-ring; Δ , skeleton in-plane bending

5.4.3 PCA analysis of tested anthocyanin SERS spectra

The 3-D principal component scores (PCA) of all tested anthocyanins can be found in Fig. 21. The PCA result is a reflection of the spectral differences from 370 – 1670 cm^{-1} . In addition, the application of SNV and second derivative filters will help one analyze the SERS pattern differences rather than peak intensities. In detail, anthocyanins that generate similar SERS patterns from Fig.20 tend to form closely-positioned or overlapping clusters within the coordinate system. It is obvious from Fig. 21 that sample spectra within the same class, i.e., purple sweet potato and purple carrots formed overlapping clusters within each other. The result also validated the previous conclusion that anthocyanin extracts from the same plant source exhibit a similar response. In this case, that is, their SERS signal. This finding is well expected since anthocyanin extracts from the same plant source tend to be chemically similar in the dominant anthocyanins and anthocyanin compositions. Such similarities will unsurprisingly generate similar SERS patterns.

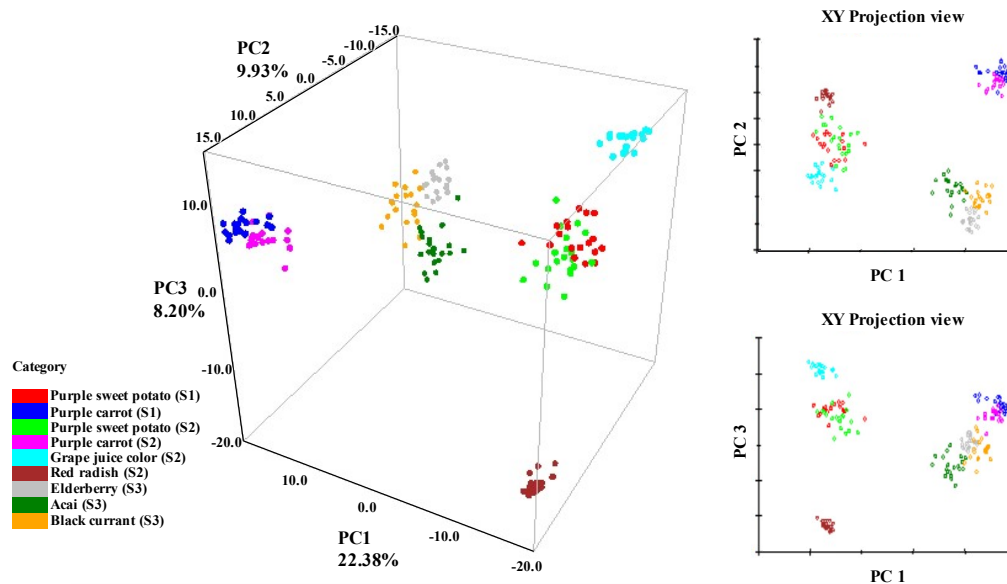


Figure 21. PCA scores of collected anthocyanin SERS signal.

It is also interesting to compare the result from Fig. 21 and Table 10. As already discussed, anthocyanins extracted from red radish, purple sweet potato, and grape juice color exhibit higher color stability than purple carrot, elderberry, acai, and black currant. Furthermore, in the PCA 2-D projection results, PC 1 clearly distinguishes and separates the stable anthocyanin from those less stable ones, which is highly in accordance with the result in Table 10. This trend indicates that there should be some correlation between the SERS spectra of anthocyanin extracts and their corresponding color stability. One obvious explanation is that the collected SERS spectra contain certain characteristic bands that translate to a stable chemical structure, especially a protected chromophore ring.

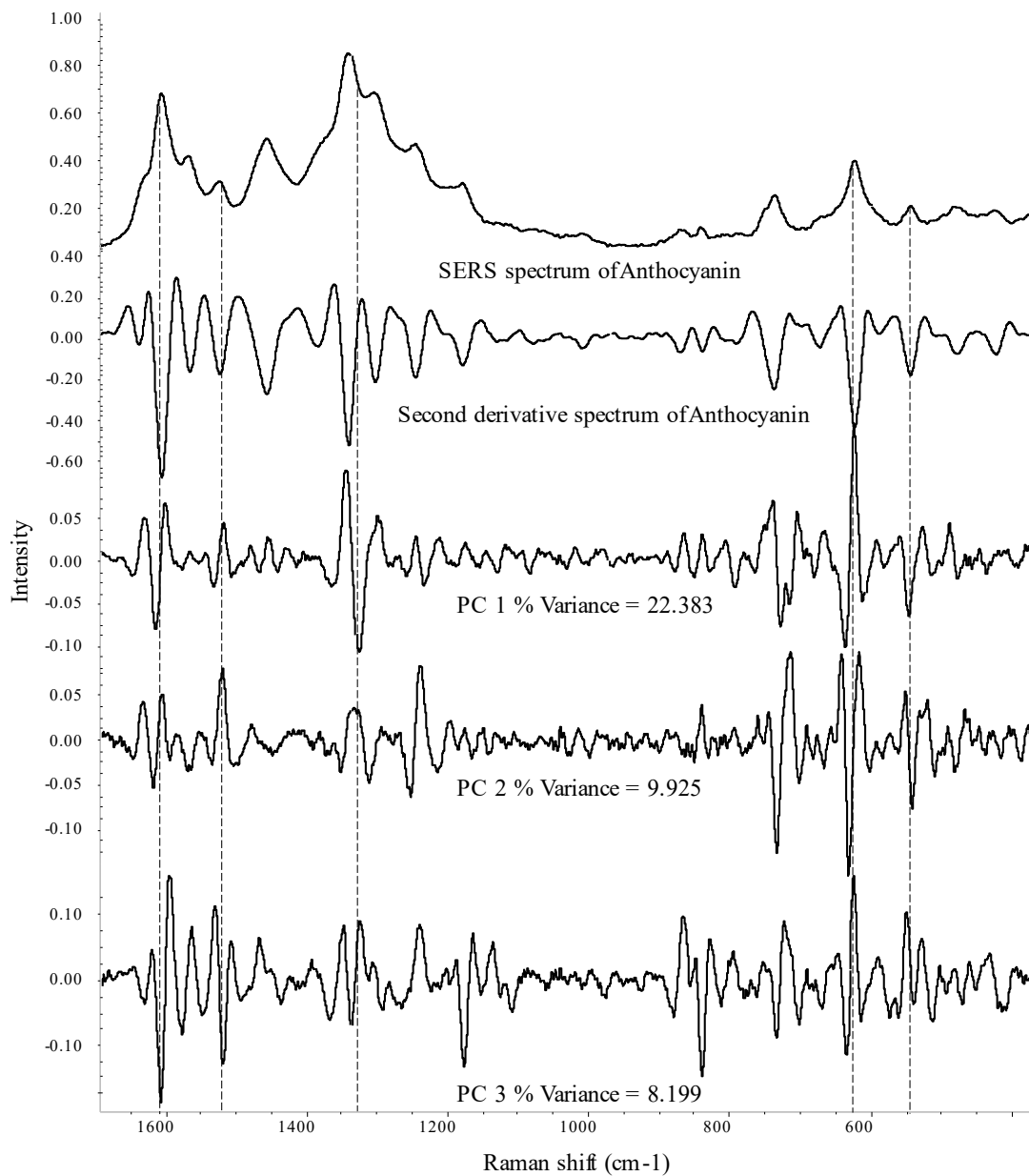


Figure 22. Principal component spectra of anthocyanin extracts.

PCA is a very powerful chemometric analytical method to compare the differences in SERS spectra for qualitative and classification analysis. The principal component spectra were presented in Fig. 22 for the diagnosis of contributing SERS bands to distinguish

anthocyanin sources, especially those stable anthocyanins. Herein, we mainly focus on the PC 1 spectrum due to its optimum performance in distinguishing the color stabilities of anthocyanins extracts. Six contributing SERS bands were spotted at ~ 1610 , 1330, 730, 715, 637, and 548 cm^{-1} , which correspond to the vibration modes in the A ring, B ring, and skeleton bending modes of anthocyanin.

5.4.4 PLSR analysis between SERS spectra and stabilization index of each anthocyanin extract

The descriptive statistics of the PLS model for each index are summarized in Table 12. In the meantime, the correlation between the collected and predicted stabilization index values from external validations can be seen in Fig. 23. From the result in Table 12, it can be concluded that the SERS spectra showed a satisfactory R^2 in the cross-validation for index 1 (0.91), index 2 (0.86), and index 5 (0.91). In addition, the RMSECV values are reported to be 4.60, 9.26, and 5.94 nm for index 1, 2, and 5, respectively. On the other hand, poor performances are observed in cross-validation models with index 3, 4, and 6, only achieving R^2 values of 0.51, 0.17, and 0.13, respectively. A similar trend is observed in the external validation, where indexes representing bathochromic shifts (index 1, 2, 5) have higher R^2 than those translating to hyperchromic shifts (index 3, 4, 6). Therefore, we suggest that the models of bathochromic performed better than those for hyperchromic shifts probably because the color intensity is relatively less stable than the color hue shift during the UV-vis measurements.

Table 12. Statistics for each stabilization index in cross- and external validations.

	Cross Validation			External Validation	
	Factors	Corr.Coeff.	RMSECV	Corr.Coeff	RMSEP
Index 1	2	0.91	4.60	0.98	2.16
Index 2	2	0.86	9.26	0.94	6.30
Index 3	2	0.52	0.10	0.88	0.06
Index 4	1	0.17	0.15	0.64	0.11
Index 5	2	0.91	5.94	0.96	4.03
Index 6	2	0.13	0.10	0.79	0.05

The results of the external validation model in Table 12 are reflected in Fig. 23. In detail, index 1 achieves the best fitting to the prediction vs. actual line, whereas index 4 generates the worst fitting plots. After comparing all PLS plots, a similar conclusion can be made: bathochromic indexes (index 1, 2, and 5) have better overall fittings than those of hyperchromic indexes (index 3, 4, and 6). The result in index 1 further confirms our initial hypothesis that there is a close correlation between anthocyanins' SERS spectra and their color stability with iron incorporation. One can potentially use the PLSR model to evaluate the stability indexes of an unknown anthocyanin sample by obtaining its SERS spectrum.

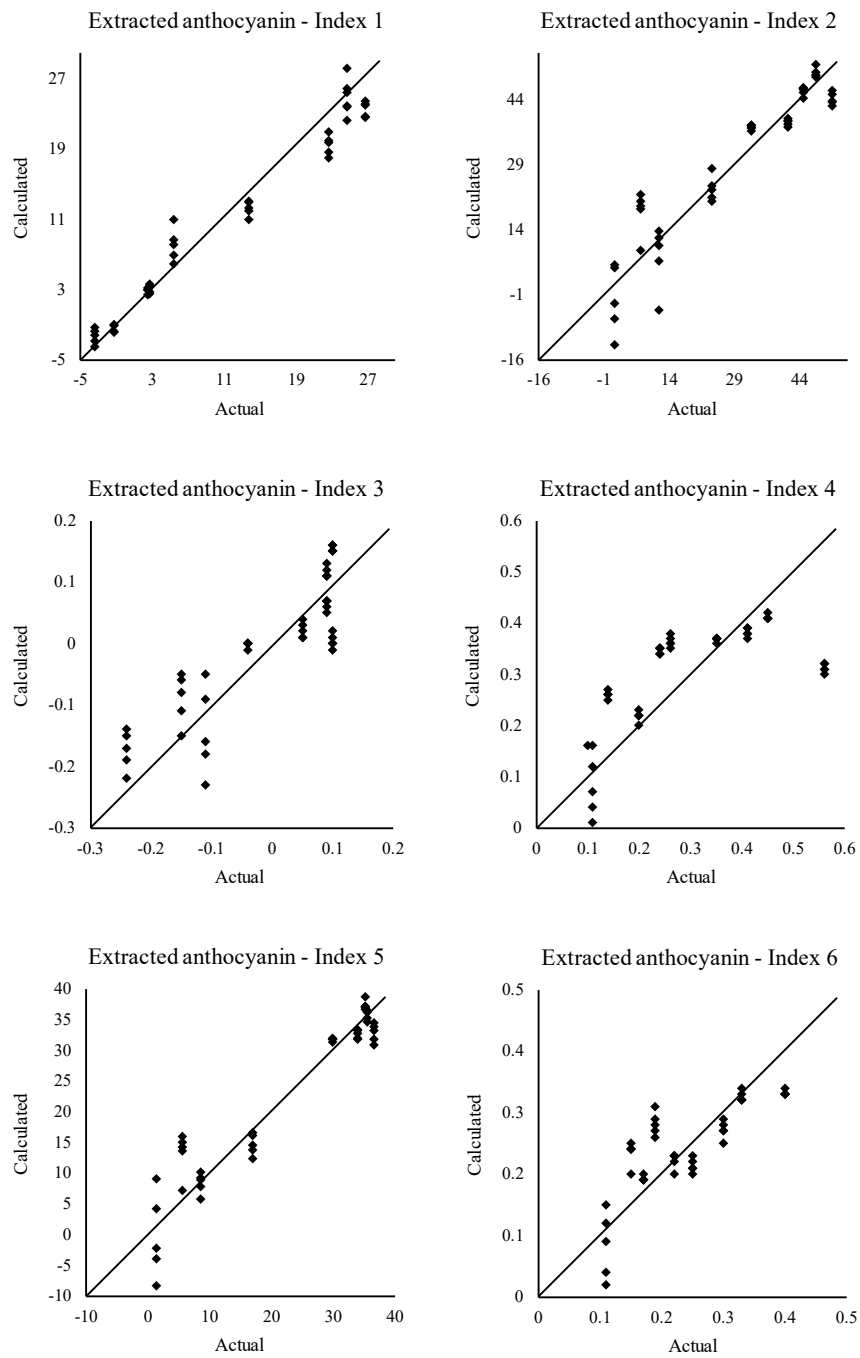


Figure 23. Actual vs. prediction PLS plot in external validation for each stabilization index.

5.4.5 Study of anthocyanin's iron stability on SERS signal

According to Table 12 and Fig. 23, index 1 is chosen to be the best model for anthocyanin color stability prediction. Hence, in Fig. 24, the PLS loading spectra of index 1 are studied to reveal the contributing Raman bands for color stability prediction of anthocyanin. In second derivative spectra, peaks pointing downwards suggest a positive influence on the development of the equation.

The major bands to predict anthocyanin stability are mainly related to anthocyanins' structural vibration modes. From the result in factor 1 and 2, the peak at ~ 1300 and 1330 cm^{-1} are closely related to the quantification and prediction of anthocyanin's color stability. Given that the ring's stretching modes are closely responsible for the signal within the spectral range of $1099\text{-}1692\text{ cm}^{-1}$,¹⁴⁹ the chromophore status can be reflected based on the SERS signal within this range. It is worth remembering that the 1330 cm^{-1} band is the inter-ring stretching mode, whose wavenumber and peak intensity are greatly affected by the location, type, and the number of the substituents. A shift to higher wavenumber was observed in most stable anthocyanin samples, including red radish (1339 cm^{-1}), purple sweet potato ($1335, 1336\text{ cm}^{-1}$), and grape juice color (1343 cm^{-1}). On the other hand, the wavenumber of this peak in most unstable anthocyanins was relatively smaller at $\sim 1329\text{ cm}^{-1}$. As previously discussed, this increase in wavenumber may be related to the delocalization of the π -electron caused by the substituents in the molecule.¹⁴⁹ Thus, it is reasonable to suggest that anthocyanin with an elevated wavelength at $\sim 1330\text{ cm}^{-1}$ tends

to exhibit higher color stability against iron, possibly due to a larger and more complex molecular structure.

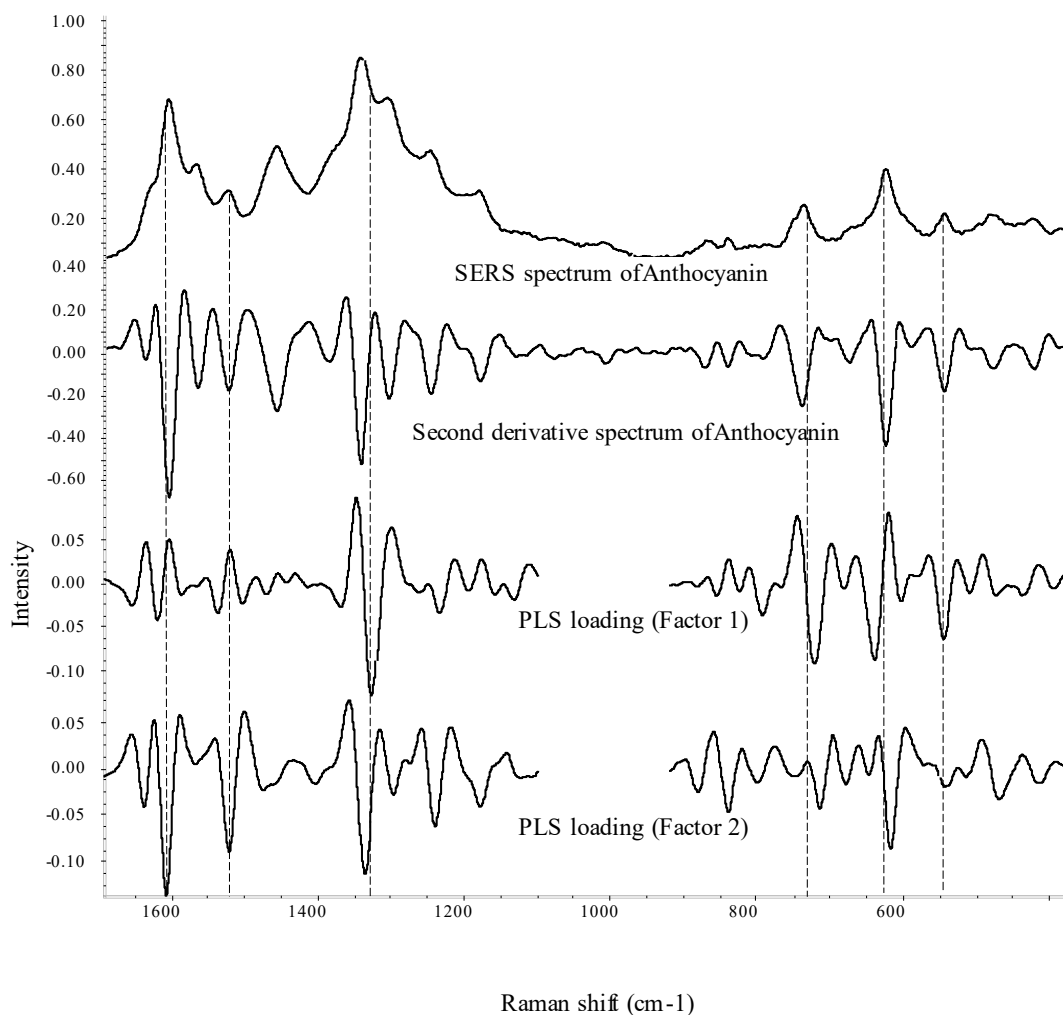


Figure 24. PLS loading spectra for stabilization index 1 using anthocyanin's SERS signal.

In addition, we suggest that the band at $\sim 1300\text{ cm}^{-1}$ may be associated with the vibration modes among the glucoside and acylated groups within anthocyanin molecules. The presence of this peak in the SERS spectrum is highly in accordance with good color

stability, especially for red radish extracts, which are known to obtain a high amount of acylated anthocyanins. SERS spectra (Fig. 20) of other samples with acylated anthocyanin, i.e., purple sweet potato, purple carrot, and grape juice color, also confirm this suggestion. The only exception is the purple carrot extract, whose dominant anthocyanin is believed to be cyanidin-3-O-(2''-xylose-6''-glucose-galactoside) by acylation with sinapic, ferulic, and p coumaric acid.^{154, 162} One possible explanation is that most purple carrot anthocyanins contain only one glycosylation position in the 3 position on the C ring. In contrast, other anthocyanins (red radish, purple sweet potato, grape juice) are believed to have sugar moieties connected in the 3 and 5 positions in the flavylum group. Furthermore, purple carrot does not contain a high amount of acylated anthocyanin. According to Malien-Aubert et al. (2001), purple carrot only contains 6.4 mg/g of acylated anthocyanin, which is significantly lower than that of red radish (116.1 mg/g).¹⁴²

Peaks around 720, 640, and 540 cm^{-1} are also strongly related to the prediction of color stability according to the PLS loading spectrum (factor 1). These three bands correspond to the vibration modes of the aromatic system, C-C skeleton in plane bending and C-C in-plane bending in anthocyanin molecules, respectively.^{148, 149, 159} Despite no apparent trends that can be concluded from the anthocyanins SERS spectra in Fig.20, most of these peaks closely relate to anthocyanin's skeleton structural vibration modes. At last, other the peak at $\sim 1610, 1520, \text{ and } 1240 \text{ cm}^{-1}$ showed a positive correlation as well. However, the significance of these bands is relatively lower than those already discussed bands.

5.5 Conclusion

The present work demonstrated a viable approach to both distinguish anthocyanin sources and predict the iron-induced color stability of extracted anthocyanins with sufficient accuracy by mean of surface-enhanced Raman spectroscopy coupled with multivariate analysis. In addition, a diagnostic of SERS signals was executed that allowed the identification of color-stable anthocyanin with the presence of iron. Based on the tested result, the anthocyanin extracts from different plant sources can be easily differentiated using collected SERS spectra coherently with their stability index. Next, a good PLS model was built with an R^2 of 0.98 and an RMSEP of 2.16 nm to predict color stability using external validations. At last, the bands ($\sim 1330\text{cm}^{-1}$) assigned to the inter-ring stretching modes and the bands reflecting skeleton vibration modes closely correlate to the anthocyanins' color stability prediction. One possible explanation is that these bands are highly coherent with the delocalization of the π -electron and the bending modes of the overall anthocyanin skeleton.

From the result of this work, it is believed that SERS can be used as a rapid and versatile tool for screening raw anthocyanin sources together with the characterization of their color stability against iron incorporation. In addition, this study has established, for the first time, that a good correlation between anthocyanin's stability indexes and SERS signal can be achieved for prediction. It also demonstrated fundamental discussions regarding anthocyanin to iron co-pigmentation from a Raman perspective. In addition, this approach greatly reduces the analysis time. As is known, the traditional way of assessing

iron-induced anthocyanin color shifts involves tedious protocols, including anthocyanin solutions preparation, anthocyanin concentration standardization, incubation with iron salt solutions, recording UV-vis spectra of target sample and control sample, and calculating the bathochromic shifts.¹⁶³ With the developed approach, one only needs to obtain the SERS spectra after preparing anthocyanin solutions to assess the color stability of anthocyanin in the presence of iron. Moreover, the outcome of this study shows great potential for real applications. For example, this model can better facilitate anthocyanin suppliers' quality control protocols or help food developers with their raw material verification and assessment.

CHAPTER 6

SUMMARY AND FUTURE RESEARCH

We have established several methods that utilize Raman spectroscopy and multivariate analysis as core methodologies for detecting and analyzing food colorants. Such applications include quantifying main colorant concentration, identification of possible adulterant or adulterated product, determination of raw ingredient plant sources, and prediction of colorants' color stability.

In the first study, a field-deployable approach was developed for quantifying saffron color strength as well as identifying saffron adulterants using TLC and Raman spectroscopy. The developed method exhibited exceptional performance in quantifying pure saffron color strength, with an RMSECV of 13 (calibration range from 0 to 400, unitless according to ISO 3632) and an R^2 of 0.99. In addition, sample adulteration can be visualized on TLC chips by means of different characteristic TLC patterns. The result of this study demonstrated a good alternative analytical method for saffron quality control out of lab settings.

After the first study, it was clear that further analysis based on TLC imaging data could be used to discriminate between pure and adulterated saffron specimens and estimate the level of adulteration with the help of chemometric models. Thus, the second study established a data fusion strategy to improve classification and quantification accuracies for adulterated saffron. The result confirmed that fused data had a better classification performance (99% accuracy) compared to each single data block (84% for imaging data

and 86% for Raman data). In addition, all spiked samples were identified and distinguished from pure saffron samples. Data fusion also slightly improved quantification accuracies in determining spike levels for each adulterant with higher R^2 values and lower errors. The completion of the first two studies established a solid TLC-Raman approach for pure saffron quality assessment and spiked saffron identification.

In the third study, complementary work has been completed to facilitate the TLC-Raman method. In brief, homemade silver nanoparticles were made into silver mirrors and stamped on TLC chips for Raman signal amplification. The result indicated that the mirror stamp technique showed the full potential of TLC-SERS substrates by enhancing the Raman signal on TLC chips without disrupting the original TLC patterns. In the meantime, compared with other sophisticated TLC-SERS techniques, which involve e-beam evaporation technology, the mirror stamp method was achieved by commercially available materials with an easy preparation protocol. The developed method would facilitate researchers to design faster and more affordable TLC-SERS approaches for complex sample analysis.

At last, a prediction model for anthocyanins' color stability against iron incorporation was completed using SERS coupled with chemometric analysis. As a result, anthocyanins from different plant sources could be clearly differentiated using PCA analysis. Then, a good PLS model was built with an R^2 of 0.98 and an RMSEP of 2.16 nm (bathochromic shift) to predict color stability. These results indicated that SERS signals allowed the identification of color-stable anthocyanins based on their spectral fingerprints.

Furthermore, a close diagnostic of the SERS spectra indicated that the bands at $\sim 1330\text{ cm}^{-1}$ closely correlate to the anthocyanins' color stability prediction. For the first time, this work has established a good SERS prediction model for anthocyanins' color stability against iron fortification. The outcome of this study not only offered a new analytical concept but also provided actual solutions for food colorant producers and product developers in their quality control protocols and raw ingredient screenings.

In conclusion, Raman spectroscopy holds significant potential for quality assessment and raw material screening of colorant samples owing to the advantages of great versatility, specificity, and portability. In addition, with the help of multivariate analysis and data fusion strategies, more meaningful results can be obtained from the spectral data. Thus, the developed methodologies from the presented studies can be applied to real-world practices, which will benefit the quality assurance for food manufacturers and government agencies.

Future works can improve the mirror stamp method and the anthocyanin-iron study. First, it is worth developing an improved mirror stamping protocol to increase mirror consistency and silver concentration per unit mirror area. In addition, developing linear mirror stamps can also expand the feasibility of this method. In this regard, the shape of the mirrors is not limited to a circle shape but can be applied along the flow direction of the mobile phase on TLC chips. Thus, this study's outcome can help one acquire all chemical distribution with one single mapping scan of the linear mirror stamp, making it easier to detect multiple analytes, including transparent samples.

Then, the introduction of X-ray fluorescence spectroscopy (XRF), a well-developed technique for elemental analysis, particularly in detecting and quantifying metal elements, can help us obtain another new perspective to further study the interactions between anthocyanins and iron fortification in complex matrices. In this case, XRF and SERS on TLC chips will evaluate the iron-binding capabilities of different anthocyanin extracts and additives (organic acids and natural chelators). The conjunction of the two techniques will provide intuitive information on elemental and chemical distribution on TLC chips. The result of this work will provide instructive information to mitigate the iron-induced color change in anthocyanin-rich food products.

At last, the established concept of predicting anthocyanins' color stability is not only limited to natural colorants analysis but can be expanded for other compounds. For instance, for a group of compounds that shares similar bone structures, their quality attributes could be estimated via similar protocols. These practices include the prediction of antioxidant activities of flavonoids, stability of carotenoids, and oxidation index of selected edible oils by means of Raman/SERS spectra. These Raman/SERS applications, if completed, would significantly improve the analytical efficiency in food quality analysis.

BIBLIOGRAPHY

- (1) Carocho, M., Barreiro, M. F., Morales, P., & Ferreira, I. C. (2014). Adding molecules to food, pros and cons: A review on synthetic and natural food additives. *Comprehensive reviews in food science and food safety*, 13(4), 377-399.
- (2) Aberoumand, A. (2011). A review article on edible pigments properties and sources as natural biocolorants in foodstuff and food industry. *WJDFS*, 6(1), 71-78.
- (3) Shim, S. M., Seo, S. H., Lee, Y., Moon, G. I., Kim, M. S., & Park, J. H. (2011). Consumers' knowledge and safety perceptions of food additives: Evaluation on the effectiveness of transmitting information on preservatives. *Food control*, 22(7), 1054-1060.
- (4) FDA, U. (2010). Overview of food ingredients, additives & colors.
- (5) Ai, Y. J., Liang, P., Wu, Y. X., Dong, Q. M., Li, J. B., Bai, Y., ... & Ni, D. (2018). Rapid qualitative and quantitative determination of food colorants by both Raman spectra and Surface-enhanced Raman Scattering (SERS). *Food chemistry*, 241, 427-433.
- (6) Martins, N., Roriz, C. L., Morales, P., Barros, L., & Ferreira, I. C. (2016). Food colorants: Challenges, opportunities and current desires of agro-industries to ensure consumer expectations and regulatory practices. *Trends in Food Science & Technology*, 52, 1-15.
- (7) Kobylewski, S., & Jacobson, M. F. (2012). Toxicology of food dyes. *International journal of occupational and environmental health*, 18(3), 220-246.
- (8) International Agency for Research on Cancer. (1993). Occupational exposures of hairdressers and barbers and personal use of hair colourants; some hair dyes, cosmetic colourants, industrial dyestuffs and aromatic amines. *IARC monographs on the evaluation of carcinogenic risks to humans*, 57.
- (9) Chung, K. T. (1983). The significance of azo-reduction in the mutagenesis and carcinogenesis of azo dyes. *Mutation Research/Reviews in Genetic Toxicology*, 114(3), 269-281.
- (10) Liu, R., Hei, W., He, P., & Li, Z. (2011). Simultaneous determination of fifteen illegal dyes in animal feeds and poultry products by ultra-high performance liquid chromatography tandem mass spectrometry. *Journal of Chromatography B*, 879(24), 2416-2422.
- (11) Gray, K. M., Walker, M. J., Burn, M. J. S., Mazur, M., Niedzwiedzka, K., Liszka, K., & Burns, D. T. (2016). Illegal dyes in food and spices—A 2006 LGC LC-UV/Visible method reviewed and updated for 19 dyes. *J. Assoc. Public Anal*, 44, 18-39.
- (12) Lehto, S., Buchweitz, M., Klimm, A., Straßburger, R., Bechtold, C., & Ulberth, F. (2017). Comparison of food colour regulations in the EU and the US: a review of current provisions. *Food Additives & Contaminants: Part A*, 34(3), 335-355.
- (13) Downham, A., & Collins, P. (2000). Colouring our foods in the last and next millennium. *International journal of food science & technology*, 35(1), 5-22.

- (14) Amchova, P., Kotolova, H., & Ruda-Kucerova, J. (2015). Health safety issues of synthetic food colorants. *Regulatory toxicology and pharmacology*, 73(3), 914-922.
- (15) Weber, R. W., Hoffman, M., Raine Jr, D. A., & Nelson, H. S. (1979). Incidence of bronchoconstriction due to aspirin, azo dyes, non-azo dyes, and preservatives in a population of perennial asthmatics. *Journal of Allergy and Clinical Immunology*, 64(1), 32-37.
- (16) McCann, D., Barrett, A., Cooper, A., Crumpler, D., Dalen, L., Grimshaw, K., ... & Stevenson, J. (2007). Food additives and hyperactive behaviour in 3-year-old and 8/9-year-old children in the community: a randomised, double-blinded, placebo-controlled trial. *The lancet*, 370(9598), 1560-1567.
- (17) Sasaki, Y. F., Kawaguchi, S., Kamaya, A., Ohshita, M., Kabasawa, K., Iwama, K., ... & Tsuda, S. (2002). The comet assay with 8 mouse organs: results with 39 currently used food additives. *Mutation Research/Genetic Toxicology and Environmental Mutagenesis*, 519(1-2), 103-119.
- (18) Ishidate Jr, M., Sofuni, T., Yoshikawa, K., Hayashi, M., Nohmi, T., Sawada, M., & Matsuoka, A. (1984). Primary mutagenicity screening of food additives currently used in Japan. *Food and chemical toxicology*, 22(8), 623-636.
- (19) Gukowsky, J. C., Xie, T., Gao, S., Qu, Y., & He, L. (2018). Rapid identification of artificial and natural food colorants with surface enhanced Raman spectroscopy. *Food Control*, 92, 267-275.
- (20) Lehto, S., Buchweitz, M., Klimm, A., Straßburger, R., Bechtold, C., & Ulberth, F. (2017). Comparison of food colour regulations in the EU and the US: a review of current provisions. *Food Additives & Contaminants: Part A*, 34(3), 335-355.
- (21) Brown, J. P., Roehm, G. W., & Brown, R. J. (1978). Mutagenicity testing of certified food colors and related azo, xanthene and triphenylmethane dyes with the Salmonella/microsome system. *Mutation Research/Fundamental and Molecular Mechanisms of Mutagenesis*, 56(3), 249-271.
- (22) Price, P. J., Suk, W. A., Freeman, A. E., Lane, W. T., Peters, R. L., Vernon, M. L., & Huebner, R. J. (1978). In vitro and in vivo indications of the carcinogenicity and toxicity of food dyes. *International journal of cancer*, 21(3), 361-367.
- (23) Mohamad, M. F., Dailin, D. J., Gomaa, S. E., Nurjayadi, M., & El Enshasy, H. (2019). Natural colorant for food: A healthy alternative. *Int J Sci Technol Res*, 8, 3161-3166.
- (24) Rodriguez-Amaya, D. B. (2019). Update on natural food pigments-A mini-review on carotenoids, anthocyanins, and betalains. *Food Research International*, 124, 200-205.
- (25) Li, X., Wang, Z., Zhang, G., & Yi, L. (2019). Improving lycopene production in *Saccharomyces cerevisiae* through optimizing pathway and chassis metabolism. *Chemical Engineering Science*, 193, 364-369.
- (26) Liu, D., Shi, J., Ibarra, A. C., Kakuda, Y., & Xue, S. J. (2008). The scavenging capacity and synergistic effects of lycopene, vitamin E, vitamin C, and β -carotene mixtures on the DPPH free radical. *LWT-Food Science and Technology*, 41(7), 1344-1349.

- (27) Bao, J., Cai, Y., Sun, M., Wang, G., & Corke, H. (2005). Anthocyanins, flavonols, and free radical scavenging activity of Chinese bayberry (*Myrica rubra*) extracts and their color properties and stability. *Journal of Agricultural and Food Chemistry*, 53(6), 2327-2332.
- (28) Wang, L. S., & Stoner, G. D. (2008). Anthocyanins and their role in cancer prevention. *Cancer letters*, 269(2), 281-290.
- (29) Reddivari, L., Vanamala, J., Chintharlapalli, S., Safe, S. H., & Miller Jr, J. C. (2007). Anthocyanin fraction from potato extracts is cytotoxic to prostate cancer cells through activation of caspase-dependent and caspase-independent pathways. *Carcinogenesis*, 28(10), 2227-2235.
- (30) Ding, M., Feng, R., Wang, S. Y., Bowman, L., Lu, Y., Qian, Y., ... & Shi, X. (2006). Cyanidin-3-glucoside, a natural product derived from blackberry, exhibits chemopreventive and chemotherapeutic activity. *Journal of Biological Chemistry*, 281(25), 17359-17368.
- (31) Weisel, T., Baum, M., Eisenbrand, G., Dietrich, H., Will, F., Stockis, J. P., ... & Janzowski, C. (2006). An anthocyanin/polyphenolic - rich fruit juice reduces oxidative DNA damage and increases glutathione level in healthy probands. *Biotechnology Journal: Healthcare Nutrition Technology*, 1(4), 388-397.
- (32) Bosetti, C., Bravi, F., Talamini, R., Parpinel, M., Gnagnarella, P., Negri, E., ... & La Vecchia, C. (2006). Flavonoids and prostate cancer risk: a study in Italy. *Nutrition and cancer*, 56(2), 123-127.
- (33) Rossi, M., Garavello, W., Talamini, R., Negri, E., Bosetti, C., Dal Maso, L., ... & La Vecchia, C. (2007). Flavonoids and the risk of oral and pharyngeal cancer: a case-control study from Italy. *Cancer Epidemiology and Prevention Biomarkers*, 16(8), 1621-1625.
- (34) Giovannucci, E. (2002). A review of epidemiologic studies of tomatoes, lycopene, and prostate cancer. *Experimental biology and medicine*, 227(10), 852-859.
- (35) Hari, R. K., Patel, T. R., & Martin, A. M. (1994). An overview of pigment production in biological systems: functions, biosynthesis, and applications in food industry. *Food Reviews International*, 10(1), 49-70.
- (36) Wu, H., Guo, J. B., Du, L. M., Tian, H., Hao, C. X., Wang, Z. F., et al. (2013). A rapid shaking-based ionic liquid dispersive liquid phase micro extraction for the simultaneous determination of six synthetic food colourants in soft drinks, sugar-and gelatin-based confectionery by high-performance liquid chromatography. *Food Chemistry*, 141, 182–186.
- (37) Gosetti, F., Frascarolo, P., Mazzucco, E., Gianotti, V., Bottaro, M., & Gennaro, M. C. (2008). Photodegradation of E110 and E122 dyes in a commercial aperitif: A high performance liquid chromatography–diode array–tandem mass spectrometry study. *Journal of Chromatography A*, 1202, 58–63.

- (38) Soy lak, M., Unsal, Y. E., & Tuzen, M. (2011). Spectrophotometric determination of trace levels of allura red in water samples after separation and preconcentration. *Food and Chemical Toxicology*, 49, 1183–1187.
- (39) Yoshioka, N., & Ichihashi, K. (2008). Determination of 40 synthetic food colors in drinks and candies by high-performance liquid chromatography using a short column with photodiode array detection. *Talanta*, 74, 1408–1413.
- (40) Sun, H., Sun, N., Li, H., Zhang, J., & Yang, Y. (2013). Development of multiresidue analysis for 21 synthetic colorants in meat by microwave-assisted extraction–solid-phase extraction–reversed-phase ultrahigh performance liquid chromatography. *Food Analytical Methods*, 6, 1291–1299.
- (41) Shen, Y., Zhang, X., Prinyawiwatkul, W., & Xu, Z. (2014). Simultaneous determination of red and yellow artificial food colourants and carotenoid pigments in food products. *Food Chemistry*, 157, 553–558.
- (42) Harp, B. P., Miranda-Bermudez, E., & Barrows, J. N. (2013). Determination of seven certified color additives in food products using liquid chromatography. *Journal of Agricultural and Food Chemistry*, 61, 3726–3736.
- (43) Kucharska, M., & Grabka, J. (2010). A review of chromatographic methods for determination of synthetic food dyes. *Talanta*, 80, 1045–1051.
- (44) Prado, M. A., Boas, L. F. V., Bronze, M. R., & Godoy, H. T. (2006). Validation of methodology for simultaneous determination of synthetic dyes in alcoholic beverages by capillary electrophoresis. *Journal of Chromatography A*, 1136, 231–236.
- (45) Yamjala, K., Nainar, M. S., & Ramiseti, N. R. (2016). Methods for the analysis of azo dyes employed in food industry—a review. *Food chemistry*, 192, 813–824.
- (46) Keresztury, G. (2006). Raman spectroscopy: Theory. *Handbook of vibrational spectroscopy*.
- (47) Sinha, S. S., Jones, S., Pramanik, A., & Ray, P. C. (2016). Nanoarchitecture based SERS for biomolecular fingerprinting and label-free disease markers diagnosis. *Accounts of chemical research*, 49(12), 2725–2735.
- (48) Almeahadi, L. M.; Curley, S. M.; Tokranova, N. A.; Tenenbaum, S. A.; Lednev, I. K. Surface Enhanced Raman Spectroscopy for Single Molecule Protein Detection. *Scientific Reports* 2019, 9 (1), 12356. <https://doi.org/10.1038/s41598-019-48650-y>.
- (49) Kneipp, J.; Wittig, B.; Bohr, H.; Kneipp, K. Surface-Enhanced Raman Scattering: A New Optical Probe in Molecular Biophysics and Biomedicine. *Theoretical Chemistry Accounts* 2010, 125 (3), 319–327. <https://doi.org/10.1007/s00214-009-0665-2>.
- (50) Nie, S.; Emory, S. R. Probing Single Molecules and Single Nanoparticles by Surface-Enhanced Raman Scattering. *Science* 1997, 275 (5303), 1102–1106. <https://doi.org/10.1126/science.275.5303.1102>.
- (51) Ding, S. Y., Yi, J., Li, J. F., Ren, B., Wu, D. Y., Panneerselvam, R., & Tian, Z. Q. (2016). Nanostructure-based plasmon-enhanced Raman spectroscopy for surface analysis of materials. *Nature Reviews Materials*, 1(6), 1–16.

- (52) Chowdhury, J. (2015). How the Charge Transfer (CT) Contributions Influence the SERS Spectra of Molecules? A Retrospective from the View of Albrecht's "A" and Herzberg-Teller Contributions. *Applied Spectroscopy Reviews*, 50(3), 240-260.
- (53) Le Ru, E., & Etchegoin, P. (2008). *Principles of Surface-Enhanced Raman Spectroscopy: and related plasmonic effects*. Elsevier.
- (54) Willets, K. A., & Van Duyne, R. P. (2007). Localized surface plasmon resonance spectroscopy and sensing. *Annu. Rev. Phys. Chem.*, 58, 267-297.
- (55) Yamamoto, Y. S., Ozaki, Y., & Itoh, T. (2014). Recent progress and frontiers in the electromagnetic mechanism of surface-enhanced Raman scattering. *Journal of Photochemistry and Photobiology C: Photochemistry Reviews*, 21, 81-104.
- (56) Han, X. X., Ji, W., Zhao, B., & Ozaki, Y. (2017). Semiconductor-enhanced Raman scattering: Active nanomaterials and applications. *Nanoscale*, 9(15), 4847-4861.
- (57) Lombardi, J. R., & Birke, R. L. (2009). A unified view of surface-enhanced Raman scattering. *Accounts of chemical research*, 42(6), 734-742.
- (58) Pang, S.; Yang, T.; He, L. Review of Surface Enhanced Raman Spectroscopic (SERS) Detection of Synthetic Chemical Pesticides. *TrAC Trends in Analytical Chemistry* 2016, 85, 73–82. <https://doi.org/10.1016/j.trac.2016.06.017>.
- (59) Xie, X.; Pu, H.; Sun, D.-W. Recent Advances in Nanofabrication Techniques for SERS Substrates and Their Applications in Food Safety Analysis. *Critical Reviews in Food Science and Nutrition* 2018, 58 (16), 2800–2813. <https://doi.org/10.1080/10408398.2017.1341866>.
- (60) Muehlethaler, C.; Leona, M.; Lombardi, J. R. Review of Surface Enhanced Raman Scattering Applications in Forensic Science. *Analytical Chemistry* 2016, 88 (1), 152–169. <https://doi.org/10.1021/acs.analchem.5b04131>.
- (61) Li, D.-W.; Zhai, W.-L.; Li, Y.-T.; Long, Y.-T. Recent Progress in Surface Enhanced Raman Spectroscopy for the Detection of Environmental Pollutants. *Microchimica Acta* 2014, 181 (1), 23–43. <https://doi.org/10.1007/s00604-013-1115-3>.
- (62) Bellot-Gurlet, L.; Pagès-Camagna, S.; Coupry, C. Raman spectroscopy in art and archaeology. *Journal of Raman Spectroscopy* 2006, 37 (10), 962–965. <https://doi.org/10.1002/jrs.1615>.
- (63) Sharma, B.; Frontiera, R. R.; Henry, A.-I.; Ringe, E.; Van Duyne, R. P. SERS: Materials, Applications, and the Future. *Materials Today* 2012, 15 (1), 16–25. [https://doi.org/10.1016/S1369-7021\(12\)70017-2](https://doi.org/10.1016/S1369-7021(12)70017-2).
- (64) Yang, T., Qu, Y., Hickey, M., Wang, W., Zhao, B., Bi, S., ... & He, L. (2019). Mapping of pesticide transmission on biological tissues by surface enhanced Raman microscopy with a gold nanoparticle mirror. *ACS applied materials & interfaces*, 11(47), 44894-44904.
- (65) Lee, K.-M.; Herrman, T. J. Determination and Prediction of Fumonisin Contamination in Maize by Surface-Enhanced Raman Spectroscopy (SERS). *Food and Bioprocess Technology* 2016, 9 (4), 588–603. <https://doi.org/10.1007/s11947-015-1654-1>.

- (66) Hudson, S. D.; Chumanov, G. Bioanalytical Applications of SERS (Surface-Enhanced Raman Spectroscopy). *Analytical and Bioanalytical Chemistry* 2009, 394 (3), 679–686. <https://doi.org/10.1007/s00216-009-2756-2>.
- (67) Dai, H., Gao, Q., & He, L. (2020). Rapid Determination of Saffron Grade and Adulteration by Thin-Layer Chromatography Coupled with Raman Spectroscopy. *Food Analytical Methods*, 13(11), 2128-2137.
- (68) Meng, J., Qin, S., Zhang, L., & Yang, L. (2016). Designing of a novel gold nanodumbbells SERS substrate for detection of prohibited colorants in drinks. *Applied Surface Science*, 366, 181-186.
- (69) Li, D., Zhu, Q., Lv, D., Zheng, B., Liu, Y., Chai, Y., & Lu, F. (2015). Silver-nanoparticle-based surface-enhanced Raman scattering wiper for the detection of dye adulteration of medicinal herbs. *Analytical and bioanalytical chemistry*, 407(20), 6031-6039.
- (70) Wu, L., Pu, H., Huang, L., & Sun, D. W. (2020). Plasmonic nanoparticles on metal-organic framework: A versatile SERS platform for adsorptive detection of new coccine and orange II dyes in food. *Food Chemistry*, 328, 127105.
- (71) Xie, Y., Li, Y., Niu, L., Wang, H., Qian, H., & Yao, W. (2012). A novel surface-enhanced Raman scattering sensor to detect prohibited colorants in food by graphene/silver nanocomposite. *Talanta*, 100, 32-37.
- (72) Yao, Y., Wang, W., Tian, K., Ingram, W. M., Cheng, J., Qu, L., ... & Han, C. (2018). Highly reproducible and sensitive silver nanorod array for the rapid detection of Allura Red in candy. *Spectrochimica Acta Part A: Molecular and Biomolecular Spectroscopy*, 195, 165-171.
- (73) Chen, J., Abell, J., Huang, Y. W., & Zhao, Y. (2012). On-chip ultra-thin layer chromatography and surface enhanced Raman spectroscopy. *Lab on a Chip*, 12(17), 3096-3102.
- (74) Zhu, Y., Zhang, L., & Yang, L. (2015). Designing of the functional paper-based surface-enhanced Raman spectroscopy substrates for colorants detection. *Materials Research Bulletin*, 63, 199-204.
- (75) Gao, F., Hu, Y., Chen, D., Li-Chan, E. C., Grant, E., & Lu, X. (2015). Determination of Sudan I in paprika powder by molecularly imprinted polymers–thin layer chromatography–surface enhanced Raman spectroscopic biosensor. *Talanta*, 143, 344-352.
- (76) Lin, Z., & He, L. (2019). Recent advance in SERS techniques for food safety and quality analysis: a brief review. *Current Opinion in Food Science*, 28, 82-87.
- (77) Zhang, Y.; Zhao, S.; Zheng, J.; He, L. Surface-Enhanced Raman Spectroscopy (SERS) Combined Techniques for High-Performance Detection and Characterization. *TrAC Trends in Analytical Chemistry* 2017, 90, 1–13. <https://doi.org/10.1016/j.trac.2017.02.006>.
- (78) Assimadhis, M. K., Tarantilis, P. A., & Polissiou, M. G. (1998). UV-Vis, FT-Raman, and 1H NMR spectroscopies of cis-trans carotenoids from saffron (*Crocus sativus* L.). *Applied Spectroscopy*, 52(4), 519-522.

- (79) Chao, K., Dhakal, S., Schmidt, W. F., Qin, J., Kim, M., Peng, Y., & Huang, Q. (2020). Raman and IR spectroscopic modality for authentication of turmeric powder. *Food chemistry*, 320, 126567.
- (80) Lussier, F., Thibault, V., Charron, B., Wallace, G. Q., & Masson, J. F. (2020). Deep learning and artificial intelligence methods for Raman and surface-enhanced Raman scattering. *TrAC Trends in Analytical Chemistry*, 124, 115796.
- (81) Cheung, W., Shadi, I. T., Xu, Y., & Goodacre, R. (2010). Quantitative analysis of the banned food dye Sudan-1 using surface enhanced Raman scattering with multivariate chemometrics. *The Journal of Physical Chemistry C*, 114(16), 7285-7290.
- (82) Hoehse, M., Paul, A., Gornushkin, I., & Panne, U. (2012). Multivariate classification of pigments and inks using combined Raman spectroscopy and LIBS. *Analytical and bioanalytical chemistry*, 402(4), 1443-1450.
- (83) Bergoin, M., Raynaud, C., Vilarem, G., & Talou, T. (2005). Investigation on Aroma Volatiles from Fresh Flowers of Saffron (*Crocus sativus* L.). *SPECIAL PUBLICATION-ROYAL SOCIETY OF CHEMISTRY*, 300, 104.
- (84) Peter, K. V. (2000). Saffron. *Handbook of Herbs and Spices*.
- (85) Er, S. V., Eksi-Kocak, H., Yetim, H., & Boyaci, I. H. (2017). Novel spectroscopic method for determination and quantification of saffron adulteration. *Food analytical methods*, 10(5), 1547-1555.
- (86) Hamidpour, R., Hamidpour, S., Hamidpour, M., & Shahlari, M. (2013). Effect of *Crocus sativus* and its active compounds for the treatment of several diseases: A review. *International Journal of Case Reports and Images*.
- (87) Assimopoulou, A. N., Sinakos, Z., & Papageorgiou, V. (2005). Radical scavenging activity of *Crocus sativus* L. extract and its bioactive constituents. *Phytotherapy Research: An International Journal Devoted to Pharmacological and Toxicological Evaluation of Natural Product Derivatives*, 19(11), 997-1000.
- (88) Verma, S. K., & Bordia, A. (1998). Antioxidant property of saffron in man. *Indian journal of medical sciences*, 52(5), 205-207.
- (89) Ashrafi, M., Bathaie, S. Z., Taghikhani, M., & Moosavi-Movahedi, A. A. (2005). The effect of carotenoids obtained from saffron on histone H1 structure and H1-DNA interaction. *International journal of biological macromolecules*, 36(4), 246-252.
- (90) Premkumar, K., Thirunavukkarasu, C., Abraham, S. K., Santhiya, S. T., & Ramesh, A. (2006). Protective effect of saffron (*Crocus sativus* L.) aqueous extract against genetic damage induced by anti-tumor agents in mice. *Human & experimental toxicology*, 25(2), 79-84.
- (91) Anastasaki, E. G., Kanakis, C. D., Pappas, C., Maggi, L., Zalacain, A., Carmona, M., ... & Polissiou, M. G. (2010). Quantification of crocetin esters in saffron (*Crocus sativus* L.) using Raman spectroscopy and chemometrics. *Journal of agricultural and food chemistry*, 58(10), 6011-6017.

- (92) Sabatino, L., Scordino, M., Gargano, M., Belligno, A., Traulo, P., & Gagliano, G. (2011). HPLC/PDA/ESI-MS evaluation of saffron (*Crocus sativus* L.) adulteration. *Natural product communications*, 6(12), 1934578X1100601220.
- (93) Sereshti, H., Poursorkh, Z., Aliakbarzadeh, G., Zarre, S., & Ataolahi, S. (2018). An image analysis of TLC patterns for quality control of saffron based on soil salinity effect: A strategy for data (pre)-processing. *Food chemistry*, 239, 831-839.
- (94) Sujata, V., Ravishankar, G. A., & Venkataraman, L. V. (1992). Methods for the analysis of the saffron metabolites crocin, crocetins, picrocrocin and safranal for the determination of the quality of the spice using thin-layer chromatography, high-performance liquid chromatography, and gas chromatography. *Journal of Chromatography A*, 624(1-2), 497-502.
- (95) Zheng, J., & He, L. (2014). Surface - enhanced Raman spectroscopy for the chemical analysis of food. *Comprehensive reviews in food science and food safety*, 13(3), 317-328.
- (96) Assimiadis, M. K., Tarantilis, P. A., & Polissiou, M. G. (1998). UV-Vis, FT-Raman, and ¹H NMR Spectroscopies of cis-trans Carotenoids from Saffron (*Crocus sativus* L.). *Applied Spectroscopy*, 52(4), 519-522.
- (97) Parker, F. S. (1983). Applications of infrared, Raman, and resonance Raman spectroscopy in biochemistry. Springer Science & Business Media.
- (98) Petrakis, E. A., & Polissiou, M. G. (2017). Assessing saffron (*Crocus sativus* L.) adulteration with plant-derived adulterants by diffuse reflectance infrared Fourier transform spectroscopy coupled with chemometrics. *Talanta*, 162, 558-566.
- (99) Schulz, H., Baranska, M., & Baranski, R. (2005). Potential of NIR - FT - Raman spectroscopy in natural carotenoid analysis. *Biopolymers: Original Research on Biomolecules*, 77(4), 212-221.
- (100) Tarantilis, P. A., Beljebbar, A., Manfait, M., & Polissiou, M. (1998). FT-IR, FT-Raman spectroscopic study of carotenoids from saffron (*Crocus sativus* L.) and some derivatives. *Spectrochimica Acta Part A: Molecular and Biomolecular Spectroscopy*, 54(4), 651-657.
- (101) ISO 3632 - 1. (2011). Saffron (*Crocus sativus* Linneaus). Part 1: Specifications. International Organization For Standardization.
- (102) ISO 3632 - 2. (2010a). Saffron (*Crocus sativus* Linneaus). Part 2: Test Methods, International Organisation for Standardization.
- (103) Socrates, G. (2004). Infrared and Raman characteristic group frequencies: tables and charts. John Wiley & Sons.
- (104) Schmidt, C., & Trentelman, K. (2009). 1064 nm dispersive Raman micro-spectroscopy for the in-situ identification of organic red colorants. *Preservation Science*, 6, 10-21.

- (105) Bruni, S., Guglielmi, V., & Pozzi, F. (2011). Historical organic dyes: a surface - enhanced Raman scattering (SERS) spectral database on Ag Lee - Meisel colloids aggregated by NaClO₄. *Journal of Raman Spectroscopy*, 42(6), 1267-1281.
- (106) Varliklioz Er, S., Eksi-Kocak, H., Yetim, H., & Boyaci, I. H. (2016). Novel Spectroscopic Method for Determination and Quantification of Saffron Adulteration. *Food Analytical Methods*, 10(5), 1547–1555. <https://doi.org/10.1007/s12161-016-0710-4>
- (107) Sabatino, L., Scordino, M., Gargano, M., Belligno, A., Traulo, P., & Gagliano, G. (2011). HPLC/PDA/ESI-MS Evaluation of Saffron (*Crocus sativus* L.) Adulteration. *Natural Product Communications*, 6(12), 1934578X1100601. <https://doi.org/10.1177/1934578x1100601220>
- (108) Cocchi, M. (2019). *Data Fusion Methodology and Applications* (ISSN Book 31) (1st ed.). Elsevier.
- (109) Borràs, E., Ferré, J., Boqué, R., Mestres, M., Aceña, L., & Busto, O. (2015). Data fusion methodologies for food and beverage authentication and quality assessment – A review. *Analytica Chimica Acta*, 891, 1–14. <https://doi.org/10.1016/j.aca.2015.04.042>
- (110) Castanedo, F. (2013). A review of data fusion techniques. *The scientific world journal*, 2013.
- (111) Salvi, M., Michielli, N., & Molinari, F. (2020). Stain Color Adaptive Normalization (SCAN) algorithm: Separation and standardization of histological stains in digital pathology. *Computer Methods and Programs in Biomedicine*, 193, 105506. <https://doi.org/10.1016/j.cmpb.2020.105506>
- (112) Zhang, Y., Zhao, S., Zheng, J., & He, L. (2017). Surface-enhanced Raman spectroscopy (SERS) combined techniques for high-performance detection and characterization. *TrAC Trends in Analytical Chemistry*, 90, 1-13.
- (113) Bin Zhang, B., Shi, Y., Chen, H., xia Zhu, Q., Lu, F., & wei Li, Y. (2018). A separable surface-enhanced Raman scattering substrate modified with MIL-101 for detection of overlapping and invisible compounds after thin-layer chromatography development. *Analytica chimica acta*, 997, 35-43.
- (114) Shen, Z., Fan, Q., Yu, Q., Wang, R., Wang, H., & Kong, X. (2020). Facile detection of carbendazim in food using TLC-SERS on diatomite thin layer chromatography. *Spectrochimica Acta Part A: Molecular and Biomolecular Spectroscopy*, 247, 119037.
- (115) Zhu, Q., Li, H., Lu, F., Chai, Y., & Yuan, Y. (2016). A widely applicable silver sol for TLC detection with rich and stable SERS features. *Nanoscale research letters*, 11(1), 1-8.
- (116) Li, D., Qu, L., Zhai, W., Xue, J., Fossey, J. S., & Long, Y. (2011). Facile on-site detection of substituted aromatic pollutants in water using thin layer chromatography combined with surface-enhanced Raman spectroscopy. *Environmental science & technology*, 45(9), 4046-4052.

- (117) Araújo, A., Caro, C., Mendes, M. J., Nunes, D., Fortunato, E., Franco, R., ... & Martins, R. (2014). Highly efficient nanoplasmonic SERS on cardboard packaging substrates. *Nanotechnology*, 25(41), 415202.
- (118) Toh, H. S., Faure, R. L., Amin, L. B. M., Hay, C. Y. F., & George, S. (2017). A light-assisted in situ embedment of silver nanoparticles to prepare functionalized fabrics. *Nanotechnology, science and applications*, 10, 147.
- (119) Qu, Y., Tan, C., Zhang, Z., & He, L. (2017). A facile solvent mediated self-assembly silver nanoparticle mirror substrate for quantitatively improved surface enhanced Raman scattering. *Analyst*, 142(21), 4075-4082.
- (120) Dai, H., Gao, Q., & He, L. (2020). Rapid Determination of Saffron Grade and Adulteration by Thin-Layer Chromatography Coupled with Raman Spectroscopy. *Food Analytical Methods*, 13(11), 2128-2137.
- (121) Anastasaki, E. G., Kanakis, C. D., Pappas, C., Maggi, L., Zalacain, A., Carmona, M., ... & Polissiou, M. G. (2010). Quantification of crocetin esters in saffron (*Crocus sativus* L.) using Raman spectroscopy and chemometrics. *Journal of agricultural and food chemistry*, 58(10), 6011-6017.
- (122) Schulz, H., Baranska, M., & Baranski, R. (2005). Potential of NIR - FT - Raman spectroscopy in natural carotenoid analysis. *Biopolymers: Original Research on Biomolecules*, 77(4), 212-221
- (123) Li, H., xia Zhu, Q., sian Chwee, T., Wu, L., feng Chai, Y., Lu, F., & fang Yuan, Y. (2015). Detection of structurally similar adulterants in botanical dietary supplements by thin-layer chromatography and surface enhanced Raman spectroscopy combined with two-dimensional correlation spectroscopy. *Analytica chimica acta*, 883, 22-31.
- (124) Chen, J., Abell, J., Huang, Y. W., & Zhao, Y. (2012). On-chip ultra-thin layer chromatography and surface enhanced Raman spectroscopy. *Lab on a Chip*, 12(17), 3096-3102.
- (125) Sinha, S. S., Jones, S., Pramanik, A., & Ray, P. C. (2016). Nanoarchitecture based SERS for biomolecular fingerprinting and label-free disease markers diagnosis. *Accounts of chemical research*, 49(12), 2725-2735.
- (126) Pyysalo, H., & Kuusi, T. (1973). The role of iron and tin in discoloration of berry and red beet juices. *Zeitschrift für Lebensmittel-Untersuchung und Forschung*, 153(4), 224-233.
- (127) Camaschella, C. (2019). Iron deficiency. *Blood, The Journal of the American Society of Hematology*, 133(1), 30-39.
- (128) Rustandi, A., Soedarsono, J. W., Priadi, D., Suprpta, D. N., Priyotomo, G., & Bakri, R. (2014). Interaction of Purple Sweet Potato Extract with Ascorbic Acid in FeCl₃ Solution. In *Applied Mechanics and Materials* (Vol. 680, pp. 32-37). Trans Tech Publications Ltd.
- (129) Cheng, G. W., & Crisosto, C. H. (1997). Iron—polyphenol complex formation and skin discoloration in peaches and nectarines. *Journal of the American Society for Horticultural Science*, 122(1), 95-99.

- (130) McGee, E. J. T., & Diosady, L. L. (2018). Development of Spectrophotometric Quantification Method of Iron-Polyphenol Complex in Iron-Fortified Black Tea at Relevant pH Levels. *Food Analytical Methods*, 11(6), 1645-1655.
- (131) Martinez-Navarrete, N., Camacho, M. M., Martinez-Lahuerta, J., Martinez-Monzó, J., & Fito, P. (2002). Iron deficiency and iron fortified foods—a review. *Food Research International*, 35(2-3), 225-231.
- (132) Adams, J. B., & Brown, H. M. (2007). Discoloration in raw and processed fruits and vegetables. *Critical Reviews in Food Science and Nutrition*, 47(3), 319-333.
- (133) Chandler, B. V., & Mary Clegg, K. (1970). Pink discoloration in canned pears I.—Role of tin in pigment formation. *Journal of the Science of Food and Agriculture*, 21(6), 315-319.
- (134) Melo, M. J., Pina, F., & Andary, C. (2009). Anthocyanins: nature's glamorous palette (pp. 134-150). Wiley: Chichester, UK.
- (135) Seitz, H. U., & Hinderer, W. (1988). Anthocyanins. *Phytochemicals in Plant Cell Cultures*, 49-76.
- (136) McCallum, J. L., Yang, R., Young, J. C., Strommer, J. N., & Tsao, R. (2007). Improved high performance liquid chromatographic separation of anthocyanin compounds from grapes using a novel mixed-mode ion-exchange reversed-phase column. *Journal of Chromatography A*, 1148(1), 38-45.
- (137) Clifford, M. N. (2000). Anthocyanins—nature, occurrence and dietary burden. *Journal of the Science of Food and Agriculture*, 80(7), 1063-1072.
- (138) Manach, C.; Scalbert, A.; Morand, C.; Rem'esy, C.; Jimenez, C. 'Polyphenols: Food Source and Bioavailability. *Am. J. Clin. Nutr.* 2004, 79 (5), 727–747.
- (139) Bueno, J. M., Sáez-Plaza, P., Ramos-Escudero, F., Jiménez, A. M., Fett, R., & Asuero, A. G. (2012). Analysis and antioxidant capacity of anthocyanin pigments. Part II: chemical structure, color, and intake of anthocyanins. *Critical reviews in analytical chemistry*, 42(2), 126-151.
- (140) Lambert, S. G.; Asenstorfer, R. E.; Williamson, N. M.; Iland, P. G.; Graham, P. Copigmentation between Malvidin-3-Glucoside and Some Wine Constituents and Its Importance to Colour Expression in Red Wine. *Food Chem.* 2011, 125 (1), 106–115.
- (141) Giusti, M. M., & Wrolstad, R. E. (2003). Acylated anthocyanins from edible sources and their applications in food systems. *Biochemical engineering journal*, 14(3), 217-225.
- (142) Malien-Aubert, C., Dangles, O., & Amiot, M. J. (2001). Color stability of commercial anthocyanin-based extracts in relation to the phenolic composition. Protective effects by intra- and intermolecular copigmentation. *Journal of agricultural and food chemistry*, 49(1), 170-176.
- (143) Fenger, J. A., Moloney, M., Robbins, R. J., Collins, T. M., & Dangles, O. (2019). The influence of acylation, metal binding and natural antioxidants on the thermal stability of red cabbage anthocyanins in neutral solution. *Food & Function*, 10(10), 6740-6751.

- (144) Krenn, L., Steitz, M., Schlicht, C., Kurth, H., & Gaedcke, F. (2007). Anthocyanin- and proanthocyanidin-rich extracts of berries in food supplements—analysis with problems. *Die Pharmazie-An International Journal of Pharmaceutical Sciences*, 62(11), 803-812.
- (145) Błkowska-Barczak, A. (2005). Acylated anthocyanins as stable, natural food colorants—A review. *Polish journal of food and nutrition sciences*, 14, 55.
- (146) Bueno, J. M., Sáez-Plaza, P., Ramos-Escudero, F., Jiménez, A. M., Fett, R., & Asuero, A. G. (2012). Analysis and antioxidant capacity of anthocyanin pigments. Part II: chemical structure, color, and intake of anthocyanins. *Critical reviews in analytical chemistry*, 42(2), 126-151.
- (147) Lee, J., Durst, R. W., Wrolstad, R. E., & Collaborators: Eisele T Giusti MM Hach J Hofsommer H Koswig S Krueger DA Kupina; S Martin SK Martinsen BK Miller TC Paquette F Ryabkova A Skrede G Trenn U Wightman JD. (2005). Determination of total monomeric anthocyanin pigment content of fruit juices, beverages, natural colorants, and wines by the pH differential method: collaborative study. *Journal of AOAC international*, 88(5), 1269-1278.
- (148) Buchweitz, M., Gudi, G., Carle, R., Kammerer, D. R., & Schulz, H. (2012). Systematic investigations of anthocyanin–metal interactions by Raman spectroscopy. *Journal of Raman Spectroscopy*, 43(12), 2001-2007.
- (149) Zaffino, C., Russo, B., & Bruni, S. (2015). Surface-enhanced Raman scattering (SERS) study of anthocyanidins. *Spectrochimica Acta Part A: Molecular and Biomolecular Spectroscopy*, 149, 41-47.
- (150) Zaffino, C., Bruni, S., Russo, B., Pilu, R., Lago, C., & Colonna, G. M. (2016). Identification of anthocyanins in plant sources and textiles by surface - enhanced Raman spectroscopy (SERS). *Journal of Raman Spectroscopy*, 47(3), 269-276.
- (151) Sigurdson, G. T., Robbins, R. J., Collins, T. M., & Giusti, M. M. (2016). Evaluating the role of metal ions in the bathochromic and hyperchromic responses of cyanidin derivatives in acidic and alkaline pH. *Food Chemistry*, 208, 26-34.
- (152) Li, A., Xiao, R., He, S., An, X., He, Y., Wang, C., ... & He, J. (2019). Research advances of purple sweet potato anthocyanins: extraction, identification, stability, bioactivity, application, and biotransformation. *Molecules*, 24(21), 3816.
- (153) Del Pozo-Insfran, D., Brenes, C. H., & Talcott, S. T. (2004). Phytochemical composition and pigment stability of Açai (*Euterpe oleracea* Mart.). *Journal of Agricultural and Food Chemistry*, 52(6), 1539-1545.
- (154) Charron, C. S., Kurilich, A. C., Clevidence, B. A., Simon, P. W., Harrison, D. J., Britz, S. J., ... & Novotny, J. A. (2009). Bioavailability of anthocyanins from purple carrot juice: effects of acylation and plant matrix. *Journal of agricultural and food chemistry*, 57(4), 1226-1230.
- (155) GIUSTI, M. M., & Wrolstad, R. E. (1996). Characterization of red radish anthocyanins. *Journal of food science*, 61(2), 322-326.

- (156) Bitsch, R., Netzel, M., Frank, T., Strass, G., & Bitsch, I. (2004). Bioavailability and biokinetics of anthocyanins from red grape juice and red wine. *Journal of Biomedicine and Biotechnology*, 2004(5), 293.
- (157) Oh, Y. S., Lee, J. H., Yoon, S. H., Oh, C. H., Choi, D. S., Choe, E., & Jung, M. Y. (2008). Characterization and quantification of anthocyanins in grape juices obtained from the grapes cultivated in Korea by HPLC/DAD, HPLC/MS, and HPLC/MS/MS. *Journal of food science*, 73(5), C378-C389.
- (158) Rubinskiene, M., Viskelis, P., Jasutiene, I., Viskeliene, R., & Bobinas, C. J. F. R. I. (2005). Impact of various factors on the composition and stability of black currant anthocyanins. *Food research international*, 38(8-9), 867-871.
- (159) Burns, A. E., Mazauric, J. P., & Cheynier, V. (2013). Resonance raman study on the pH dependence on grape anthocyanins. In *Physical Methods in Food Analysis* (pp. 127-135). American Chemical Society.
- (160) Tiwari, B. K., Patras, A., Brunton, N., Cullen, P. J., & O'donnell, C. P. (2010). Effect of ultrasound processing on anthocyanins and color of red grape juice. *Ultrasonics sonochemistry*, 17(3), 598-604.
- (161) Li, X. D., Li, J., Wang, M., & Jiang, H. (2016). Copigmentation effects and thermal degradation kinetics of purple sweet potato anthocyanins with metal ions and sugars. *Applied Biological Chemistry*, 59(1), 15-24.
- (162) Assous, M. T. M., Abdel-Hady, M. M., & Medany, G. M. (2014). Evaluation of red pigment extracted from purple carrots and its utilization as antioxidant and natural food colorants. *Annals of Agricultural Sciences*, 59(1), 1-7.
- (163) Sigurdson, G. T., Robbins, R. J., Collins, T. M., & Giusti, M. M. (2016). Evaluating the role of metal ions in the bathochromic and hyperchromic responses of cyanidin derivatives in acidic and alkaline pH. *Food Chemistry*, 208, 26-34.